STRATOSPHERIC CIRCULATION:

A NARROWBAND FILTER SPECTROPHOTOMETER FOR

TOTAL OZONE DETERMINATION

A thesis presented for the degree of

Doctor of Philosophy in Physics

in the University of Canterbury,

Christchurch, New Zealand.

by

Reid E. Basher

1975

ABSTRACT

This thesis describes the use of ultraviolet narrowband interference filters in the spectrophotometric determination of local atmospheric total ozone burdens.

An investigation of a prototype interference filter spectrophotometer shows that its total ozone measurements are in error owing to the breadth of the filters' passband skirts and to the transmittance sideband leakages of the filters. Accurate spectral transmittance measurements, extending down to transmittances of 10^{-7}, are described and show that the leakage sidebands generally occur close to the passbands and in the near infrared spectral region.

An outline of the design and construction of a new, more accurate filter spectrophotometer is given. The use of stacks of two filters at each wavelength greatly improves the narrowness of the passband skirts and significantly decreases the transmittances of the leakage sidebands. In addition a very effective sideband blocking filter is used. The considerably improved performance of this new spectrophotometer is confirmed by the results of a direct comparison of the instrument with a standard Dobson prism spectrophotometer.

A study is presented of the effects of filter non-uniformity, orientation, aging and temperature. This enables the establishment of criteria in these regards for accurate total ozone measurement. A similar study is made of the instrument's photomultiplier detector.

The effects of the filters' finite bandwidths are analysed by a numerical simulation of the spectral characteristics of the whole measurement process. The theory involved is given. Calculations show that double stacked filters perform considerably better than single filters. Over the usual operating ranges of airmass and total ozone, the error in the total ozone measurement due to the filter bandwidth effect, is found to be about ±1.0% for the doubled-filter instrument. Corrections for the error are tabulated.

ACKNOWLEDGEMENTS

Few theses can be considered as the work solely of their authors, and this thesis is no exception. Much credit is due to many people in the Physics Department and elsewhere for their willing assistance and advice during the course of this project.

I am particularly indebted to Dr Grahame J. Fraser, my Project Supervisor, for his unfailing support and encouragement. He is an attentive and sympathetic listener, and has the ability to inspire the self-confidence and enthusiasm so necessary for original research. He has promoted the development of the narrow-band filter spectrophotometer from the beginning through the supervision of Dr W. Andrew Matthews' Ph.D. project and then of mine. My gratitude also goes to Dr Matthews for his help and advice in the early stages of my project.

My appreciation is extended to the very able staffs of the Physics Department's Mechanical and Electronic Workshops for their help in constructing the two filter spectrophotometers, especially to Bruce Bradshaw for mechanical construction, and to Alex Black and Ray Borrell for electronic design and construction. My thanks also go to Ross Ritchie for varied technical help, and to Laurie Hunter for his fine photographic work.

The spectrophotometers' construction was materially aided by the generous financial support of the New Zealand Meteorological Service. I wish to express my appreciation to the Service's officers and scientists for their interest, and

particularly to Edith Farkas for calibrating and operating the Dobson spectrophotometer for the direct comparison with the filter instrument, for analysing the raw data, and for providing help at other times.

I am very appreciative of the many useful clarifying discussions I have had with Joan, my wife, and on a different level, with my postgraduate companion, now Dr David S. Wratt. To Joan also go my warm thanks for the application of her literary talents to the thesis to make it more readable.

Finally, acknowledgement is due to the University of Canterbury and to the Head of the Physics Department, Professor A.G. McLellan, for the continued support of a Teaching Fellowship and for the provision of the many facilities required during the course of the project.

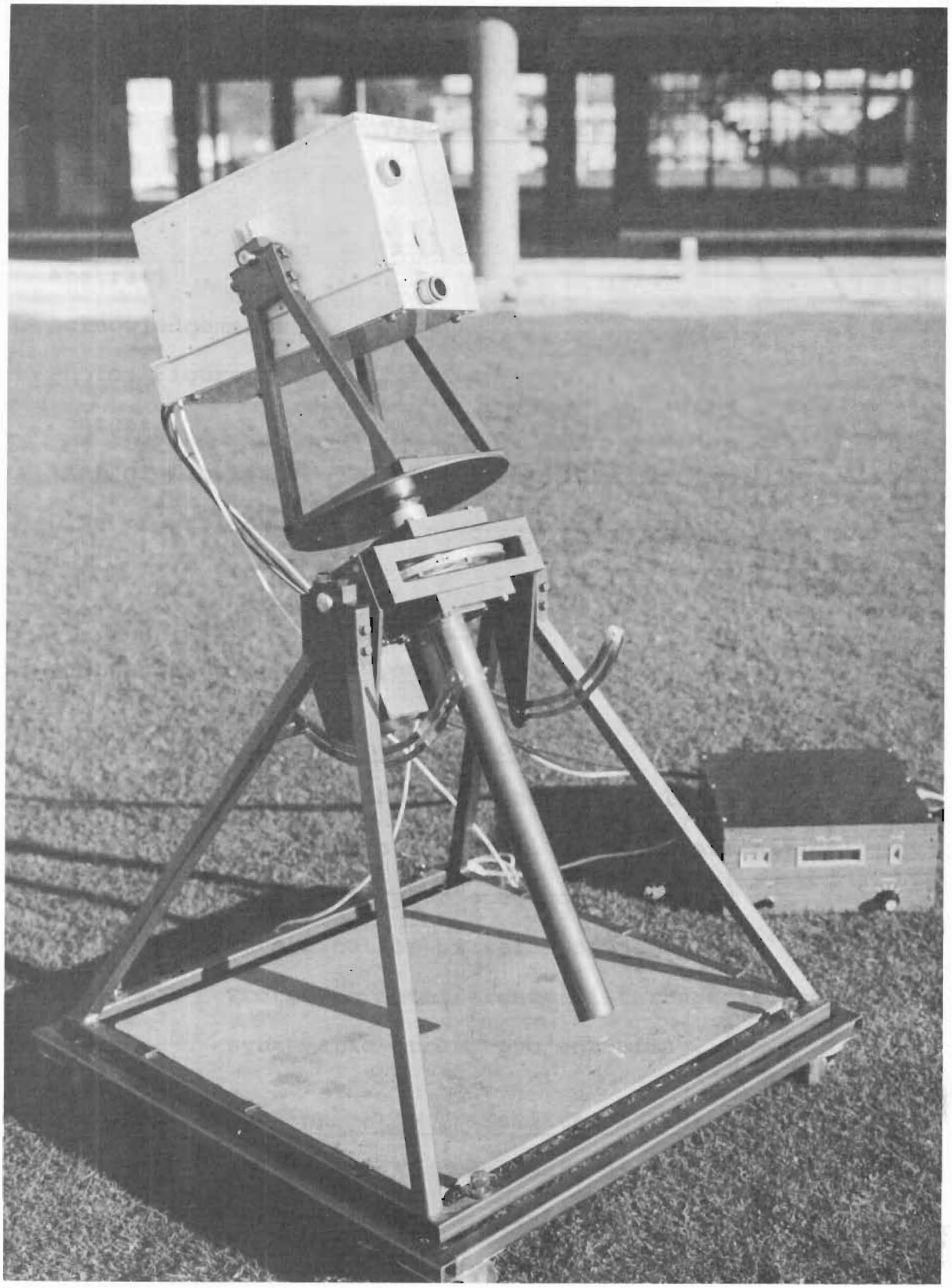

FIG. 1.1 NEW INTERFERENCE-FILTER SPECTROPHOTOMETER FOR TOTAL OZONE MEASUREMENT.

The white photometer can be seen mounted on the equatorial sun-follower and is about one metre above the ground, while the electronic data display unit is on the right. The construction and accuracy of the spectrophotometer are the main concerns of this thesis.

TABLE OF CONTENTS

Page

PART II: NEW FILTER SPECTROPHOTOMETER

Page

Page

LIST OF FIGURES

LIST OF TABLES

PART I: BACKGROUND

Preliminary Remarks

The thesis divides naturally into four parts. This first part, Part I, provides the basis from which the remaining parts develop. Part II, which describes the new filter instrument, and Part III, which analyses the filter bandwidth effect, form the major portions of the work, while the remaining part, Part IV, is a conclusion.

Part I contains two chapters. In Chapter 1, a brief outline of the main areas of ozone research, and the idea of total ozone and its measurement is given, along with a description of the theory involved. The advantages of an interference filter spectrophotometer for total ozone measurement are listed, and a prototype instrument and its systematic error are discussed. The project aims are also given.

Chapter 2 describes an experimental procedure which was devised to investigate transmission leakages in the prototype instrument's interference filters. Experimental measurements are compared with the theory. The fuller understanding of the filters which is gained forms a necessary basis for the instrument development of Part II, and the filter measurement theory of Part III.

CHAPTER 1: GENERAL INTRODUCTION

1.1 Ozone in the Atmosphere, Total Ozone, Instruments for Total Ozone Determination

Studies made over many years have shown atmospheric ozone to be intimately involved in the atmosphere's circulation, heat budget, and state of pollution. The outlines of these aspects which follow are based on the detailed and well referenced reviews of Craig (1965) and Griggs (1966).

Ozone is formed in the atmosphere through the reaction of atomic and molecular oxygen above about 50 km in altitude, the atomic oxygen having been produced by photodissociation of molecular oxygen. Ozone's concentration is small, being generally less than 20 mg/g even at its maximum in the lower stratosphere (15 km to 30 km) where it tends to accumulate. Despite its low abundance, ozone has the power to reduce, through absorption, the solar ultraviolet spectrum between 200 nm and 300 nm to an unobservable level at the ground.

Ground based measurement of atmospheric ozone traditionally relies on spectrophotometric measurements at the edge of this strong absorption band in the region of 300 nm to 340 nm, and has as its basic quantity the total amount of ozone in a vertical atmospheric column. The instrument usually used is the Dobson quartz prism spectrophotometer.

Systematic studies made over long periods have shown the total ozone to have significant day to day, seasonal and geographical variations which cannot be explained solely by in-situ photochemical models. However, the models do show that

in the lower stratosphere, ozone is photochemically stable with a lifetime of between a month and a year, and that hence the ozone (air) mixing ratio is a quasi-conservative property of air masses at these altitudes. Therefore, variations in total ozone can be explained as being the result of stratospheric transport processes, on both local and global scales. The corollary is that stratospheric transport processes can be investigated through study of the spatial and temporal variations in total ozone.

As well as being an indicator of transport processes, ozone also has a direct effect on such processes owing to its strong absorption of ultraviolet radiation. Although the amount of energy is small (less than 3% of the total incident radiant energy of the sun), it is absorbed within the low density air of the upper stratosphere and therefore causes this air to be of relatively high temperature. This absorption must be taken into account when modelling the earth's heat balance.

Ozone has a significant role in air pollution chemistry. At ground level it is produced by photochemical reactions of the hydrocarbons and nitrogen oxides emitted in vehicle exhausts, and may reach toxic concentrations in densely populated regions. More importantly, it is believed that at lower stratospheric altitudes, the nitrogen oxides in the exhausts of supersonic aircraft have the reverse effect, that of depleting the local ozone density. Owing to the long lifetime of ozone at these altitudes, any ozone used up in reactions is not readily replaced, and so a reduction in density occurs. This is a serious matter, since the lowered ozone density would cause local and global increases in the

earth's exposure to biologically damaging solar ultraviolet radiation.

A more recent fear is that stratospheric ozone is being depleted as a result of reactions involving the propellants released from spray cans. Large quantities of propellant are released each year and although relatively inert at ground level, by gradual diffusion to stratospheric altitudes and subsequent photodissociation, the materials could introduce products of significant reactivity.

As can be seen from the preceding paragraphs, atmospheric ozone has a key role in ensuring the wellbeing of mankind as well as being of purely scientific interest. Its continued measurement is therefore of great importance.

The pre-eminent instrument in ozone measurement is the Dobson prism spectrophotometer. Over the last forty years it has provided the bulk of the data on total ozone, for which it is regarded as the standard instrument, and on the vertical distribution of ozone using the umkehr technique. It measures the difference between the atmospheric absorption of solar ultraviolet radiation in two narrow wavelength bands. The bands are separated by prisms and slits. It is described in detail by Dobson (1957).

Despite its widespread use, the instrument has some disadvantages. The use of prisms and slits requires it to be large and well engineered. This results in it being rather cumbersome and heavy (75 kg), and yet at the same time, in it requiring care in handling. It must be operated manually, and several minutes may be needed to take the measurements for a single total ozone determination. In addition, there is reason

to believe that its reliability, sensitivity and price are not satisfactory (Matthews 1971, pl.11). Significantly, in 1973, it was reported to be out of production (Brewer 1973).

The need for an alternative instrument prompted Dr G.J. Fraser of the University of Canterbury Physics Department to promote the development of a spectrophotometer which uses narrowband interference filters to select the desired ultra-violet wavelength bands. Interference filters are very suitable for use in total ozone measurement by virtue of the fact that they do not need the precisely engineered mounting that a prism and slit system does, and by virtue of their small size and weight, flexibility in design, and relatively low price.

The project was initially undertaken by W.A. Matthews and was subsequently continued by the author. As is described in his thesis (1971), Matthews constructed a compact, robust filter spectrophotometer whose measurements compared favour-ably with those of a Dobson instrument. This prototype filter instrument is further discussed in Section 1.3.

Another interference filter spectrophotometer is reported by Osherovich et al. (1969). It is intended as a replacement for the M83 Russian total ozone instrument which uses broad-bandwidth coloured glass filters. Brewer (1973) describes an alternative instrument which uses a diffraction grating as its dispersing element. Attempts are also being made to automate a Dobson instrument (Raeber 1973). All three instrument types; filter, prism and grating, rely on the same basic measurement theory. A formulation of the theory follows in Section 1.2.

1.2 Basic Theory of Spectrophotometric Determination of Total Ozone

The theory of total ozone measurement was originally developed for use with the Dobson spectrophotometer, but it is also applicable to other instruments which have essentially monochromatic passbands. A good account of it is given in Craig (1965) and forms the basis of the presentation given here.

Following Beer's Law, the fractional change in solar flux $W(\lambda)$ in between wavelengths λ and $\lambda+d\lambda$, in going from height z to z+dz, and due to ozone absorption, molecular scattering and aerosol scattering, can be expressed as

$$dW(\lambda)/W(\lambda) = [\alpha(\lambda)\rho_3(z) + K(\lambda)\rho(z) + \delta(\lambda,z)]\sec\psi(z)dz \tag{1.1}$$

where

$\alpha(\lambda)$ = ozone absorption coefficient at wavelength λ

$K(\lambda)$ = molecular scattering coefficient at wavelength λ

$\delta(\lambda,z)$ = fraction scattered by aerosols at height z and wavelength λ

$\rho_3(z)$ = ozone number density at height z

$\rho(z)$ = number density of air at height z

$\psi(z)$ = solar zenith angle at height z.

Integrating equation (1.1) from the earth's surface to the outer limit of the atmosphere gives

$$\ln[W(\lambda)/W_\infty(\lambda)] = -\alpha(\lambda)\int_0^\infty \rho_3(z)\sec\psi(z)dz - K(\lambda)\int_0^\infty \rho(z)\sec\psi(z)dz - \int_0^\infty \delta(\lambda,z)\sec\psi(z)dz \tag{1.2}$$

where $W_\infty(\lambda)$ is the flux outside the atmosphere.

The integrals are approximated as follows. In the first integral, sec $\psi(z)$ is considered constant and is evaluated at z = 22 km, near the ozone's centre of mass, to become μ_h. The second integral is written as $\beta(\lambda)\mu_m$ where $\beta(\lambda)$ is the value of the term for vertical incidence and is calculated from the theory described in Appendix H, and where μ_m is the airmass, a function which accounts for atmospheric refraction and sphericity, and which is expressed in Appendix G, section 5. In the third integral, sec $\psi(z)$ is replaced by μ, the secant of the ground level zenith angle, since most aerosols exist near the earth's surface, and the remaining part of the integral is represented by $\delta(\lambda)$. Hence

$$\ln[W(\lambda)/W_\infty(\lambda)] = -\mu_h X\alpha(\lambda) - \mu_m\beta(\lambda) - \mu\delta(\lambda) \qquad (1.3)$$

where X is the total number of ozone molecules per unit base area of a vertical atmospheric column. It is called the total ozone and is usually expressed as a thickness of pure ozone at S.T.P. The ozone absorption coefficient is then expressed per unit thickness.

The factors μ_h, μ_m and μ can be called column ratios. Since they are very nearly equal for $\mu < 3.0$, they are often corporately called the airmass in the rest of the thesis.

Equation (1.3) is more useful if written in terms of $P(\lambda)$, the electrical response of a spectrophotometer to the flux $W(\lambda)$ where

$$P(\lambda) = C(\lambda)W(\lambda) \qquad (1.4)$$

and $C(\lambda)$ represents the instrument's spectral characteristics. Thus

$$\ln[P(\lambda)/P_{\infty}(\lambda)] = -\mu_h X\alpha(\lambda) - \mu_m\beta(\lambda) - \mu\delta(\lambda) \qquad (1.5)$$

or

$$P(\lambda) = P_{\infty}(\lambda)\exp -[\mu_h X\alpha(\lambda) - \mu_m\beta(\lambda) - \mu\delta(\lambda)] \qquad (1.6)$$

The total ozone is found by comparing the instrument response, $P(\lambda)$, for two wavelength bands. Writing out equation (1.5) for the two bands, at λ_1 and λ_2, and subtracting them gives the expression

$$X = \frac{\ln[P_{\infty}(\lambda_1)/P_{\infty}(\lambda_2)]-\ln[P(\lambda_1)/P(\lambda_2)]-\mu_m[\beta(\lambda_1)-\beta(\lambda_2)]-\mu[\delta(\lambda_1)-\delta(\lambda_2)]}{\mu_h[\alpha(\lambda_1)-\alpha(\lambda_2)]} \qquad (1.7)$$

Since the aerosol scattering coefficient $\delta(\lambda)$ is generally not known, it is often assumed that the coefficient is independent of wavelength so that the term $\delta(\lambda_1)-\delta(\lambda_2) = 0$. In fact this is not a good assumption. A better procedure is to take measurements at two pairs of wavelengths and express the total ozone by taking the difference of the two equations corresponding to equation 1.7. Then the differences of $[\delta(\lambda_1)-\delta(\lambda_2)]$ terms are set equal to zero.

This practice is recommended in Dobson (1957), and is supported by the theoretical calculations of Thomas et al. (1974) and the experimental work of Rat'kov (1969). For the Dobson instrument, it is tantamount to assuming that the aerosol scattering coefficient is linear with wavelength since the wavelength separation of the bands in each pair is approximately the same.

The term $\ln[P_\infty(\lambda_1)/P_\infty(\lambda_2)]$ is called the extraterrestrial constant, because $P_\infty(\lambda)$ is the response the instrument would have outside the atmosphere. It can be seen from equation (1.4) that each $P_\infty(\lambda)$ includes a solar flux constant $W_\infty(\lambda)$, as well as an instrumental constant $C(\lambda)$. The extraterrestrial constants are determined experimentally by the following method.

The measurement equation for a single wavelength band, equation (1.5), can be written as

$$\ln[P(\lambda)/P_\infty(\lambda)] = -\mu_h\gamma(\lambda) \tag{1.8}$$

where $\gamma(\lambda)$ represents the band's total atmospheric attenuation. Writing equation (1.8) for two bands and subtracting them gives

$$\ln[P(\lambda_1)/P(\lambda_2)] = \ln[P_\infty(\lambda_1)/P_\infty(\lambda_2)] - \mu_h[\gamma(\lambda_1)-\gamma(\lambda_2)] \tag{1.9}$$

Now if the atmospheric attenuation term, $\gamma(\lambda_1)-\gamma(\lambda_2)$ is constant, measurements of $\ln[P(\lambda_1)/P(\lambda_2)]$ will be linear in μ_h and their extrapolation to zero airmass will yield the extraterrestrial constant, $\ln[P_\infty(\lambda_1)/P_\infty(\lambda_2)]$.

Accurate determinations of the constants require measurements to be taken over a large range of airmass, particularly since no measurements are possible between the noon airmass and zero airmass. However, during the long periods needed, the atmospheric attenuation, especially that due to ozone and aerosols, is likely to change, and contradictory results are often found. Further discussion of

the method and its accuracy can be found in Dobson and Normand (1962).

It should be noted that in the above theory the instrument passbands are treated as monochromatic. It is subsequently referred to in this thesis as the monochromatic theory.

1.3 Prototype Interference Filter Spectrophotometer, Systematic Error, Project Aims

The prototype narrowband filter spectrophotometer is fully described by Matthews (1971). It consists of a lens-less collimator of 1.5° field of view, a rotating frame containing four interference filters which correspond to the Dobson standard A and D pairs of wavelength bands, and a photo-multiplier detector. The detector's output is logarithmically amplified and is fed, along with phasing pulses derived from reed relays and a magnet on the filter frame, to a mini-computer for on-line data acquisition.

The photometer unit is relatively small and light, being about 20 cm in each dimension, and weighing 5 kg. To track the sun, it is rotated in the equatorial plane under the control of a sunlight-sensitive servo system. Therefore, once set up, the instrument is able to operate automatically and can accumulate measurements over a whole day.

The 2.3 nm to 5.0 nm halfbandwidths of the filters are larger than the 1.0 nm and 3.0 nm slitwidths of the Dobson instrument, but are much smaller than those of the Russian M83 filter instrument. Better resolution results in higher total ozone accuracy. The filters, like the Dobson slitbands, are treated as monochromatic so that the theory of Section 1.2 of this Chapter can be used.

Matthews (1971 and 1972) describes a comparison of the instrument with the Dobson No. 17 instrument operated by the New Zealand Meteorological Service at Invercargill ($46^{o}25'S$). The instrument performed well, with the individual total ozone values agreeing to within 5% over a 15% range in total ozone, and a range of 1.2 to 2.8 in airmass. The comparison period was brief though, and only five days' data are presented.

At the end of Matthews' thesis study then, it appeared that a total ozone filter spectrophotometer had been developed which could be considered a viable alternative to the Dobson instrument. However, it later became apparent that the instrument had the following major systematic fault.

Figure 1.2 is a sample graph of $\log[P(\lambda_1)/P(\lambda_2)]$ against airmass for the instrument's A and D wavelength pairs. According to equation 1.9, the data should lie on a straight line, provided that the atmospheric attenuation is constant. A satisfactory linearity is to be seen for the D wavelength pair, and also for the A wavelength pair up to an airmass of 2.0, but beyond this airmass the A pair data show an increasing divergence which cannot be explained by atmospheric changes alone.

The nonlinearity is erroneously interpreted by the usual total ozone determination as a systematic reduction in total ozone with airmass. For example, the data of figure 1.2 will show a 30% total ozone reduction between airmasses 2.0 and 3.0. The non-linearity also increases the difficulty of extrapolating the data to find the extraterrestrial constants (Section 1.2).

It is the solution of this problem with which the present thesis is concerned. Matthews' work clearly demonstrates the

FIG. 1.2
LOG RESPONSE
DIFFERENCE
VERSUS
AIRMASS

A-PAIR
AND
D-PAIR

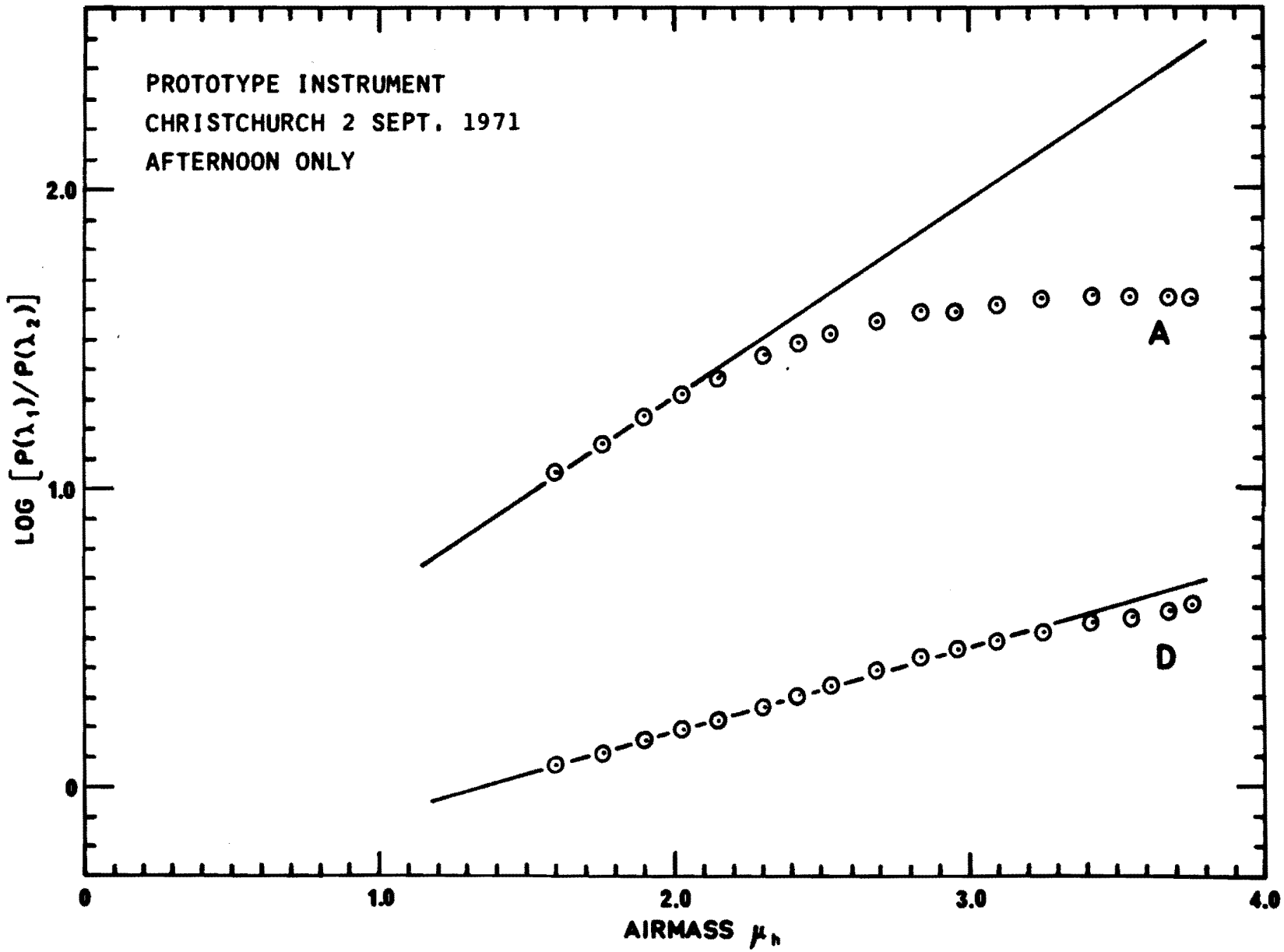

potential value of filter spectrophotometers for total ozone measurement, but there still remains the above nonlinearity problem, as well as other lesser problems with filters and electronics, some of which are touched on by Matthews.

The aims of the present project, therefore, are firstly to carry out a full investigation of the instrument's accuracy, with particular reference to the interference filters used, and secondly, on the basis of these studies, to design and construct a new and improved instrument.

CHAPTER 2:

MONOCHROMATIC TRANSMITTANCE LEAKAGE BAND MODEL

2.1 Introduction, Hypothesis of Transmittance Leakage to Explain Systematic Error

In the first chapter, the filters are modelled as a single monochromatic passband, in just the same way that the Dobson instrument slitbands are. In this chapter, however, a single , small, monochromatic leakage sideband is added to the model, with a view to explaining the systematic error in the filter instrument's total ozone measurements which was described in Section 1.3.

A leakage sideband on the long wavelength side of a filter passband will suffer less atmospheric attenuation than the passband, and hence, as the airmass increases, it will contribute an increasing proportion of the filter's total transmitted radiation. If the 305 nm filter had such a leakage, the increasing proportion of additional radiation would cause a steady reduction in the A wavelength pair's log intensity ratio with airmass, and a consequent steady reduction in determined total ozone. This is just the behaviour described in Section 1.3.

If, however, the sizes and whereabouts of the leakages were known, it would be possible to correct the total ozone for their effect. The leakage bands could be measured on a spectrophotometer, but at the time of the investigation, this was considered undesirable as the removal of the filters from the photometer would require a subsequent redetermination of the instrument's extraterrestrial constants.

The need to measure the leakage bands in situ prompted a consideration of silica glass (ordinary window glass), whose transmittance spectrum, figure 2.1, is very similar to the atmosphere's, attenuating shorter wavelength radiation more strongly than longer wavelength radiation. Therefore, a sufficient thickness of glass could be used to completely block out a filter passband, and thus allow measurement of the transmitted leakage bands.

The method proved to be very successful insofar as it enabled the accurate identification of a leakage band at 346 nm in the 305 nm filter, and the measurement of sufficient parameters to provide for the band's correction. The theory which follows in the next Section, 2.2, is simple, and leads to some very tidy experimental results as is shown in Section 2.3.

2.2 Theory of Monochromatic Leakage Band Model, Use of Glass Filters

Let P_1 by the photometer's electrical output response (in current, voltage or frequency) to radiation transmitted only by a filter's essentially monochromatic passband at wavelength λ_1, and let P_2 be the response due only to the filter's single, essentially monochromatic leakage band at wavelength λ_2. In this case the photometer's total response P to this filter is

$$P = P_1 + P_2 \qquad (2.1)$$

If, however, n identical plates of glass are introduced into the photometer's measurement beam, where each plate has

transmittance A_1 at λ_1, and A_2 at λ_2, then the total response P becomes

$$P = A_1^n P_1 + A_2^n P_2 \tag{2.2}$$

Now if $A_1 << A_2$, then for a sufficiently large value of n, equation 2.2 reduces to

$$P = A_2^n P_2 \tag{2.3}$$

From looking at the glass transmittance spectrum, figure 2.1, one can see that this situation would arise for a longer wavelength leakage in the 305 nm filter. The leakage band response, P_2, can be defined in terms of equation (1.6) as

$$P_2 = P_{\infty 2} e^{-\mu \gamma_2} \tag{2.4}$$

where $P_{\infty 2}$ is the photometer's extraterrestrial response to the band, μ is the atmospheric airmass, and γ_2 is the band's atmospheric attenuation coefficient. γ_2 accounts for ozone absorption, molecular scattering and aerosol scattering.

As with the monochromatic theory of Section 1.2, variability in the response P_2 due to spectrally flat changes in aerosol attenuation and in the instrumental component of the extraterrestrial response, is accounted for by comparison with the measurement of another filter band. The 340 nm filter was chosen for this task as its atmospheric attenuation coefficient is relatively small and constant.

Combining equations (2.3) and (2.4) and taking logarithms gives

$$\ln P = n \ln A_2 + \ln P_{\infty 2} - \mu\gamma_2 \qquad (2.5)$$

from which two conclusions can be made.

Firstly, for constant airmass μ and attenuation coefficient γ_2, ln P is proportional to the number of glass plates n, with gradient $\ln A_2$ and intercept $\ln P_{\infty 2} - \mu\gamma_2$.

Secondly, for any constant number of glass plates n, ln P is proportional to airmass μ, with gradient $-\gamma_2$ and intercept $n \ln A_2 - \ln P_{\infty 2}$.

Therefore, by carrying out experiments to test the above conclusions, it should be possible to find values of γ_2 and $P_{\infty 2}$ which can be used to eliminate the effects of the leakage band on the total ozone measurements. Furthermore, if either or both γ_2 and A_2 is known, the wavelength of the leakage λ_2 can be found.

2.3 In Situ Experimental Analysis of Leakage in 305 nm Filter Using Silica Glass Plates

The basic experiment was to measure the photometer's response for all four filters, as a function of airmass μ and number of glass plates n.

This involved operating the photometer on the automatic data acquisition system (Section 1.3) and taking measurements at minute intervals while various numbers of glass plates were held in front of the entry aperture. From one to six, 7 mm thick plates were used, in cyclic fashion. Every second or third measurement was made without glass so that background changes in the extraterrestrial responses ($P_{\infty 2}$) could be monitored.

Measurements were made on 7 Sept 1971, a cold, clear, spring day, for three hours centred on noon, when the airmass was relatively constant at about 1.65, and for 1.5 hours in the mid-afternoon during which the airmass rose to 3.7. The following discussion is restricted to the 305 nm filter as the others show little evidence of transmittance leakages. For convenience, decimal logarithms have been used.

The model proposed is well confirmed in figure 2.3 for the 305 nm filter. The introduction of one glass plate produces a marked reduction in the photometer's output P corresponding to the strong attenuation of the 305 nm passband by the glass. From $n = 2$ to $n = 6$, the excellent linearity of the data implies that the passband is completely blocked out, and that only a single, less strongly attenuated, and therefore longer wavelength leakage band remains.

The straight line is described by equation (2.5), and has a gradient which yields

$$A_2 = 0.670 \pm 0.003 \qquad (2.6)$$

and an intercept of

$$\log P_{\infty 2} - \mu\gamma_2 = 3.18 \pm 0.01 \qquad (2.7)$$

The measurements of figure 2.3 were taken within a few minutes during which the airmass was essentially constant, at $\mu = 1.615 \pm 0.004$, and during which the leakage band's atmospheric attenuation coefficient could be considered constant.

More support for the model comes from figure 2.4, which shows the leakage band's attenuation as a function of airmass. The data are again described by equation 2.5 and yield an average leakage band attenuation coefficient of

$$\gamma_2 = 0.29 \pm 0.01 \qquad (2.8)$$

With the aid of the value of A_2 given in equation (2.6), the intercepts of figure 2.4 can be used to find an average value of the log of the leakage band's extraterrestrial response

$$\log P_{\infty 2} = 3.65 \pm 0.01 \qquad (2.9)$$

Log $P_{\infty 2}$ can also be found by inserting the value of γ_2 (equation 2.8) into equation (2.7), which holds at airmass $\mu = 1.619 \pm 0.004$, to give

$$\log P_{\infty 2} = 3.66 \pm 0.03 \qquad (2.10)$$

which agrees very well with equation (2.9).

The centre wavelength of the leakage band, λ_2, can be found in two ways. Firstly, if the glass transmittance spectrum (figure 2.1) is monotonic, there will be a unique wavelength corresponding to the transmittance A_2 given in equation (2.6). In this way the wavelength is found to be

$$\lambda_2 = 345.8 \pm 0.4 \text{ nm} \qquad (2.11)$$

Secondly, if the leakage band's atmospheric attenuation is due solely to molecular scattering (there is negligible ozone absorption at 346 nm), a unique wavelength can be found

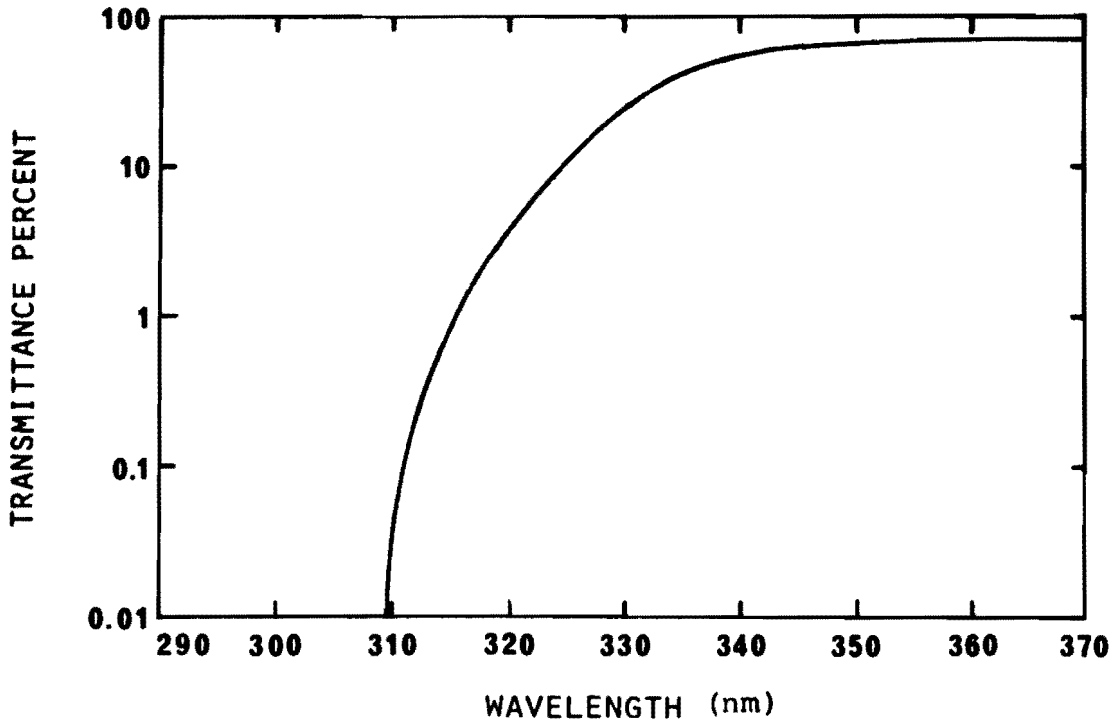

FIG.2.1 TRANSMITTANCE SPECTRUM OF ONE 7mm THICK GLASS PLATE.

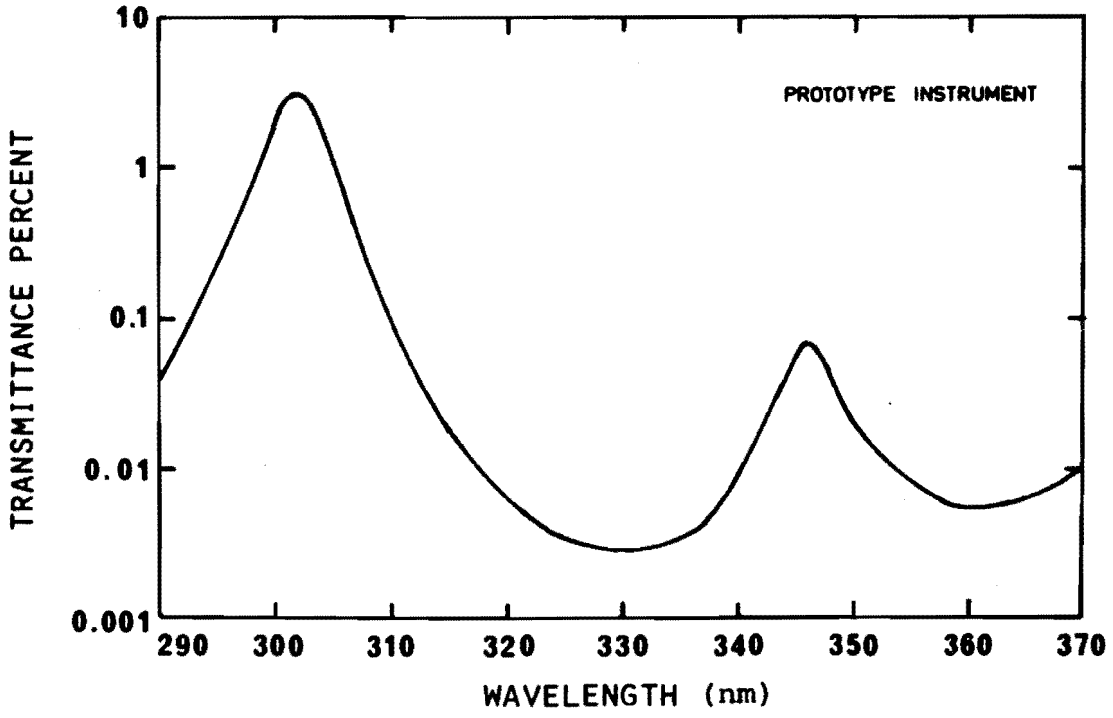

FIG.2.2 TRANSMITTANCE SPECTRUM OF 305nm INTERFERENCE FILTER.

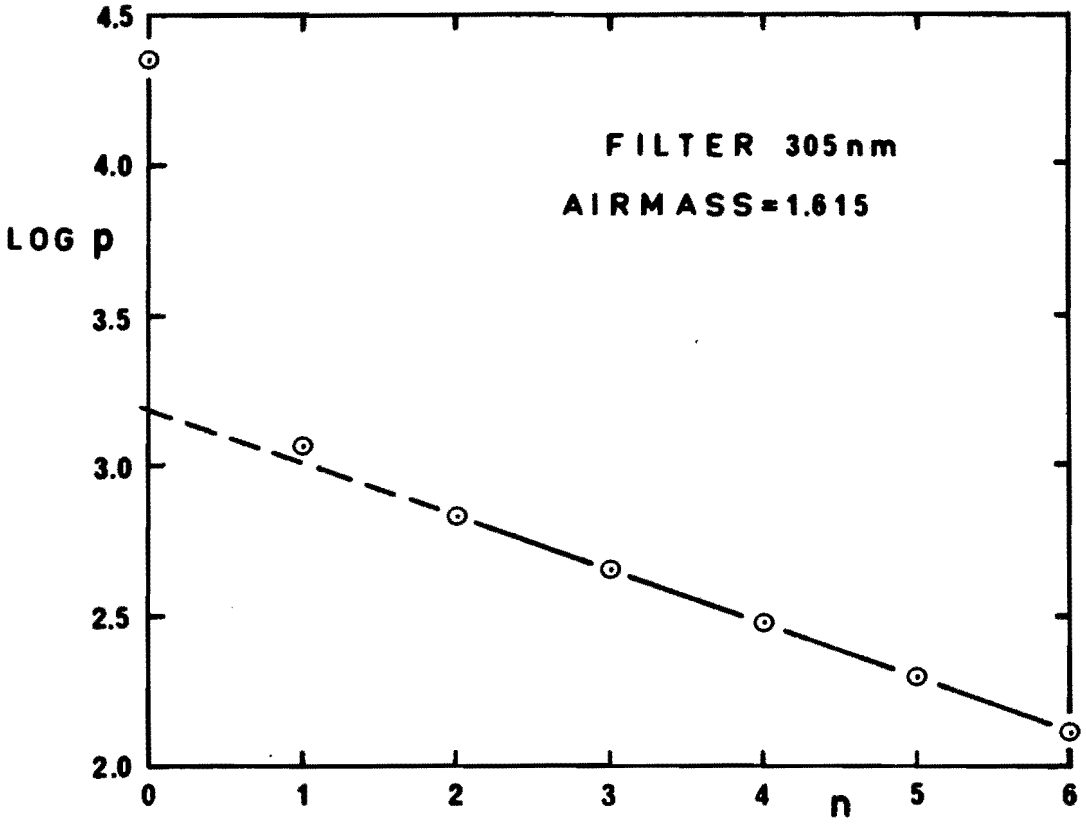

FIG.2.3 LOG OF INSTRUMENT RESPONSE, P, VERSUS n, THE NUMBER OF GLASS PLATES.

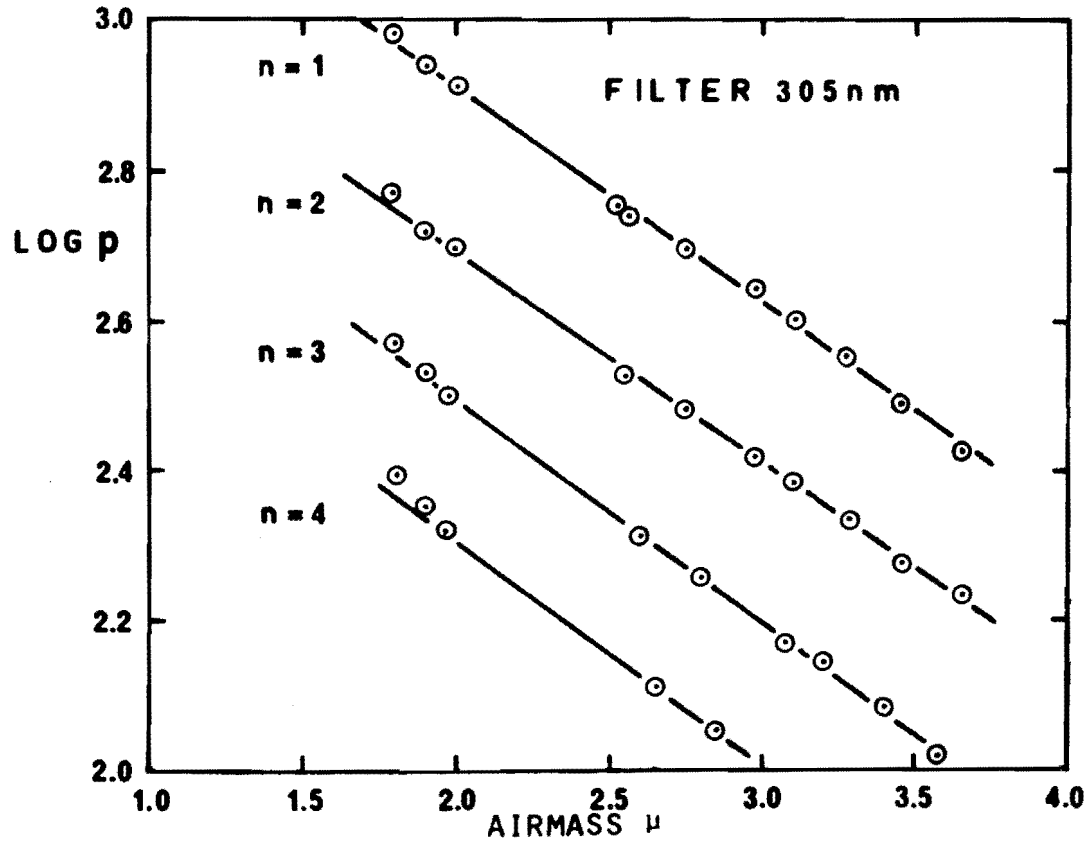

FIG.2.4 LOG OF INSTRUMENT RESPONSE P VERSUS AIRMASS FOR n=1,2,3 & 4 GLASS PLATES.

which corresponds to the band's attenuation coefficient γ_2 given in equation 2.8. It is

$$\lambda_2 = 346 \pm 3 \text{ nm} \tag{2.12}$$

The agreement between equations (2.11) and (2.12) suggests that, on the day of the measurements, the band's aerosol scattering coefficient was very small, being less than the uncertainty in the attenuation coefficient given in equation (2.8).

The experiments described above give remarkably consistent results, and confirm beyond doubt the existence of a single, essentially monochromatic leakage band in the 305 nm filter. They also allow the band's size and wavelength to be measured to good accuracy, which enables the effect of the band on determined total ozone to be corrected for.

It should be noted that the method requires the glass to have a large transmittance difference between the passband and leakage band wavelengths. The silica glass was fortunately very suitable for isolating the leakage band found in the 305 nm filter, but it would be of little use for isolating similar leakage bands in the 325 nm filter say, or leakage bands on the short wavelength side of a passband.

2.4 Conclusion, Attempts to Correct Systematic Error, Implications for Future Instruments

The contribution to the 305 nm filter's electrical output response from the leakage band can be subtracted out with the aid of equations (2.4), (2.8) and (2.9). When the correction was applied to the already accumulated data, a considerable improvement resulted, the A wavelength pair log intensity ratios becoming much more linear with airmass. However, there was still a decreasing trend in the ratio which became increasingly noticeable beyond an airmass of about 3.0.

This nonlinearity was unreasonably large considering the accuracy and consistency of leakage band data, and was little improved by the addition of more of the blocking filter, nickel sulphate hexahydrate. It remained somewhat of a problem until the filter's transmittance spectrum, shown in figure 2.2, was eventually measured. (The measurement of this, and all the other transmittance spectra presented in this thesis, is described in detail in Appendix A.)

The spectrum does have a large leakage band near 346 nm as expected, but neither the leakage band nor the passband is narrow enough to be treated as monochromatic. In fact, both bands have broad spreading bases, or skirts, which clearly will transmit significant quantities of radiation. In particular, the long wavelength skirt of the passband will contribute an increasing proportion of radiation with increasing airmass, in just the same way as the leakage band does, and therefore will give rise to nonlinearity in the log of the intensity ratio.

The reason why no effects of the skirt transmission appear in the glass plates experiment can be found by comparing

figures 2.1 and 2.2. The transmittance of just one glass plate decreases very rapidly in going from the leakage band at 346 nm to the edge of the passband skirt at about 320 nm, and hence the glass excludes virtually all the skirt radiation along with the rest of the passband. (Note that the addition of a glass plate to the filter is represented by the addition of the two graphs.)

A similar reason explains the relative failure of the nickel sulphate to effectively reduce the nonlinearity. From its transmittance spectrum, figure 4.9, it can be seen that nickel sulphate hexahydrate is only useful as a blocking filter at wavelengths beyond 340 nm, and is hence completely ineffective in reducing the skirt transmission.

The transmittance spectra of the remaining three filters have the same passband shape as the 305 nm filter, but have no significant leakage bands.

There are two major conclusions to be drawn from this chapter. The first has an important bearing on the design of the new filter instrument, whose description fills Part II, while the second is the germinal idea of the bandwidth effect, with which Part III is concerned.

Firstly, it is clear that for accurate total ozone determination, over a good range of airmass, the present 305 nm filter is inadequate. The 305 nm filter, and the other filters, need to be narrower at all transmittance levels, and any leakage bands in them need to be considerably smaller than the one just described. The maximum permissible sizes of leakage bands are calculated for all filters in Appendix B, and along with the knowledge of the need for narrow bandwidths,

form the basis of the specifications of a new filter set, which is described in Chapter 4.

The second conclusion is that filter leakage bands and passband skirt transmission act in exactly the same way to produce inaccuracy in the determined total ozone. Evidently, all parts of the spectrum will contribute to the error, and therefore any correction procedure must take into account a filter's whole transmittance spectrum. It is this concept that forms the foundation of the bandwidth effect theory of Part III.

PART II: NEW FILTER SPECTROPHOTOMETER

Preliminary Remarks

This part of the thesis contains a general description of the second total ozone filter spectrophotometer, developed by the author, and shown in figure 1.1, as well as chapters which assess, in detail, the relevant characteristics of the instrument's filters and photomultiplier.

The instrument's design criteria were that it have as near the accuracy of the Dobson spectrophotometer (~ ±2%) as possible, but that it be much simpler than that instrument, i.e., lighter, smaller, cheaper, more rugged, easier to operate, and that it be automatic with computer-compatible data output, e.g. paper or magnetic tape. The need for a good design was accentuated by the involvement of the New Zealand Meteorological Service in the project, as the Service wished to put an instrument into regular operational use.

The author was responsible for designing, drawing and supervising the construction of the photometer, its photo-switches, and the equatorial mount, while the electronic system was designed and built in the Physics Department's Electronics Workshop. The design criteria were largely met by the two instruments built, one fully automatic and permanently installed in the Physics Dept, and the other semi-automatic and mobile.

A description of these instruments by Dr W.A. Matthews, Dr G.J. Fraser and the author was read to the European Geophysical Society's September 1974 meeting, and will be published in Pure and Applied Geophysics early in 1975.

Provisional patents on the instrument have been filed.

The chapters on filters and photomultipliers describe the many significant sources of error which arise in the use of these items. Direct experimental measurements are presented along with quantitative assessments of the effect of each aspect of behaviour on either the ozone absorption coefficients, or the total-ozone. A preliminary study of some of these effects is to be found in Matthews (1971).

The final chapter in Part II contains a discussion of the instrument's calibration and accuracy, and lists some suggested design changes aimed at further improving the instrument's performance.

CHAPTER 3: GENERAL DESCRIPTION OF INSTRUMENT

3.1 Photometer, Construction and Functions

The layout of the photometer is shown in figures 3.1, 3.2 and 3.3. It basically consists of a rotating disc of six ultraviolet narrowband filters at the front, a photomultiplier at the rear, and a set of collimating apertures in between.

The rotation of the filter disc enables the radiation entering the quartz window to be viewed by each filter in sequence, the rate of 2 cycles/sec giving each a sampling period of 22 ms. The whole filter disc can be quickly removed from its supporting shaft, so that discs can be easily interchanged or calibrated without the removal of individual filters.

For simplicity, the field of view is defined by a series of apertures, rather than by quartz lenses. Two fields of view of 2.3^{o} and 4.6^{o} are available, the smaller intended for direct sun measurements, where the skylight should be minimised, and the larger intended for zenith sky measurements, where the radiation intensity is low. The theoretical calculations of Thomas et al. (1974) show that the effect of radiation scattered by molecules and aerosols into the measured beam is negligible for fields of view less than about 5^{o}. However, it will be shown in Section 4.5 that there is good reason for using the smaller aperture for both types of measurement where possible.

The 2.3^{o} field of view gives the photometer an alignment tolerance of $\pm 0.9^{o}$. Two neutral density filters can be

introduced to attenuate the beam to 0.1 or 0.01 if necessary for photomultiplier protection.

The lens, mirror and screen contained in the base of the photometer, enable the accurate alignment of the photometer on the sun. It is possible to align the sun's 32' image on the screen graticule to within ±3', and because the light is focussed, alignment may be made on even a very weak sun.

The light sealing must be very effective as the ultra-violet fluxes transmitted by the filter are very small compared to the total external radiation flux. For this reason, all joints are rubber sealed, and the filter disc has circular grooves in it which fit over matching circular baffles in its supporting wall and the front cover. To reduce internally scattered light, baffles are provided and surfaces are painted matt black.

3.2 Electronic Design, Data Acquisition

The purpose of the electronic system is to measure the constantly changing light intensity provided by the rotating filter disc, and to record or display the information in a convenient form. The system used with the mobile instrument is shown in figure 3.4.

The photomultiplier's output current, which is directly proportional to the incident light flux, is converted by the current-controlled oscillator to a fixed-voltage pulse train, whose frequency is directly proportional to the current input as is shown in figure 3.5. Each filter intensity is then measured by counting the pulses over a fixed period during the scan of the filter.

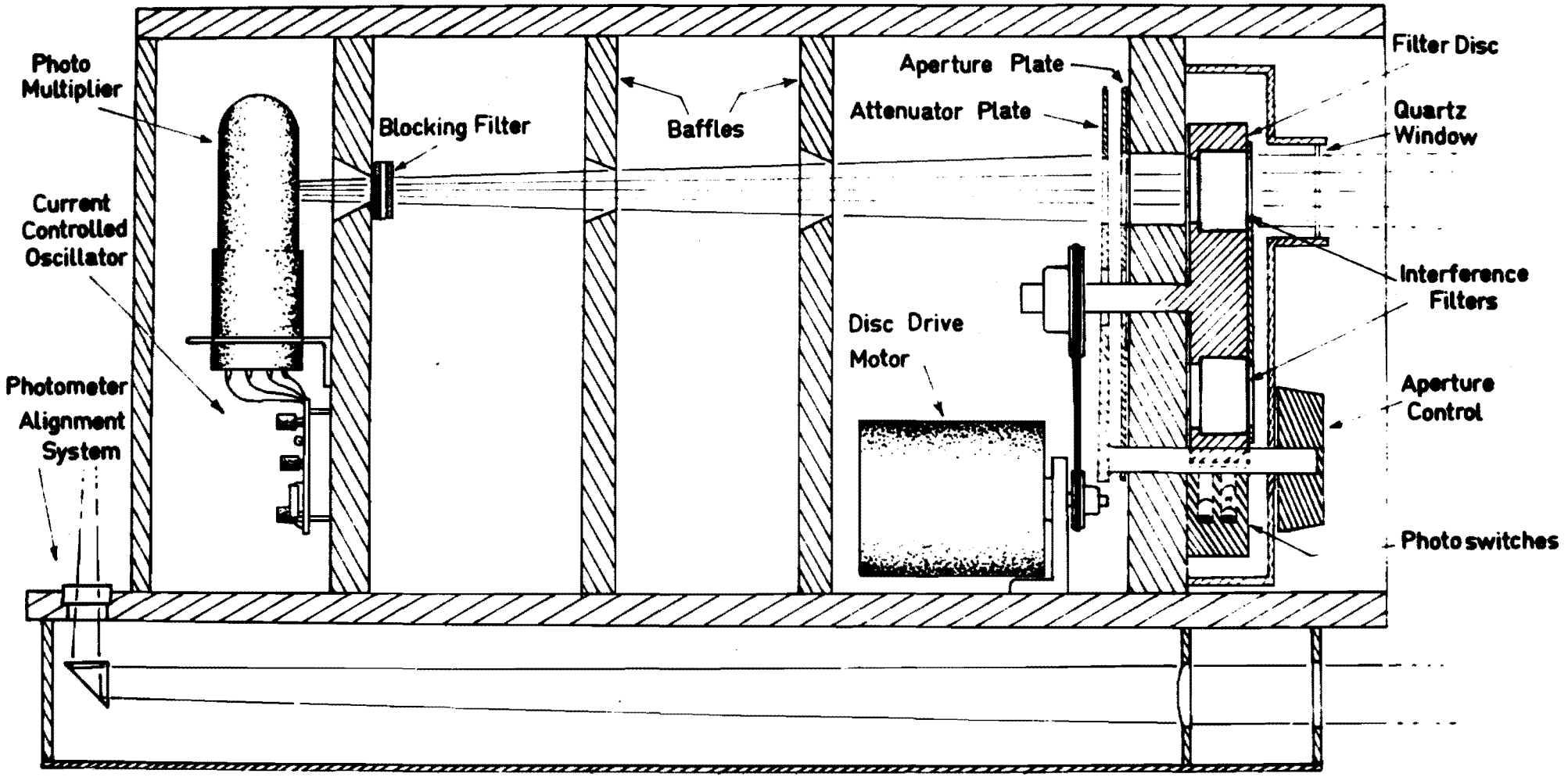

SIMPLIFIED DIAGRAM OF FILTER OZONE SPECTROPHOTOMETER (SIDE VIEW)

Fig 3-1

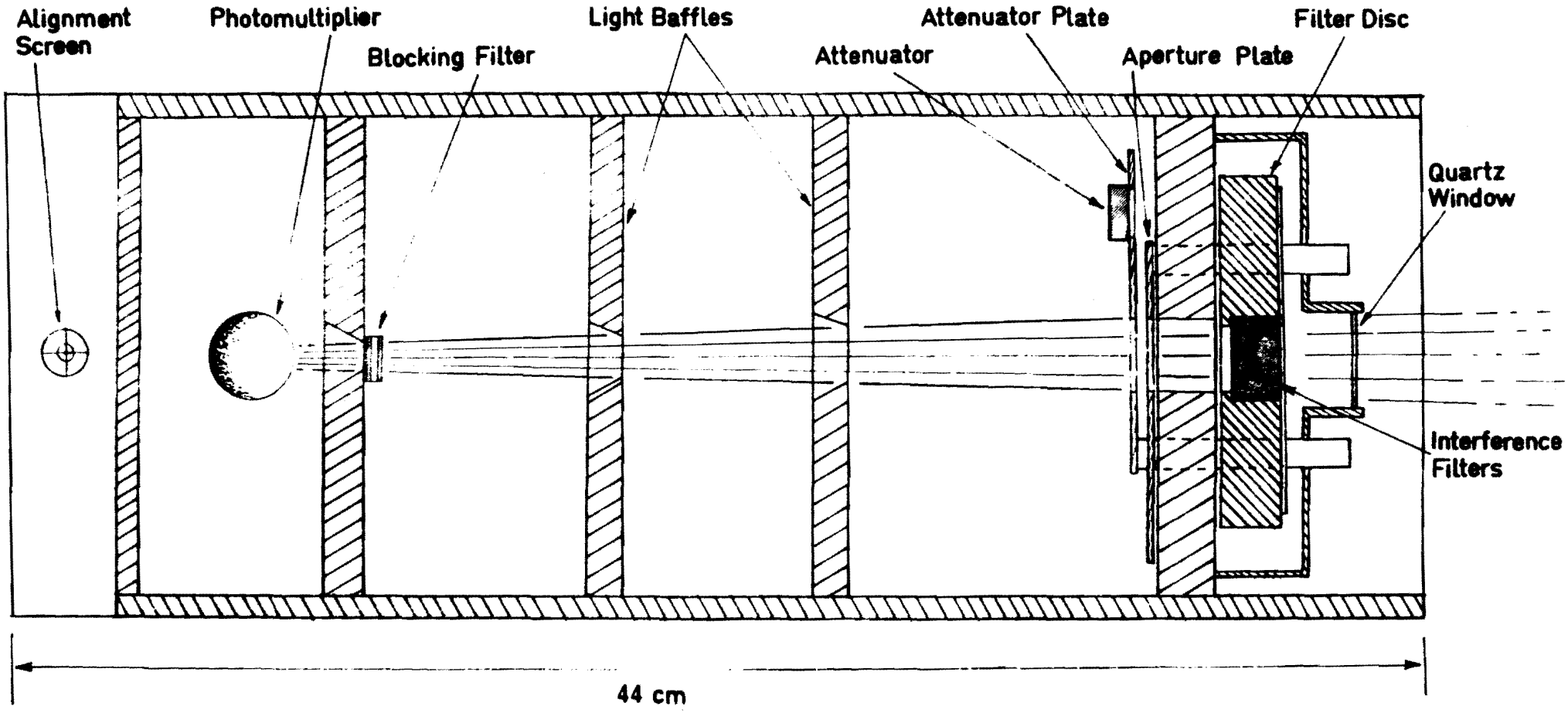

SIMPLIFIED DIAGRAM OF FILTER OZONE SPECTROPHOTOMETER (TOP VIEW)

Fig 3-2

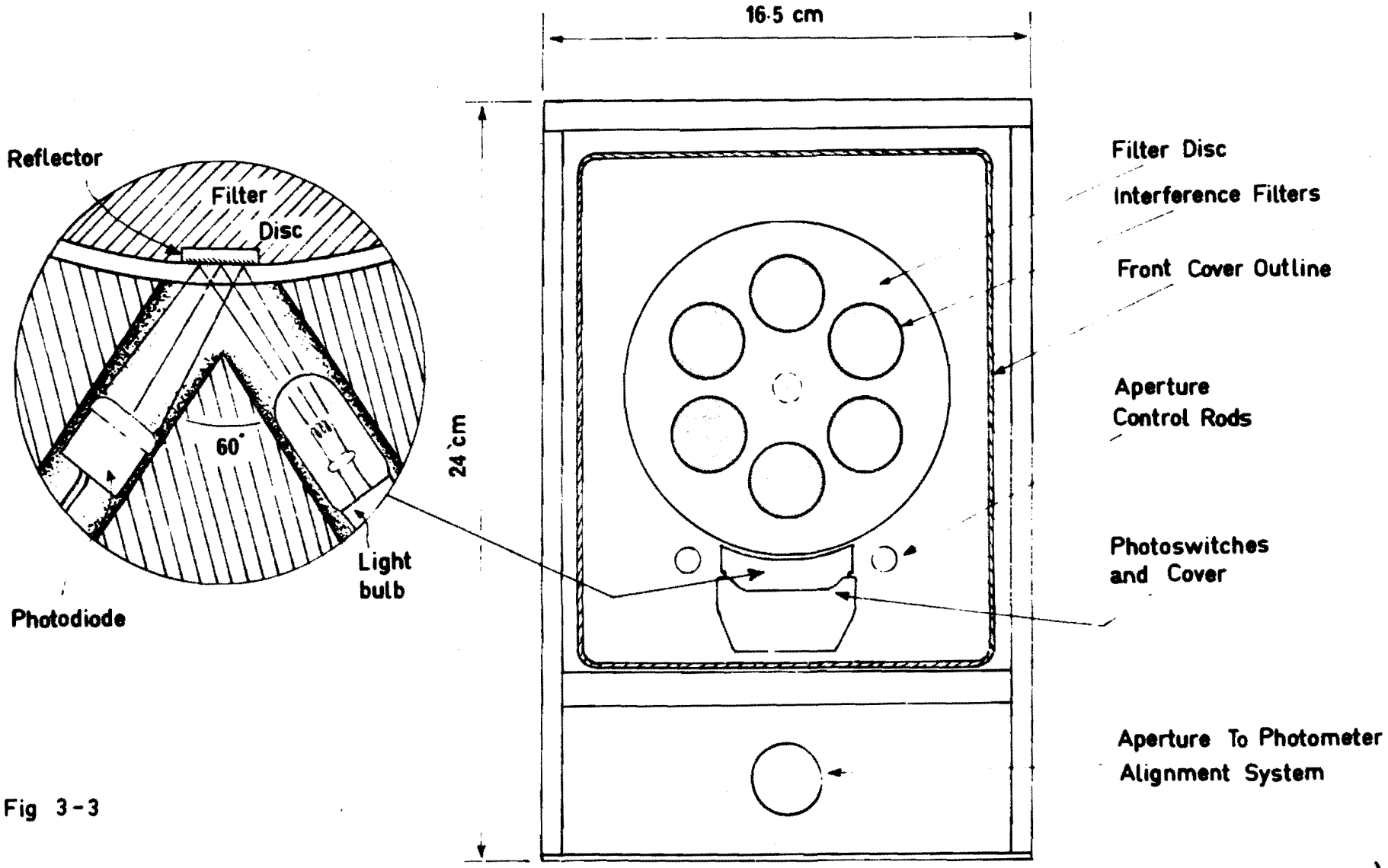

Fig 3-3

SIMPLIFIED DIAGRAM OF FILTER OZONE SPECTROPHOTOMETER (FRONT VIEW)

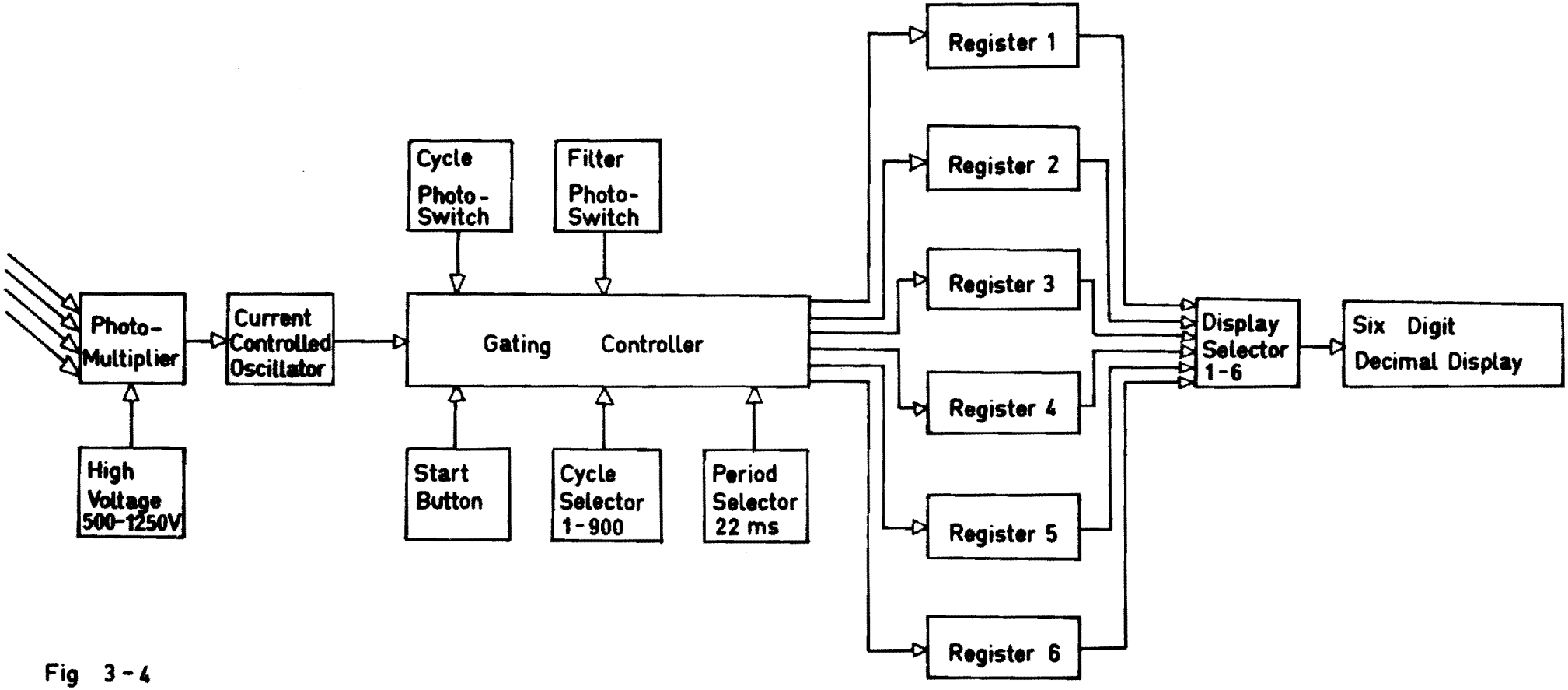

Fig 3-4

DIAGRAMMATIC REPRESENTATION OF ELECTRONICS
MOBILE FILTER OZONE SPECTROPHOTOMETER

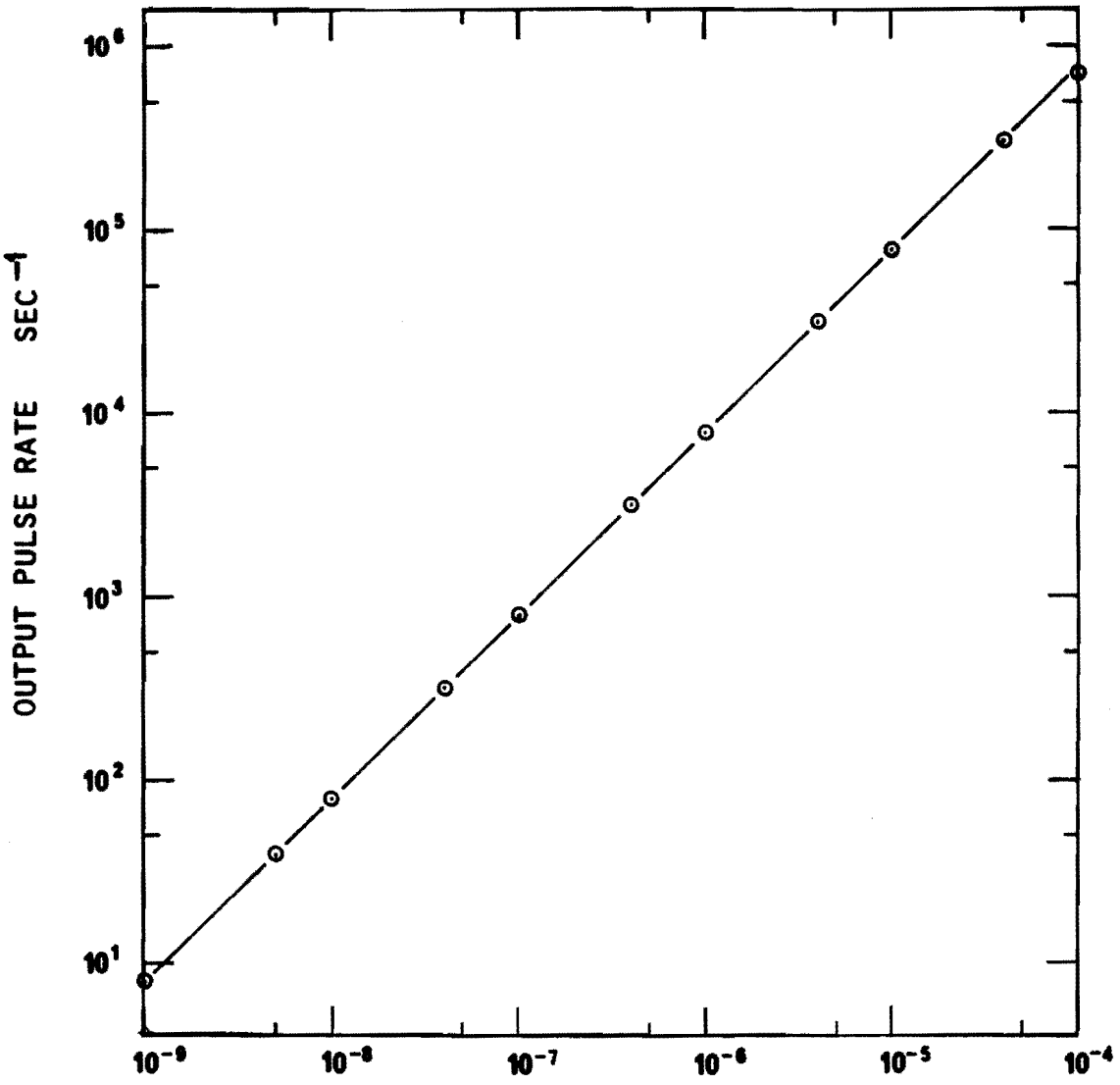

FIG. 3.5 CURRENT CONTROLLED OSCILLATOR RESPONSE

To identify each filter band, phasing pulses are generated by two photoswitches, each consisting of a small lamp and photodiode, as shown in figure 3.3, when light is reflected off small mirrors set into the edge of the rotating disc. One photoswitch marks the beginning of a cycle of the disc, while the other marks the filter positions. Together they initiate the scan periods for each filter and also select the appropriate data register in which the pulses are counted. For precision, the scan period of 22 ms is electronically timed.

The counts from up to 900 cycles of the disc may be integrated before being read. The content of each register is selected to appear on the decimal display, and the resulting six, six-digit numbers are recorded manually.

A second, fully automatic instrument was built using a mini-computer as the counting device. The current-controlled oscillator pulse train and the photoswitch pulses are fed to the computer which is programmed to control the whole counting process, to store the intensity data along with time-of-day data, and to output the data, on command, onto page and paper tape ready for further processing. This system needs setting up only once each day, and can very easily accumulate a great deal of data. Further comment on the use of the mini-computer is given in Appendix C.

The mobile instrument is also very productive. For example, a data set consisting of an integration over twenty cycles, and therefore representing twenty independent measurements of each wavelength, is made in less than ten seconds and can be recorded within a further forty seconds. Thus, measurements may be made every minute.

The relatively rapid rotation rate of the filter disc is designed to ensure that the filter measurements are as nearly simultaneous as possible. Significant changes due to cloud variation can still occur, but their effect is reduced by the averaging effect of integrating the measurements over many cycles.

Both instruments are linear in their response over a dynamic range of about four decades in intensity. By varying the photomultiplier supply voltage, the number of cycle integrations, and the density of the optical attenuation filters, the total operational range may be extended. The lower limit is determined by photomultiplier dark current, while the upper limit is determined by nonlinearity in the current controlled oscillator response, which may be seen in figure 3.5. (Although the nonlinearity is barely noticeable in figure 3.5, it in fact sets in at about 10 μA and by 100 μA amounts to a 12% reduction in the output pulse rate.)

The linearity of the current controlled oscillator at low currents enables the accurate measurement of dark currents as low as 0.5 nA. The logarithmic amplifier of the prototype instrument was limited to measuring currents above 5.0 nA.

The dark current is at present measured by capping the photometer's window and taking an average of all six channel counts. This is unsatisfactory if the dark current is large and in need of regular measurement, particularly for the automatic instrument. It is proposed that future instruments have a seventh channel, whose filter aperture is closed off to enable continual monitoring of the dark current.

3.3 Equatorial Mount, Purpose and Construction

The small size of the filters allows the construction of a light, compact instrument (14 kg, 44 x 25 x 17 cm), which is easily mounted on an automatic sun follower. The equatorial mount, seen in figure 1.1, is designed to maintain alignment on the sun throughout a day.

This is done by rotating the photometer about an axis parallel to the Earth's axis, and at the same rotational speed as the Earth's (relative to the sun), but in the opposite direction. It is called an equatorial mount because the plane of the rotation is parallel to the plane of the equator. The changing angle of declination between the sun and the equatorial plane is eadily accommodated since its maximum rate of change of 0.04° per hour, occurring at the equinoxes, is small enough to be considered as constant during a day.

The mount can be adjusted to suit any latitude, requiring only an initial adjustment of the rotation axis at each location. The photometer is rotated at constant speed by a positive drum and wire drive system and a small A.C. synchronous motor. The stability of the A.C. mains frequency yields an excellent rotation accuracy of better than 0.01° per 360°.

Compared to a servo system, this constant speed system has the advantages of simplicity, and ability to maintain alignment irrespective of the density of the cloud cover.

CHAPTER 4: INTERFERENCE FILTERS

4.1 Introduction, Elementary Description of Theory and Construction

The central role of the interference filters in the photometer is such that a very careful evaluation of their characteristics is essential to ensure, firstly, that the most suitable filters are acquired, and secondly, that once in use, their limitations are clearly understood.

To this end, this chapter considers the problems of specifying the relevant filter characteristics, in Section 4.2, of transmittance leakages and optical non-uniformity in Sections 4.3 and 4.4, and of effects due to filter orientation, aging and temperature in Sections 4.5, 4.6 and 4.7. The problem of the bandwidth effect, which results from the inevitable use of finite filter bandwidths, is discussed separately in Chapters 7 and 8 of Part III. The remainder of this section, 4.1, is a brief consideration of interference filter theory and construction, provided as a basis for the later sections.

Interference filters are based on the interference of light in thin dielectric films, hence their name. The elementary theory of film interference is given in comprehensive textbooks such as Born and Wolf (1965), and can be explained as follows.

The optical path difference between the rays reflected off the top and bottom surfaces of a thin film is $2nd \cos \theta$ where n is the film's refractive index, d is its thickness and θ is the internal angle of incidence. If this difference is

equal to an integer number m, of free space wavelengths λ, then the two rays will be in phase and will constructively interfere.

In this case:

$$m\lambda = 2nd \cos \theta, \tag{4.1}$$

while for destructive interference,

$$(m+\tfrac{1}{2})\lambda = 2nd \cos \theta. \tag{4.2}$$

The transmittance and reflectance spectra are then each a set of alternate bright and less bright bands. The destructive interference is not complete, however, since the delayed ray is of lesser intensity than the other ray, having undergone an additional reflection. (It is assumed that the refractive index of the film is greater than that of its surroundings. Where this is not so, the phase reversal at the bottom surface must be accounted for.)

The construction of a narrowband filter involves two steps. Firstly, in order to intensify the destructive interference, and narrow down the transmitted bands, as many as forty or more films, of two alternately high and low refractive index dielectrics, and of precisely controlled thicknesses, are stacked on a substrate to form a filter element. This element is sometimes called a cavity, referring to the thicker cavity-like central layer, and also called a period. Secondly, in order to attenuate the transmitted band on either side of the particular desired band, called the passband, other filter elements may be added whose designs allow transmission at the passband but not at the adjacent

bands, while outside these immediate bands, standard absorption blocking filters are used. The attenuated adjacent bands are called sidebands.

It is useful to now reconsider figure 2.2, the transmittance spectrum of the prototype instrument's 305 nm filter which was investigated in Chapter 2. It can be seen that this filter's leakage band is just a sideband which is not sufficiently well attenuated. Further examples of filter spectra will be seen later in figures 4.1 to 4.6.

Since the thickness of each dielectric layer is only of the order of a few wavelengths, essentially all the filter thickness is formed by the substrate and blocking glass, which together are generally less than 1.0 cm thick. The filter is therefore small and light.

Further insight into interference filter design may be gained from Baumeister's (1965) review which, beginning from first principles, considers several basic filter designs and contains many references to the original papers. Delano and Pegis (1969) describe the mathematical methods of filter design, and also include a long chapter on basic theory.

4.2 Specification of Filter Characteristics, Measured Characteristics

All the interference filters used by the author were commercially made, being designed by the manufacturer to meet, as closely as possible, a given set of spectral specifications: of centre wavelength, peak transmittance, bandwidth and blocking. Specific design information, such as the materials used or the number of filter elements, is usually not needed by the user, and is generally not supplied by the maker. A typical set of specifications sent to manufacturers for quotation is given in table 4.1 below.

Table 4.1: Typical Filter Set Specification

Wavelength ±1.0nm	Bandwidth ±1.0nm	Power Ratio less than
305.5	2.5	5×10^{-6}
311.5	2.0	1×10^{-4}
317.5	2.0	3×10^{-4}
325.5	2.0	3×10^{-4}
332.5	2.0	3×10^{-4}
340.5	2.0	3×10^{-4}

All filters to have transmittances >5% and be sealed in metal holders with usable diameters of 2.2 cm. (The Power Ratio is defined in Appendix B.)

It can be seen that the six filters are chosen to match the standard Dobson A, C and D wavelength pairs to within the manufacturing tolerances. This choice allows the well known Dobson formalism to be applied to the filter instrument and therefore enables better comparison of the measurements of the two instruments.

As an aside, it should be pointed out that, although only the A, C and D wavelength pairs are considered throughout the thesis, it is possible to compare any two of the six individual filter intensity measurements which are made. It is also possible to make a double wavelength pair determination of total ozone using just three filter intensity measurements. The fixed wavelength-band relationships within the A, C and D wavelength pairs are a consequence of the design of the Dobson spectrophotometer.

In Table 4.1, the specified ±1.0 nm tolerance in centre wavelength is satisfactory since the filter bandwidths are much greater than the characteristic detail in both solar irradiance (figure 8.1), and ozone absorbance (figure 8.3). However, there is an advantage in placing the passbands over regions of maxima in the ozone absorption spectrum, since the maxima are least affected by stratospheric temperature. Further consideration is given to this point in Appendix D.

The bandwidth specified is the half-bandwidth, the wavelength interval between the half peak transmittance points. (Where the shape of the passband is important, it may be desirable to specify the 0.9, 0.1, and 0.01 etc., band-widths.) Because the purpose of a filter is to select essentially monochromatic radiation, its bandwidth should be the minimum which is consistent with transmitting a measurable amount of light. For the filter instrument, the minimum is about 1.0 nm, but it seems that the narrowest ultraviolet filters produced have bandwidths of at least 2.0 nm. This fact is reflected in the specifications.

The specified power ratios are based on calculations made in Appendix B, but from the manufacturer's point of view, are

unrealistically small. As a general rule, a given power ratio requires a ten-times greater rejection ratio, but the typical rejection ratio is only about 10^{-4}. This problem can be resolved, fortunately, by the use of the stacked double filter as will be explained later in Section 4.3.

The transmittance specification is relatively unimportant, so only a minimum value is set. The sealing increases the filters' long term stability, as is discussed in Section 4.6 of this chapter, while the holder ensures that the stresses due to mechanical clamping are not borne by the filter itself. Additional filter characteristics, such as uniformity, and stability with age and temperature, may be specified to possible advantage (but at certain increased cost).

It is clear from the responses of the ten or so manufacturers to whom the above specifications were sent, that it is rather difficult to make ultraviolet filters with the narrow bandwidths and good rejection required, and that the difficulty increases as the filter centre wavelength decreases. As an extreme, and unfortunate example, one order resulted in a manufacturer's complete failure to make the shortest wavelength item, and failure to meet the specifications of three of the remaining five items.

Despite these problems, another manufacturer was able to make six satisfactory filter sets whose characteristics are listed in table 4.2 below. (Their measurement is described in Appendix A.)

Table 4.2: Measured Filter Characteristics

Wavelength ±0.5nm	Bandwidth ±0.5nm	Power Ratio (Ultraviolet only)	Transmittance %
305.4	2.0	1×10^{-3}	22 → 24
311.5	2.2	5×10^{-3}	14 → 19
317.0	2.4	1×10^{-3}	7 → 18
324.5	2.3	5×10^{-4}	10 → 23
331.0	2.5	2×10^{-4}	6 → 16
340.5	2.7	2×10^{-4}	24 → 26

The illustrative transmittance spectra, figures 4.1 to 4.6 show the passband shape, and sideband positions and sizes typically found in two-cavity filters. Note should be taken of the particular improvement in the 305 nm filter (figure 4.1) over that of the prototype instrument (figure 2.2).

The problems that arise in the use of the filters for total-ozone measurement are considered in detail in the following sections.

4.3 Ultraviolet and Infrared Leakage Bands, Composite Blocking Filter, Stacked Filters

As shown in Chapter 2, it is important to effectively block out the filter leakage bands which lie within the spectral region bounded by the short wavelength radiation cut-off and by the long wavelength photomultiplier sensitivity cut-off. This region includes the sidebands shown in figures 4.1 to 4.6, as well as infrared leakage bands not shown.

The prominent short wavelength leakage band in the 340 nm filter (figure 4.6) was at first thought to be of little importance, but the calculations detailed in Section 8.3 show

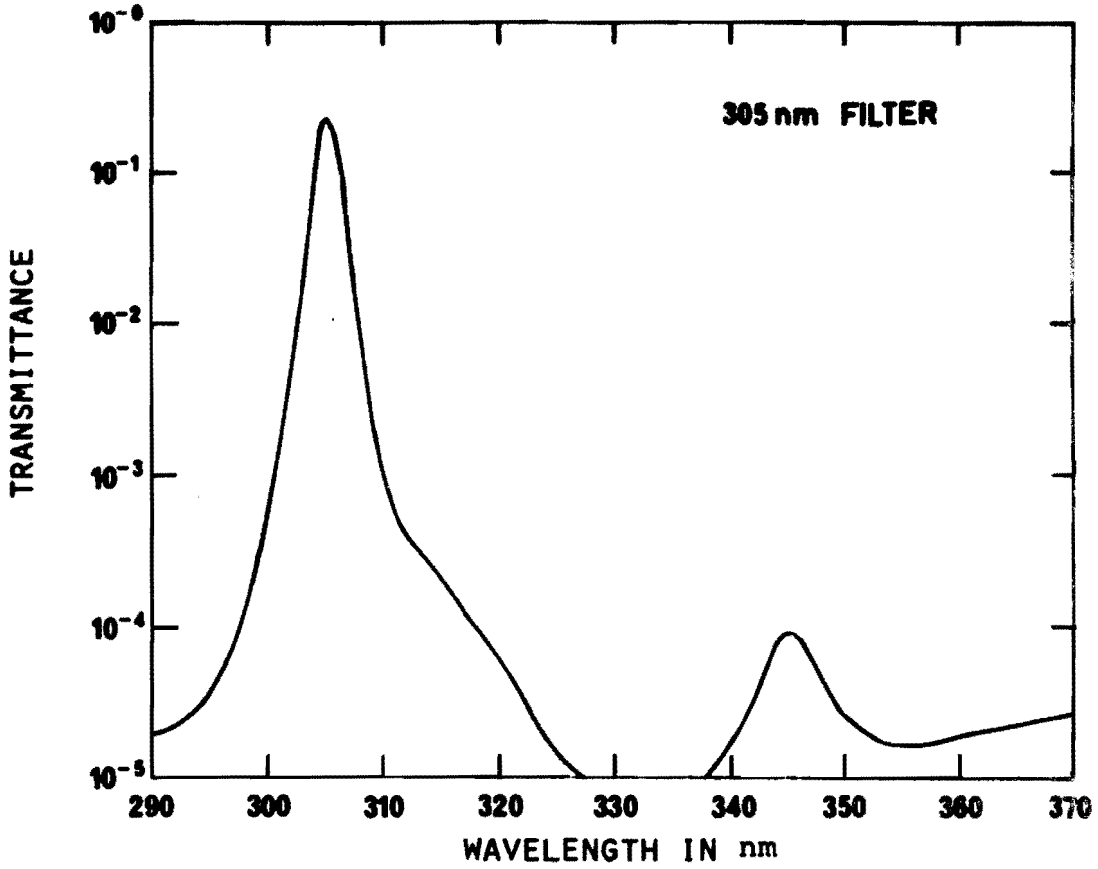

FIG. 4.1 FILTER SPECTRAL TRANSMITTANCE

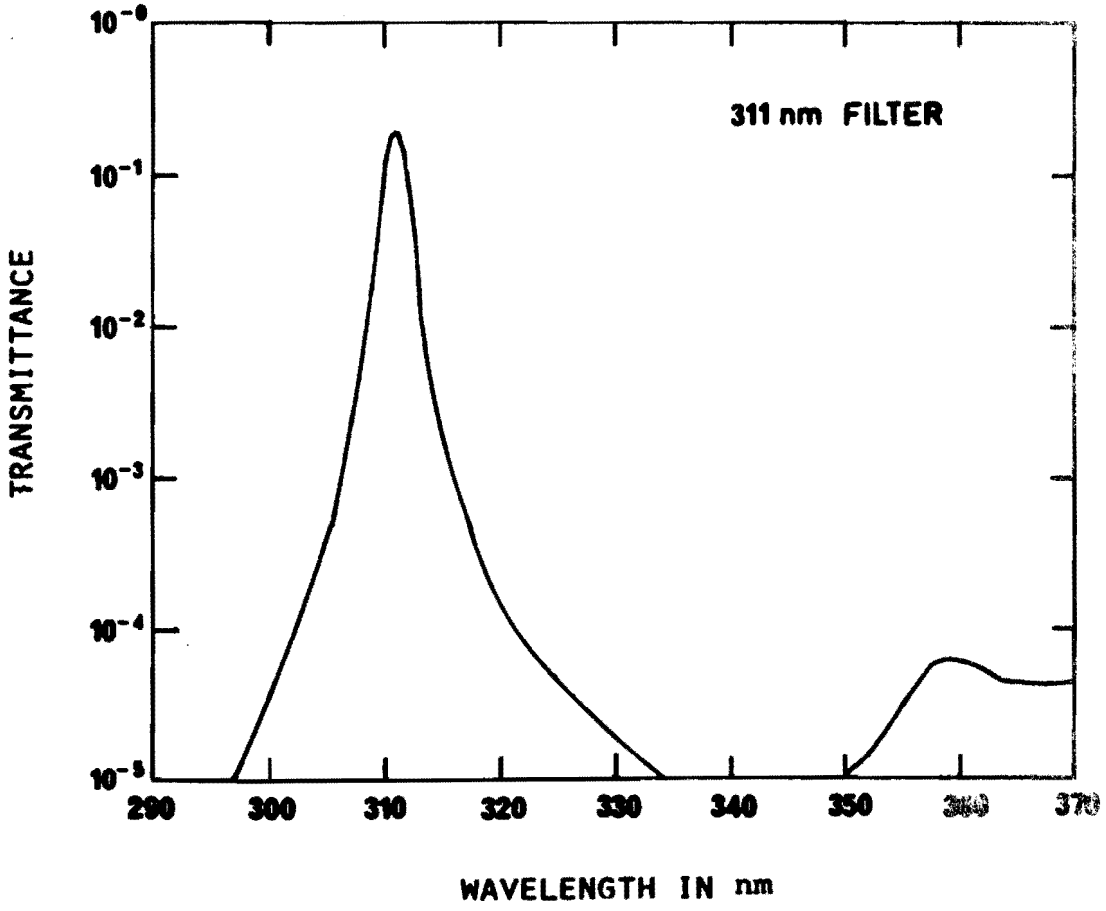

FIG. 4.2 FILTER SPECTRAL TRANSMITTANCE

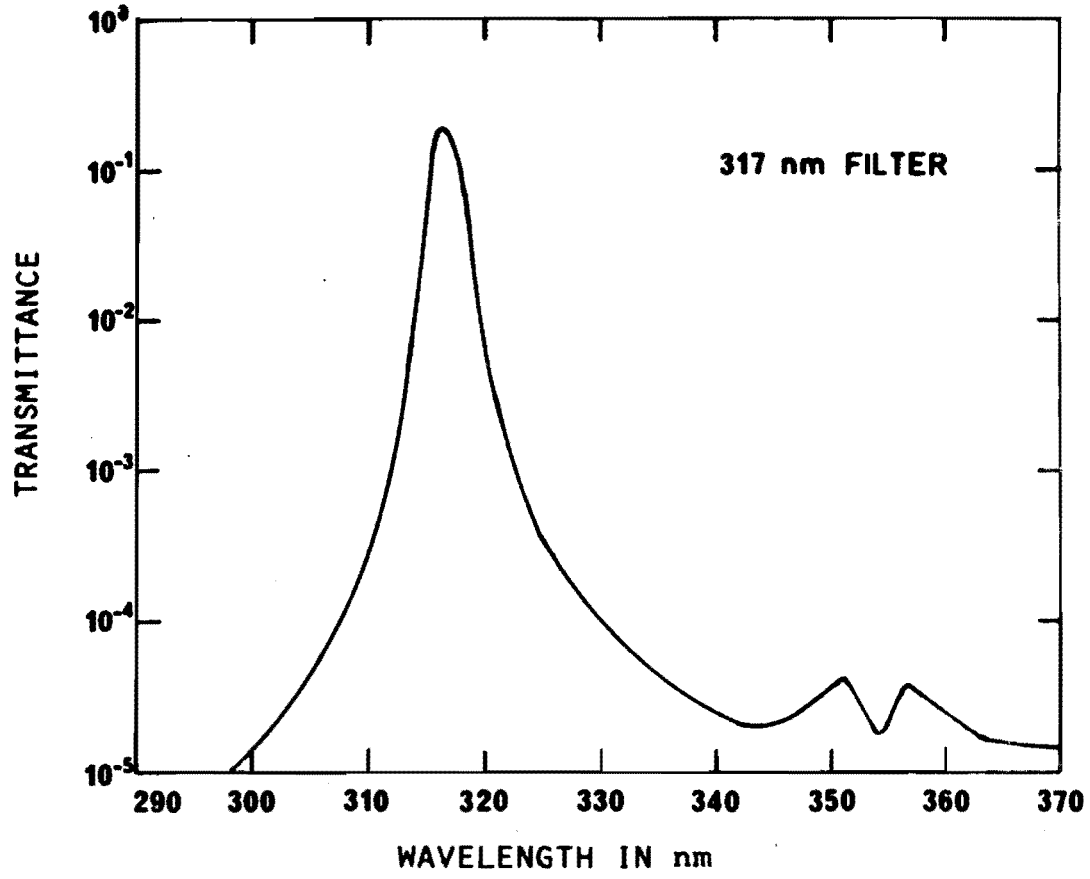

FIG. 4.3 FILTER SPECTRAL TRANSMITTANCE

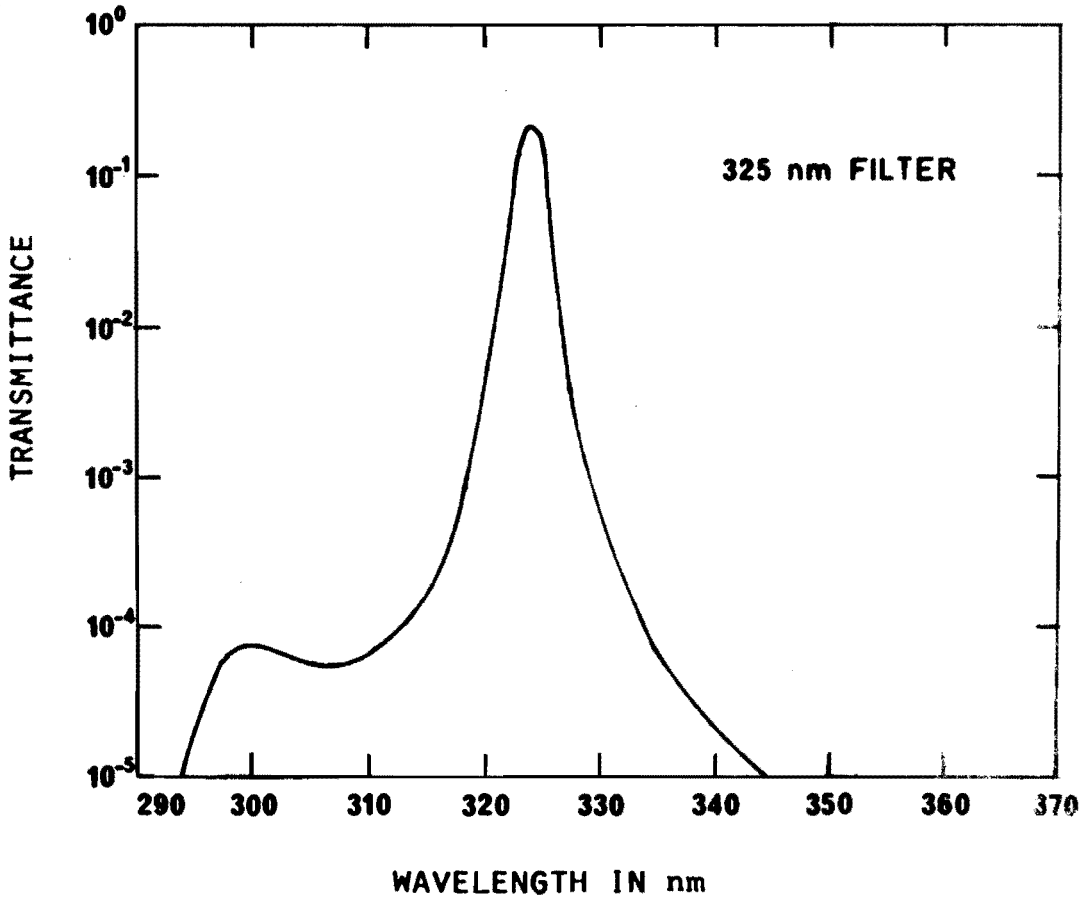

FIG.4.4 FILTER SPECTRAL TRANSMITTANCE

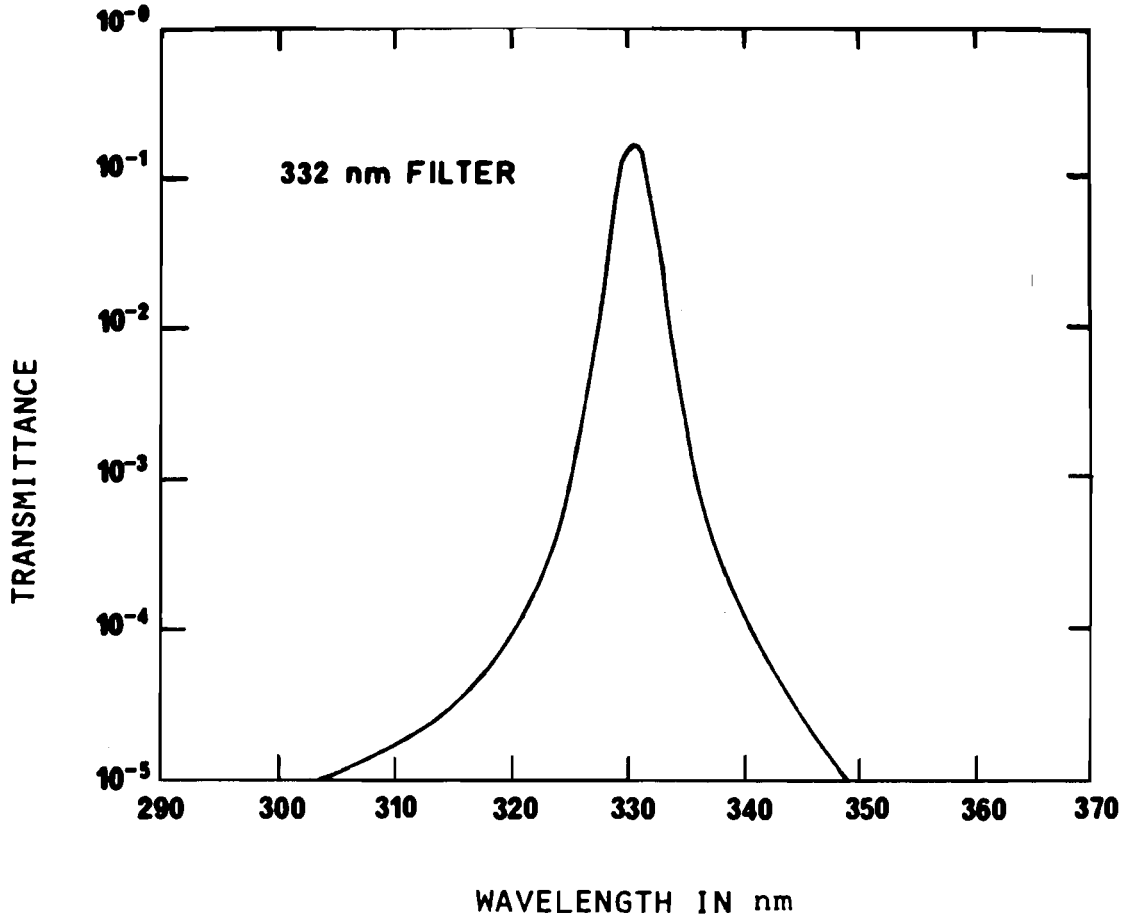

FIG.4.5 FILTER SPECTRAL TRANSMITTANCE

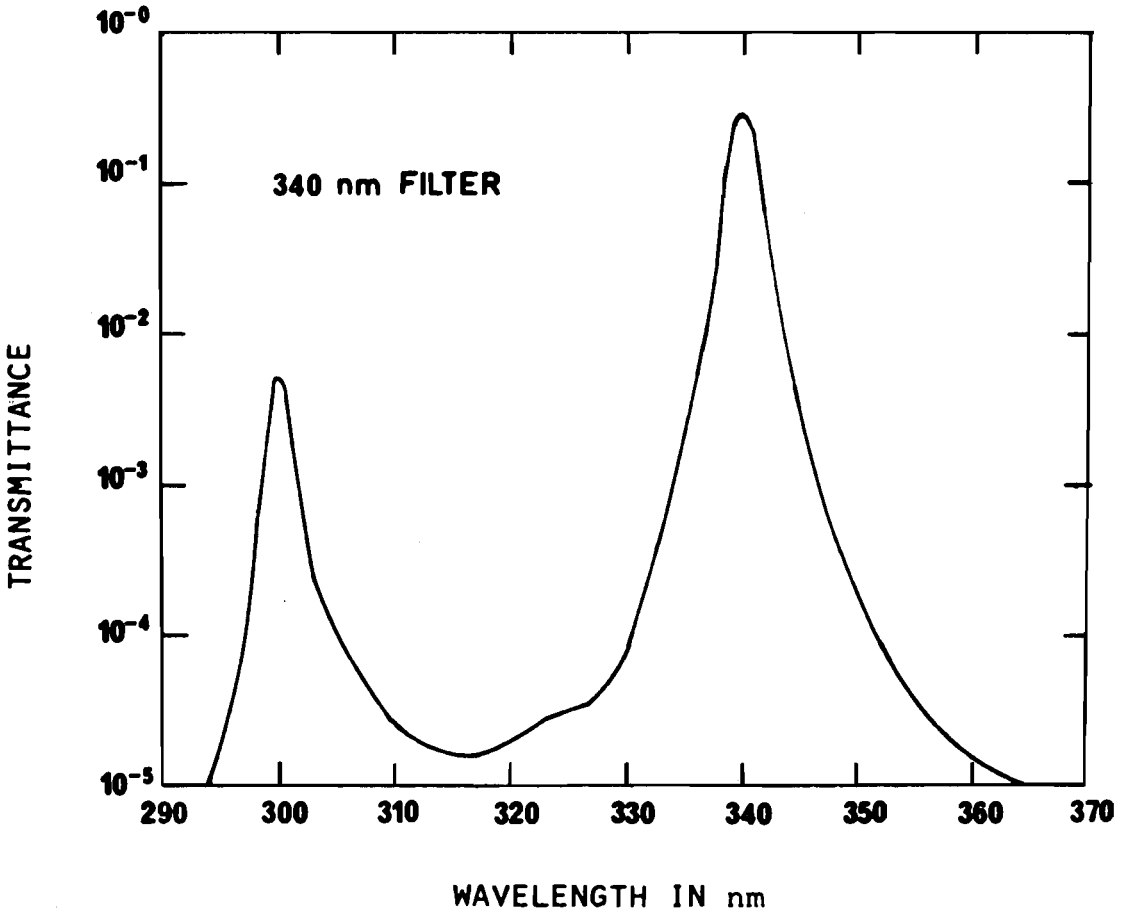

FIG.4.6 FILTER SPECTRAL TRANSMITTANCE

that this is not so. Its large transmittance results in a considerable bandwidth effect (See Part III) for the filter. Fortunately, it can be reduced to negligible proportions by the application of silica window glass (see figure 2.1).

Other leakage bands tend to lie at about 370 nm in the near ultraviolet and 720 nm in the near infrared. The worst case is that of the 311 nm filter, whose transmittance spectrum from 260 nm to 1260 nm is shown in figure 4.7. Details of its particularly large infrared leakage bands are summarised in table 4.3 below.

Table 4.3: 311 nm Filter Infrared Leakage Bands

Wavelength	720	1080	nm
Half Bandwidth	35	100	nm
Transmittance	3.5	0.08	%
Power Ratio	3.7	0.24	

The enormity of these infrared leakage bands will be seen by comparing the power ratios of table 4.3 with those specified in table 4.1.

Their contribution to the instrument's response is heavily reduced by the relative insensitivity of the photomultiplier to infrared radiation (see figure 5.1), but the preferential attenuation of the passband by the atmosphere has the opposite effect. With the two effects combined, the bands can still contribute up to 40% of the response at an airmass of 4. Extra blocking is clearly needed.

A well known ultraviolet-transmitting, visible-region blocking filter is the Corning CS 7-54 type, or Schott UG-11 type absorption glass, whose transmittance spectra is shown in figure 4.8. It is effective for blocking the visible region from 400 nm to 680 nm, and, as can be seen from figure 4.7, is used for this purpose by our filter manufacturer. However, the use of more of it would obviously have little effect on the remaining ultraviolet and infrared leakage bands.

A better filter for our purposes is nickel sulphate hexahydrate, whose transmittance spectrum is given in figure 4.9. It has the double advantage of being able to block both the ultraviolet and infrared leakage bands, and its spectrum is complementary to that of the CS 7-54 type glass. In addition, its crystalline form is relatively easy to grow, is easily cleaved to make optically flat plates, and is chemically and optically stable.

As described in Appendix E, a composite blocking filter was made, comprising a 4 mm layer of nickel sulphate hexahydrate crystal sealed between two 3 mm thick pieces of Corning CS 7-54 glass. Its transmittance spectrum is shown in figure 4.10. A comparison of this spectrum with figure 4.7 shows the composite blocking filter to be very effective at removing the 311 nm filter's three leakage bands at 370 nm, 720 nm and 1080 nm.

The final and most important topic in this section is that of the stacked filter. Originally only single interference filters were sought as per the specifications in table 4.1, each one representing as close to the ideal filter as then known. Then one manufacturer wrote that, at each wavelength, he makes a large filter plate which is cut to size

later, and that for the size required, six filters could be produced for the price of one. It was a simple step then to realise that by merely superimposing two or more such filters, a vastly improved "stacked filter" would be produced.

The ideal transmittance characteristics of a stacked filter are to be seen in figure 4.11, in which the transmittance of a 305 nm filter is squared to give a double stacked filter spectrum. The results are: narrower bandwidth, steeper transmittance skirts, and greatly increased sideband rejection, although at the expense of peak transmittance.

Since rejection ratios (but not power ratios) are squared when filters are double stacked, the 305 nm filter's undesirably large ratio of 5×10^{-4} becomes satisfactorily small at 2.5×10^{-7}. Therefore, with the exception of the short wavelength leakage band in the 340 nm filter, the near ultraviolet leakages in the doubled filters are negligibly small. The same is not true of the 311 nm filters' infrared leakage bands, since their peak transmittances are not significantly smaller than that of the passband, and therefore the squared rejection ratio is not very small. For this reason, the composite blocking filter (figure 4.10) is retained.

The superior monochromaticity of the double stacked 305 nm filter is emphasised by the comparison of its transmittance spectrum, figure 4.11, with that of the prototype instrument's 305 nm filter, figure 2.2. The benefit of the sharper passbands becomes evident in the reduced bandwidth effect (see Part III) calculated in Sections 8.2 and 8.3.

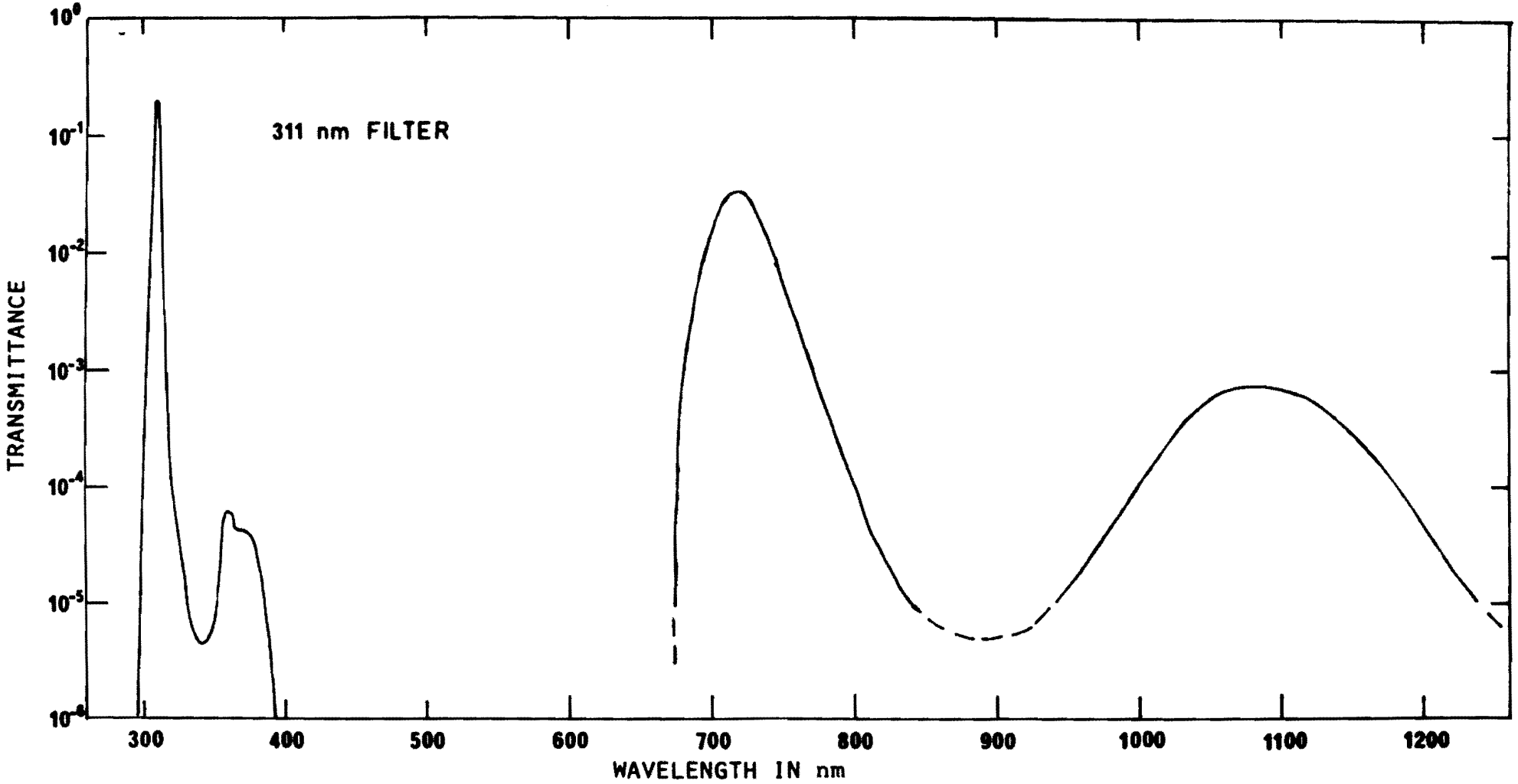

FIG.4.7 311 nm FILTER EXTENDED TRANSMITTANCE SPECTRUM

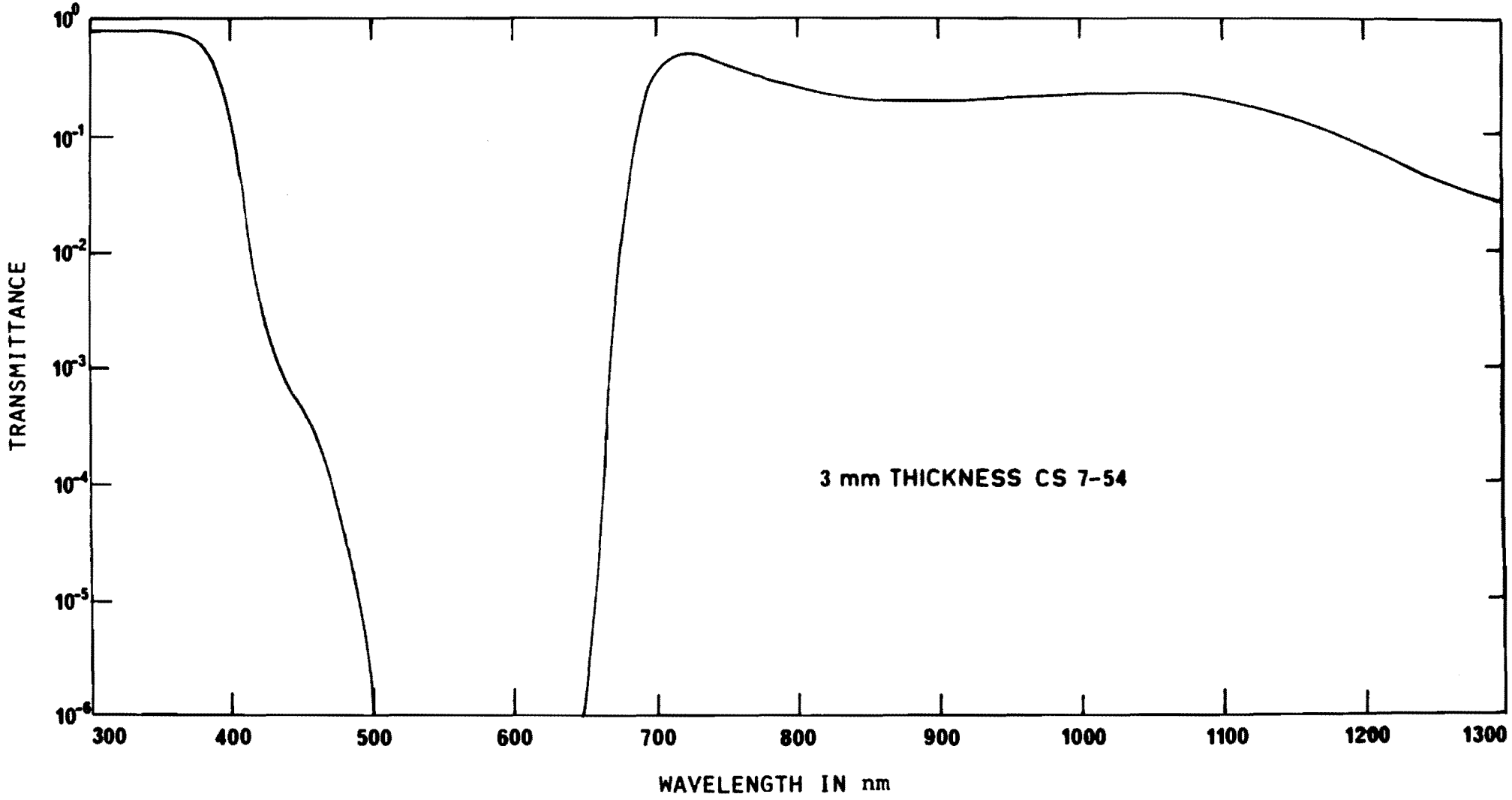

FIG.4.8 CORNING CS 7-54 GLASS SPECTRAL TRANSMITTANCE

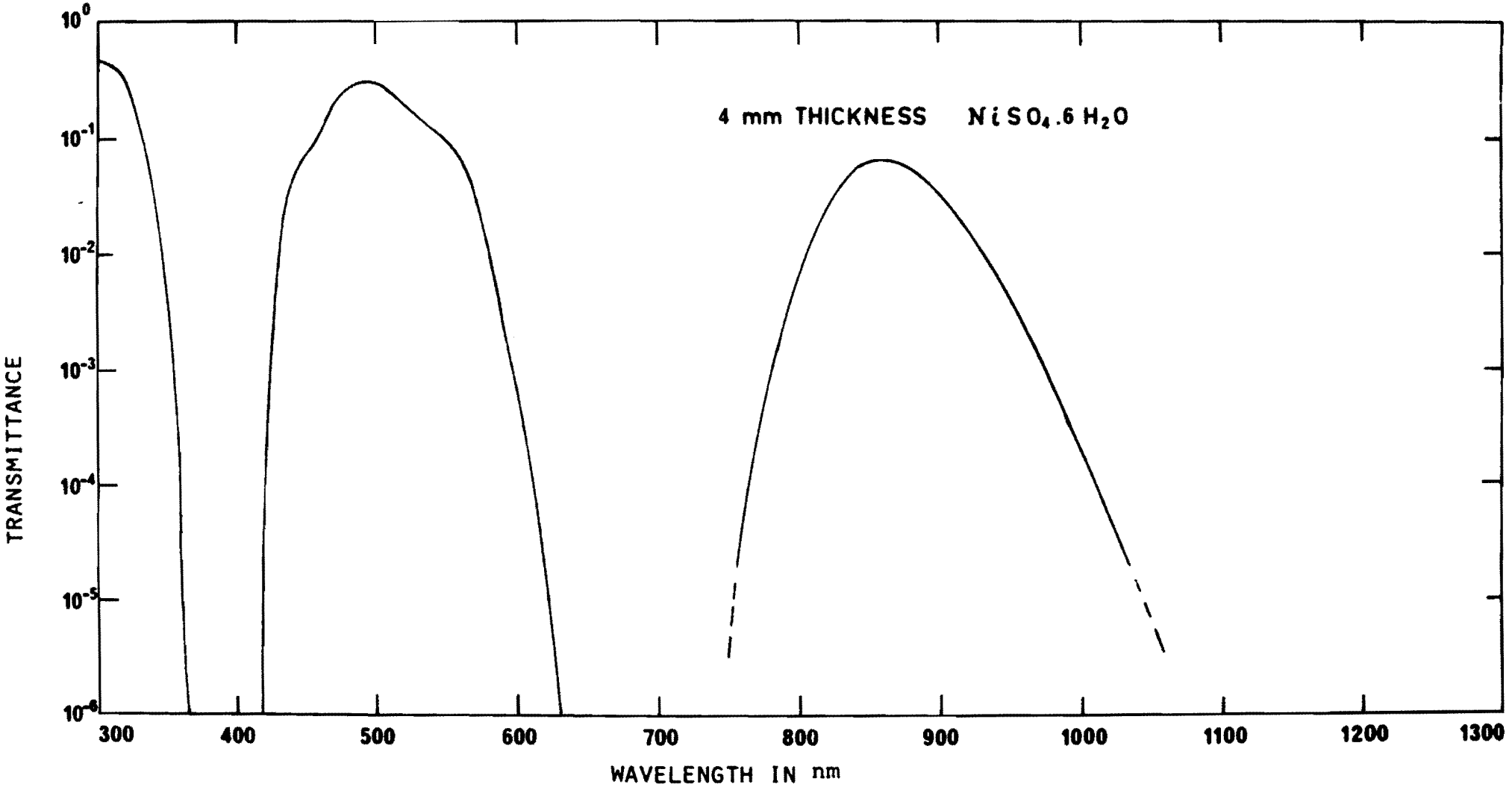

FIG. 4.9 NICKEL SULPHATE HEXAHYDRATE SPECTRAL TRANSMITTANCE

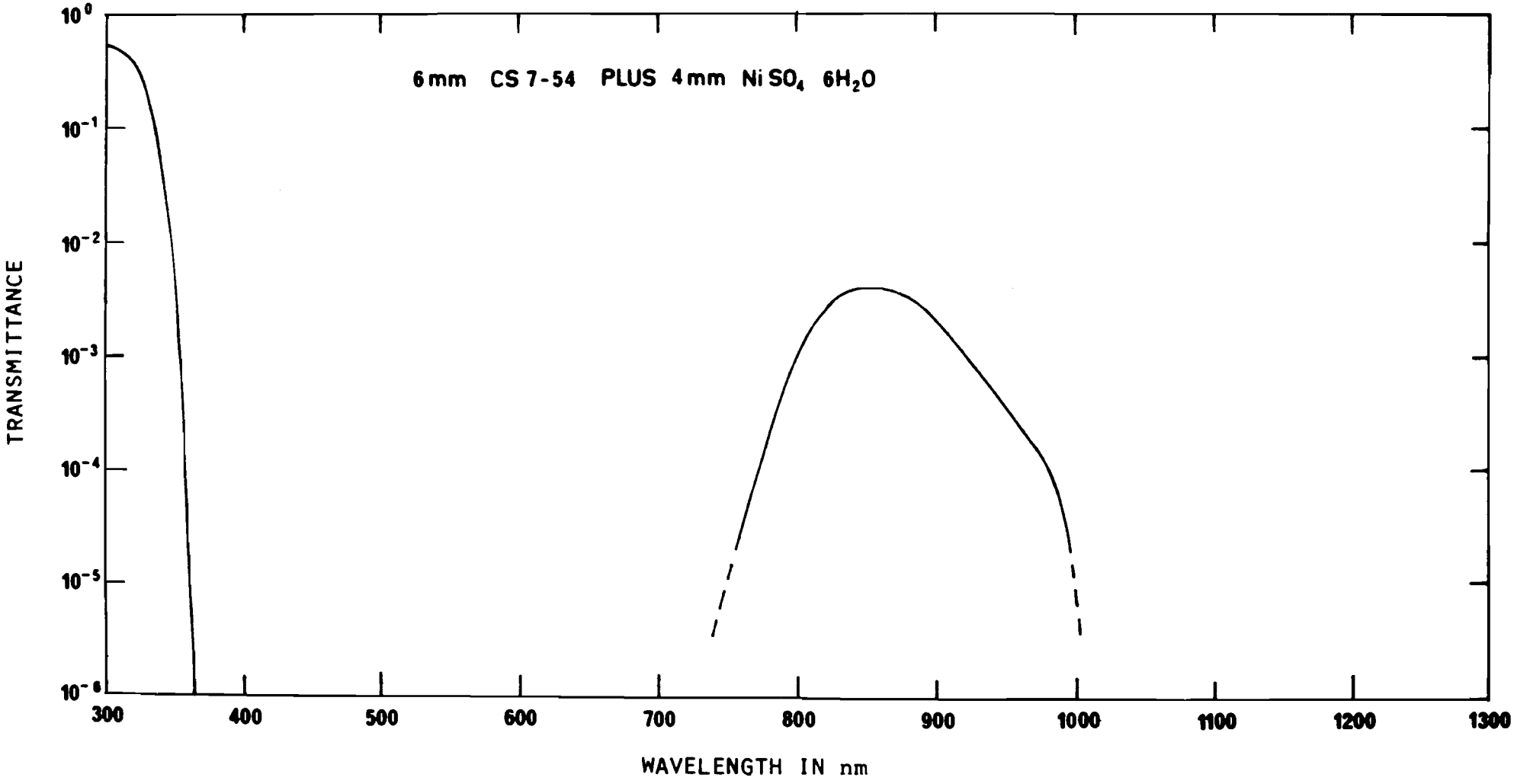

FIG.4.10 COMPOSITE BLOCKING FILTER SPECTRAL TRANSMITTANCE

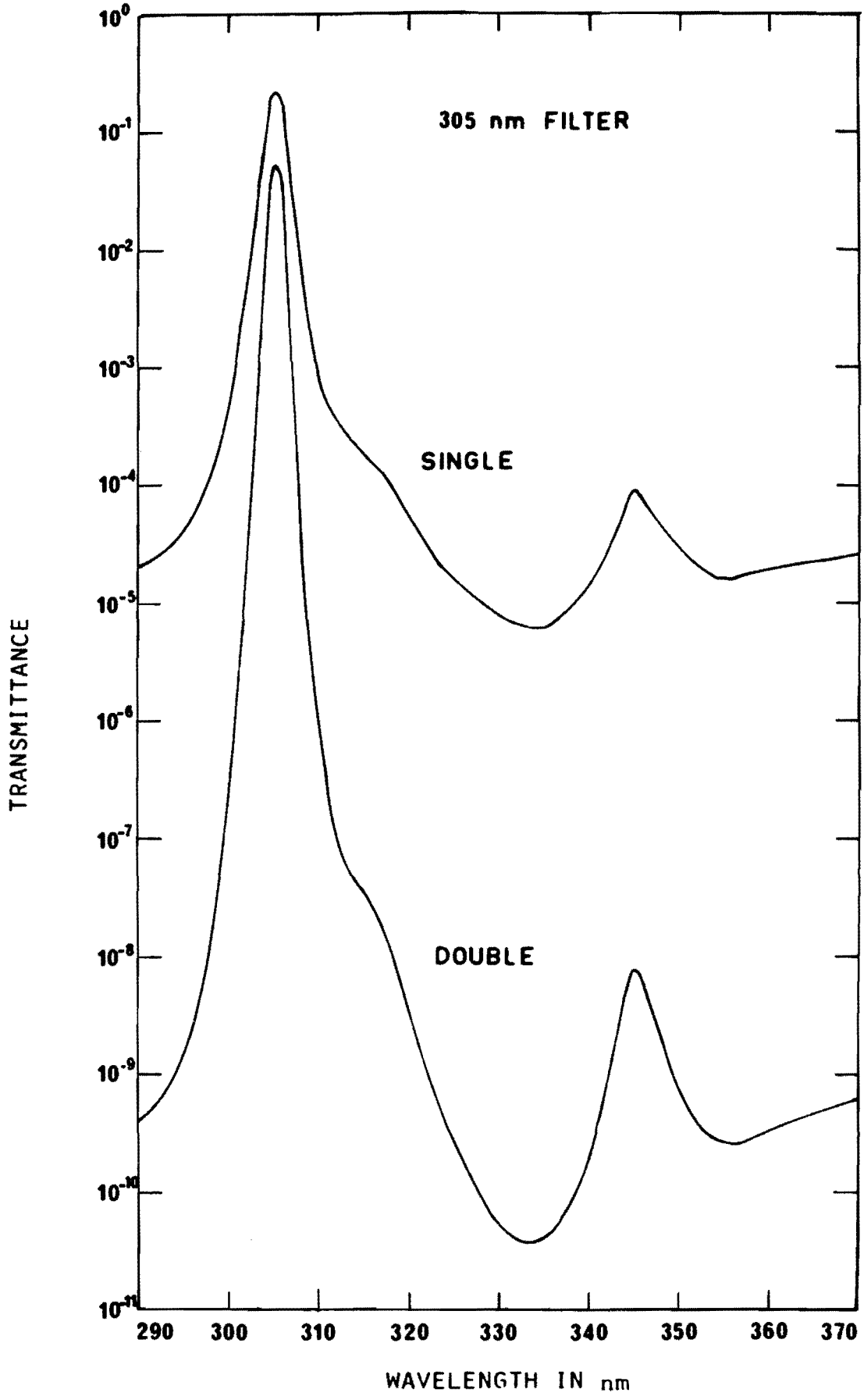

FIG.4.11 SPECTRAL TRANSMITTANCE OF 305 nm FILTER, SINGLE AND DOUBLED.

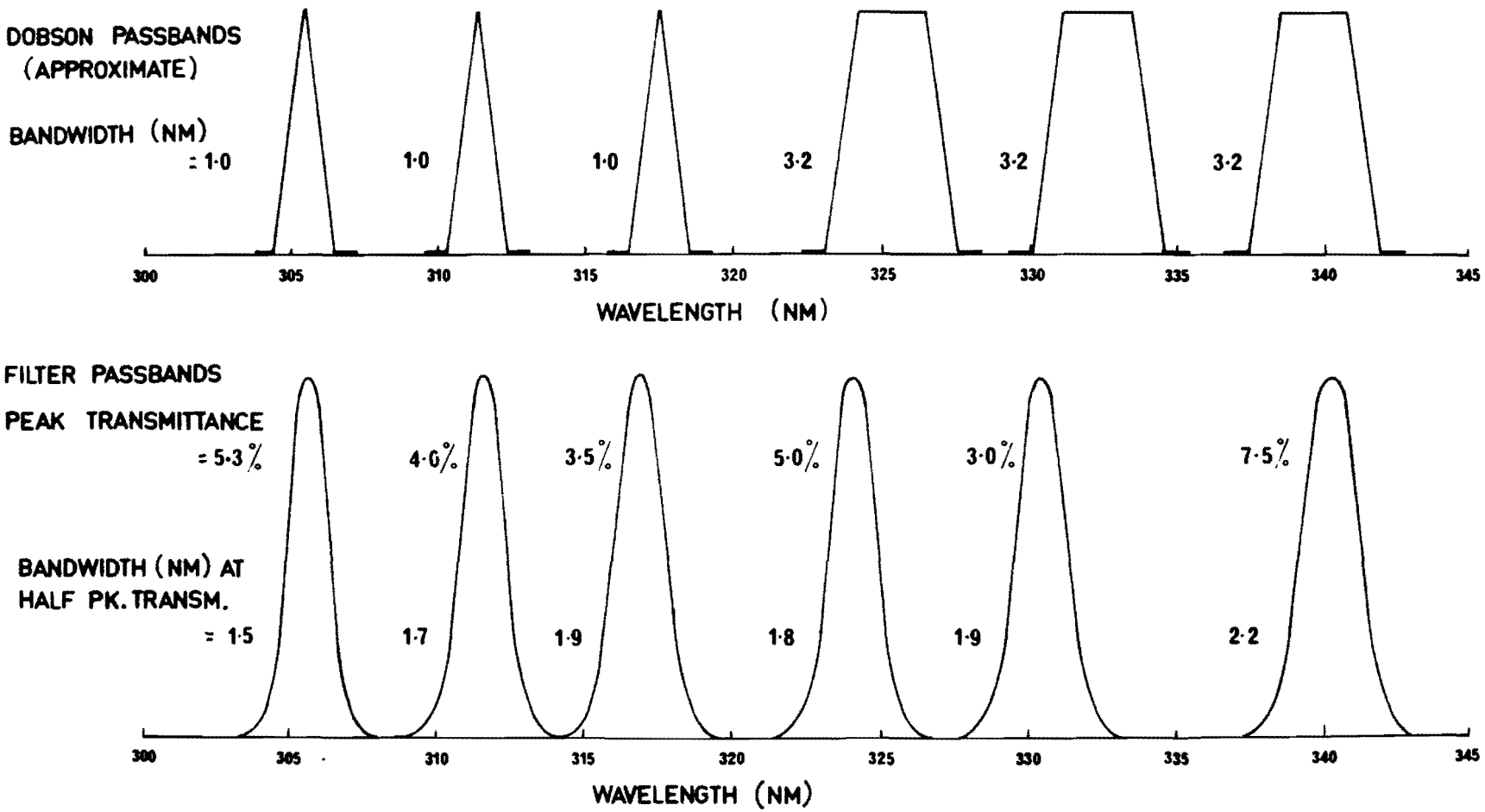

Fig 4-12 COMPARISON OF PASSBANDS OF THE FILTER SPECTROPHOTOMETER AND THE DOBSON SPECTROPHOTOMETER

The value of stacked filters has separately been realised by Goldberg and Klein (1974), although they used individually made filters of relatively large bandwith. Of course, for effective stacking, the filters' centre wavelengths should differ by less than, say, 0.2 times their bandwidth. In our case, this is about 0.5 nm, which at present appears attainable only by cutting the filters from a large plate as described.

The number of filters in a stack is limited by the sensitivity desired of the instrument and the cost of the filters. Double stacked filters were chosen for the filter instrument, and are hereafter referred to as double filters, or doubled filters. Their passbands are shown in figure 4.12, along with the equivalent slitbands of the Dobson instrument. The comparison is very favourable to the filters.

4.4 Non-Uniformity across Filter Surface of Transmittance and Centre Wavelength

Owing to the difficulty of accurately depositing the many, very thin, dielectric layers of an interference filter, the optical characteristics of the filter may not be uniform across its surface. Variations in peak transmittance of up to 20% are reported in the very useful paper on interference filter performance by Blifford (1966).

To test the behaviour of the instrument's filters, a procedure similar to Blifford's was used, involving the rotation of each filter past a small fixed hole placed at about two-thirds of the filter radius. Initial testing at fixed peak wavelengths, and with a 2 mm hole, showed the variation in peak transmittance across the 20 mm diameter

filters to be within a few percent for most filters. The exception was a 10% variation for the 305 nm filter.

However, subsequent measurements of the whole 305 nm filter passband at six equally spaced positions around the filter showed the variation of peak transmittance to be only 3%, which, together with a bandwidth variation of 4%, yields a total worst-case variation in transmitted power of 7%. The larger 10% transmittance variation in the first test was found to be caused by a significant shift in wavelength of the whole passband. A similar shift, for an infrared filter, was reported by Nichols et al. (1965).

To find the maximum variation in the centre wavelength of the filter, it was rotated in a continuous manner past a smaller 0.5 mm hole, whose area represented about 0.06% of the filter's total area. The two extreme spectra are shown in figure 4.13, and are separated by 0.6 nm. Maximum variations for all other filters are less than 0.1 nm, and smaller variations can be expected for stacked filters.

There are thus two problems to consider; the effect of variations in transmitted power, and the effect of variations in the passband centre wavelength.

Both variations mean that the area of a filter used in its calibration must correspond to the area used operationally. In practice, this is difficult as the filter instrument and calibrating spectrophotometer have dissimilar beam geometries. Once any satisfactory calibrations have been made, a fixed, constant area of each filter must be used. To this end, the filters are maintained in fixed orientations in the disc of the filter instrument.

The following situations cause difficulty. Firstly, owing to the 27 cm separation of the photomultiplier and filters, and the 2.3^{o} tolerance in instrument alignment, the photomultiplier will 'see' the direct sun through a varying region of each filter. Secondly, if for zenith sky measurements the larger aperture is chosen, a different region of each filter will be used. Lastly, for both direct sun and zenith sky measurements, the filter regions used will vary owing to the variation in the speed of the filter disc's drive motor.

These problems can be circumvented in future instruments by placing the photomultiplier and filters as close together as possible, using only one size of aperture, and electronically stabilising the filter disc drive motor speed.

Of course, the variations are spatially averaged, both in calibration, where the beam cross section is about 15 x 2 mm, and in use, where, owing to the size of the detector aperture, the measured radiation "sweeps" through 30% of total filter area, while the alignment uncertainty keeps this 30% within a fixed 60% of the filter area. Because of this, the experimental maximum variations of transmitted power and of centre wavelength given earlier, will be reduced. A reduction to a tenth, say, gives variations of 0.7% and 0.05 nm respectively, which are about the same size as the filter calibration uncertainties (Appendix A, section 1).

The actual effect of variations in transmitted power is to give the filter instrument variable extraterrestrial constants. From equation 1.4 and 1.7, it can be seen that a 1% variation in transmitted power of a single filter will

cause a change of 0.0043 in an extraterrestrial constant, and a consequent maximum change in total ozone of $0.0043/\Delta\alpha$ atm cm, where $\Delta\alpha$ is the ozone absorption coefficient difference for either single or double pairs of filters. Thus, a 1% variation in transmitted power yields the following approximate changes in total ozone: A pair 0.003, C pair 0.005, D pair 0.012, AD double pair 0.003, all in atm cm.

The effect of varying centre wavelength is to cause variations in the filters' atmospheric attenuation coefficients, particularly in the ozone absorption coefficient which changes rapidly with wavelength (figure 8.3). A wavelength shift of only 0.05 nm, or 0.017%, can result in a 1% change in the ozone absorption coefficient. (See figure 8.14, and Section 8.4.)

In general then, the variations in transmitted power and centre wavelength across a filter's surface will each give rise to errors in measured total ozone of 1% or less.

A final point is that, when averaged over the filter area used, the variable passband will give a broader nett passband, and therefore a larger, and perhaps more uncertain bandwidth effect (see Part III). However, provided that the passband variation is not excessive, any resulting errors in the bandwidth effect corrections, already very small, will be insignificant.

4.5 Orientation Effects, Effect on Field of View and on Filter Calibration

Interference filter transmittance characteristics depend on the angle of incidence of the incoming radiation. With increasing angle, Blifford (1966) observed a shifting of the passband to shorter wavelengths, with decreasing peak transmittance and increasing bandwidth. Some changes are to be expected, since the interference in a single thin film, as described by equation (4.1), is angle-dependent.

These observations were confirmed experimentally by the author for the 305 nm and 311 nm filters. The measurements are displayed in figures 4.14, 4.15 and 4.16, using the same format as Blifford's, and are sufficiently similar to be taken as representative of the whole filter set.

From figure 4.14, it can be seen that, for small angles, the shift in centre wavelength, $\Delta\lambda$, with angle of incidence, θ, will follow the linear, theoretically-based formula of Lissberger and Wilcock (1959)

$$\frac{\Delta\lambda}{\lambda_0} = -B\,\frac{\theta^2}{2} \qquad (4.3)$$

where λ_0 is the centre wavelength at normal incidence and B is a parameter which depends on the filters' materials and geometry. From the gradient of the straight line in figure 4.14, a value of $B = 0.5 \pm 0.1$ is found for these filters. Blifford reports a range in P of 0.22 to 0.51.

Recalling that a simple shift in passband of 0.05 nm or 0.017% can give a 1% change in the band's ozone absorption coefficient, it can be calculated that 1^{o}, 2^{o}, 3^{o} and 4^{o}

changes in angle of incidence will result in 0.45%, 1.8%, 4.0% and 7.2% changes in ozone absorption coefficient respectively.

There are thus several situations to consider. The first and most important is that of calibration, since the sample beam of the calibrating instrument, a Cary 14 (described in Appendix A) converges in two mutually perpendicular planes at semiangles of about 4^{o} and 1.4^{o}.

For an axially-symmetric convergent beam, Lissberger and Wilcock (1959) show the passband shift to be half that of tilting the filter through the same semiangle. Unfortunately their analysis is not easily extended to the Cary 14, because its beam is rectangular and does not converge to a point, but if, as a first approximation, their ratio of 1/2 is used here, then the Cary will shift the passband centre wavelength by 0.06% causing a 3.6% error in the ozone absorption coefficient of the 305 nm filter.

The centre of the beam is nearly parallel, however, so that simply by masking the outer divergent parts, it is possible to reduce this calibration error by at least a factor of ten.

Applying the conclusion of Lissberger and Wilcock to the 2.3^{o} and 1.15^{o} semiangles of the filter instrument's fields of view, shows the passbands' centre wavelength shifts to be 0.08% and 0.02% respectively. The resulting errors in the ozone absorption coefficient are about 4.8% and 1.2% respectively, which indicate that the smaller field of view should be used wherever possible. These errors do not apply to direct sun measurements since the dominating, direct solar radiation is subtended by the sun at a semiangle of only 0.3^{o} and thus causes negligible error.

To maintain measurement accuracy, the filters must be aligned as nearly perpendicular as possible to the incident sunlight. The 0.5^{o} alignment accuracy needed to keep the ozone absorption coefficient error to less than 0.1% is easily attainable with the aid of the instrument's alignment system (see Chapter 3).

The remaining figures, 4.15 and 4.16, show that, for filter orientation angles of less than 2^{o}, the changes in peak transmittance and half bandwidth are negligible.

It should be noted that, in the tests carried out by the author on surface non-uniformities (Section 4.4), the observing hole was fixed relative to the beam, and the filter was rotated. In this way, variations due to different beam angles within the beam were avoided.

4.6 Aging Effects, Dependence on Moisture, Need for Hermetic Sealing

The optical characteristics of interference filters change with time (aging), the most significant change being an increase in centre wavelength, of between 0.1% and 2% immediately after manufacture, and of smaller values at other times. (Furman and Levina (1972)).

The importance of this change will be realised when it is again recalled that a centre wavelength shift of only 0.05 nm, or 0.017%, can result in a 1% change in a filter's absorption coefficient. The aging effect produces much larger changes than this, and must therefore be either very well controlled, or regularly corrected for.

Fortunately, the problem has been largely solved as a result of a comprehensive set of experiments carried out by Furman and Levina (1972) to determine the role of moisture in aging. They show, by heating and cooling various filters in moist and dry air, that moisture absorbed by, or dessicated from the filters, is the primary cause of centre wavelength shifts. They derive an approximate expression for the centre wavelength shift as a function of the change in water content of a filter, and as an example, use it to calculate the minimum volume of air of 80% relative humidity, needed to shift a centre wavelength by 0.1 nm, presuming that all the moisture is absorbed. For their sample, this volume would be enclosed by a window 0.2 mm from the filter.

Of course, once the air volume is sealed in, subsequent changes in its relative humidity, and therefore in the filter's water content and centre wavelength, will be much less, perhaps by an order of magnitude. Even allowing a generous margin for the approximations in the theory, and for variations among filters, one can conclude that by placing a window directly against the filter, i.e. within 0.02 mm, and hermetically sealing the edges, the centre wavelength is stabilised against moisture effects to 0.01 nm or less.

As can be seen from an earlier calculation, this 0.01 nm wavelength uncertainty represents a 0.2% uncertainty in absorption coefficient, and is therefore adequate for our purposes. The filters described in a previous section are sealed in this way by the manufacturer, and hence stability is assured.

Furman and Levina (1972) mention that the bandwidths and peak transmittances of some of their filters changed during their experiments, but they do not pursue the matter. It is indicated that the changes are small and temporary, and that, since in opposite directions, their effects tend to cancel. If, in the filter instrument, all the filters are similarly affected, the net effect on the measurements would be negligible.

Although Furman and Levina's work has shown moisture absorption to be the major cause of short term aging, there is no certainty that other processes, such as crystallization of the dielectric layers, do not have a significant effect over longer periods. Further study of this question is needed since the successful long-term use of the filter instrument requires long-term optical stability of the filters.

4.7 Temperature Effects, Linear Shift of Centre Wavelength with Temperature

There are regular changes in the optical characteristics of interference filters with temperature, again the most significant of these being changing centre wavelength, with values of up to +0.005% per ^{o}C being observed (Blifford (1966), and Furman and Levina (1971)). Remembering that a 0.017% shift in wavelength can result in a 1% change in the ozone absorption coefficient, it can be seen that the effect is of some importance.

The changes arise through the temperature dependence of the refractive indices and thicknesses of the filters' dielectric layers. This is made clear by equation (4.1) for a

single layer, although in multilayer filters the dependence may be complicated by the different rates of change of the two dielectrics. The temperature dependence should not be confused with the effects of absorption and expulsion of moisture which are also temperature dependent.

Blifford (1966) shows that, in the ±60^{o}C temperature range, the centre wavelength shift is positive, linear, and has no hysteresis, and that the changes in half-bandwidth and peak transmittance are small, being less than 0.001 nm per ^{o}C and 0.01% per ^{o}C respectively.

Several of the filter instrument filters were tested for centre wavelength shift in the manner described in Appendix A section 5 and the measurements for two filters are shown in figure 4.17. An average temperature coefficient of passband shift of 0.0105 ± 0.0005 nm/^{o}C was found. It is equivalent to 0.0033%/^{o}C. This value implies a maximum error in the filters' ozone absorption coefficients of 0.2% per ^{o}C.

Complete calculations of the effect of shifting passbands are made in Section 8.4. The results may be applied to shifts caused by surface variations, orientation and aging, and in the case of temperature effects, may be used to provide correction to total ozone as a function of temperature.

There exists the possibility of compensating for the temperature shift in passband centre wavelengths by tilting the filters to produce equal but opposite shifts. As can be seen from Section 4.5, the filter peak transmittances and bandwidths would change little for the small tilt angles (< 5^{o}) required. Such a system could be automatic, but would have the disadvantage of mechanical complexity, especially since

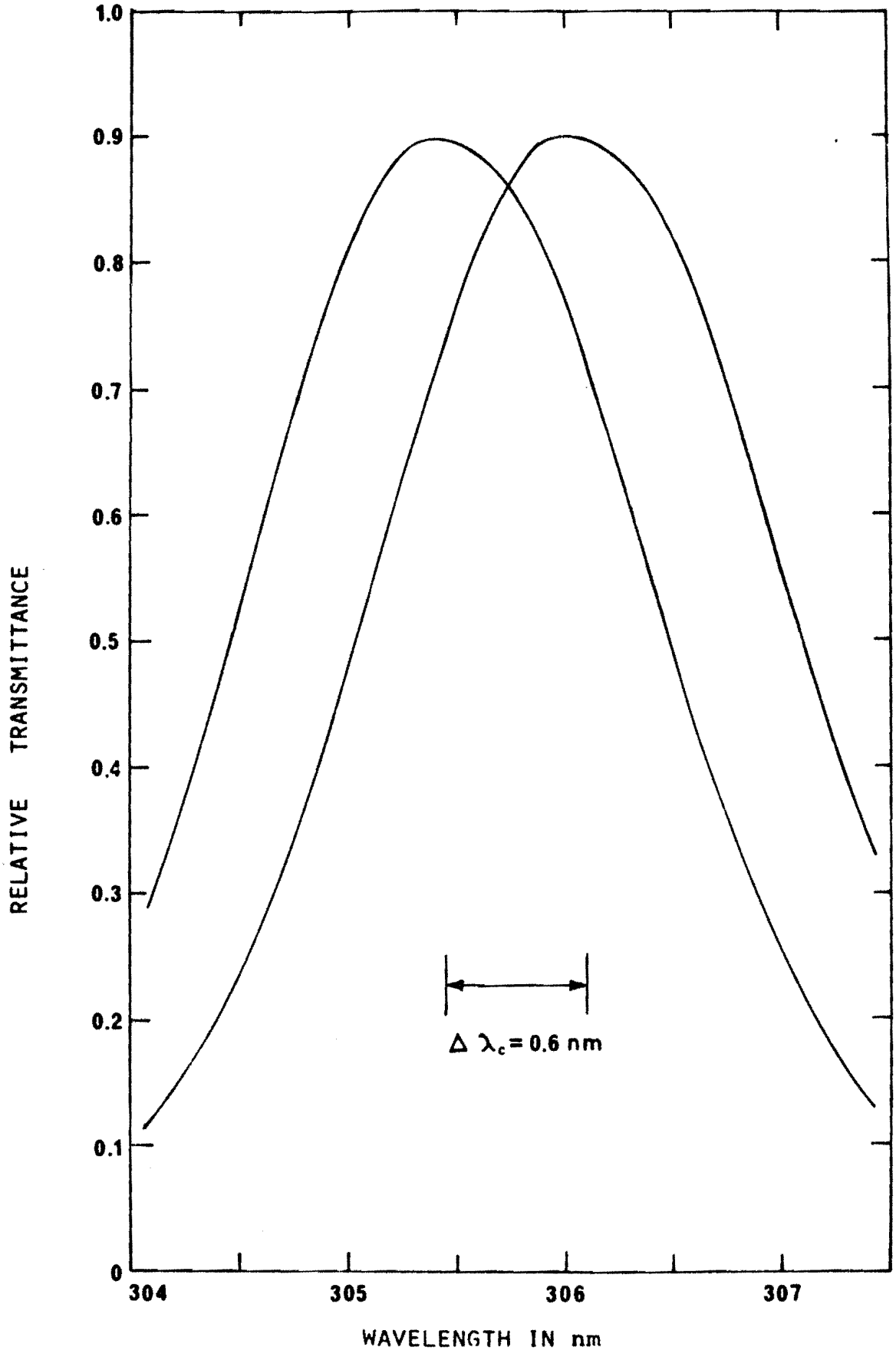

FIG.4.13 305 nm FILTER SPOT SPECTRAL TRANSMITTANCE SHOWING THE EXTREMES OF CENTRE WAVELENGTH.

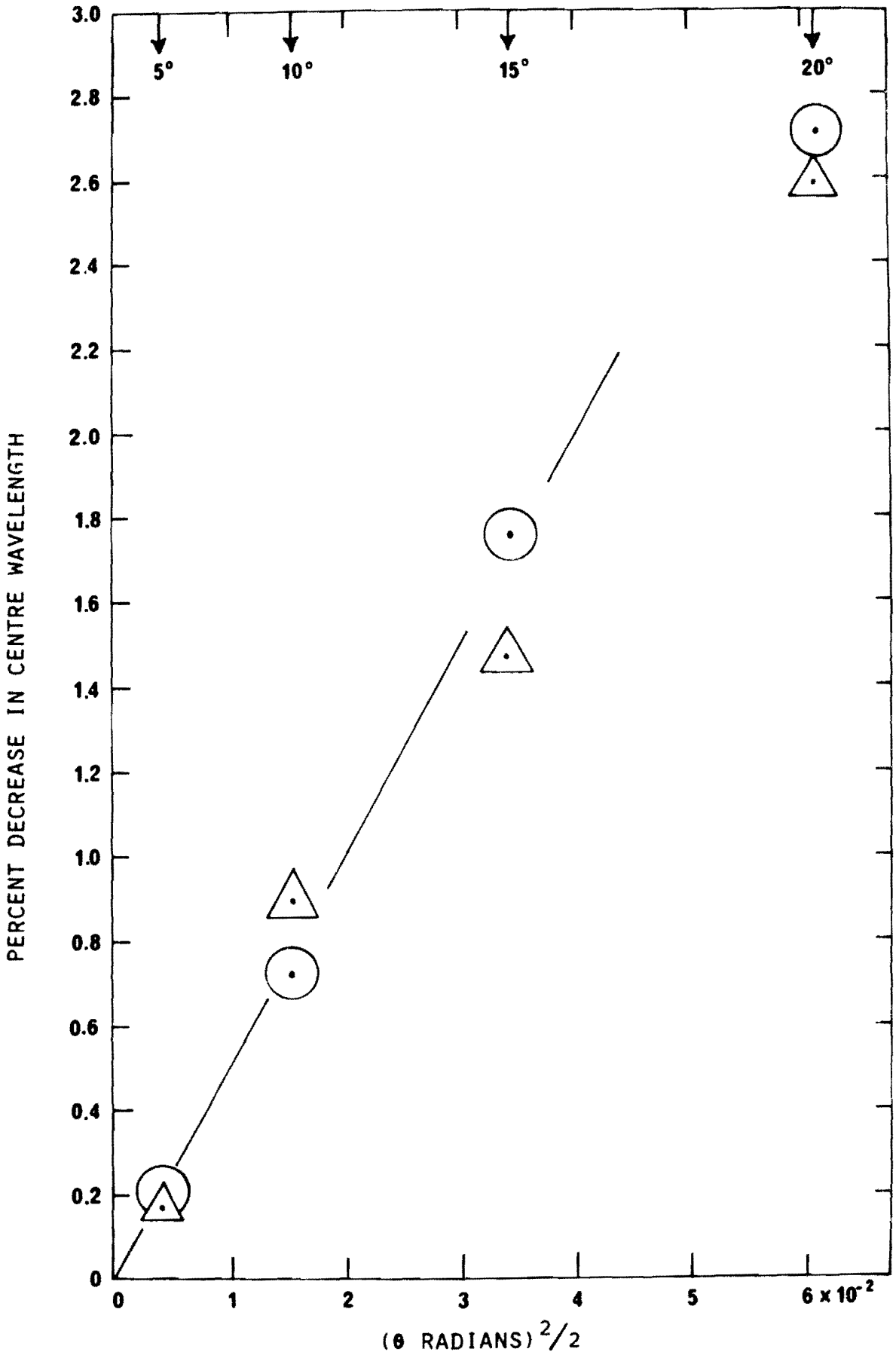

FIG.4.14 VARIATION OF FILTER CENTRE WAVELENGTH WITH RADIATION ANGLE OF INCIDENCE 305 nm FILTER ○, 311 nm FILTER △.

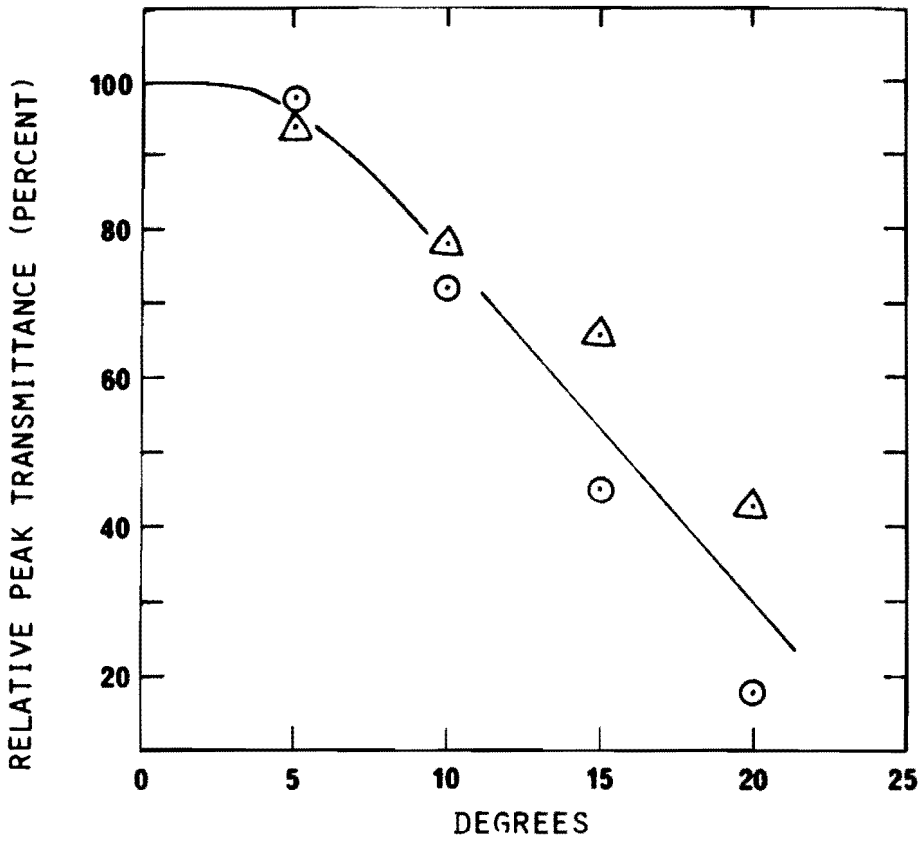

FIG.4.15 VARIATION OF FILTER PEAK TRANSMITTANCE WITH RADIATION ANGLE OF INCIDENCE 305 nm FILTER ⊙, 311 nm FILTER △.

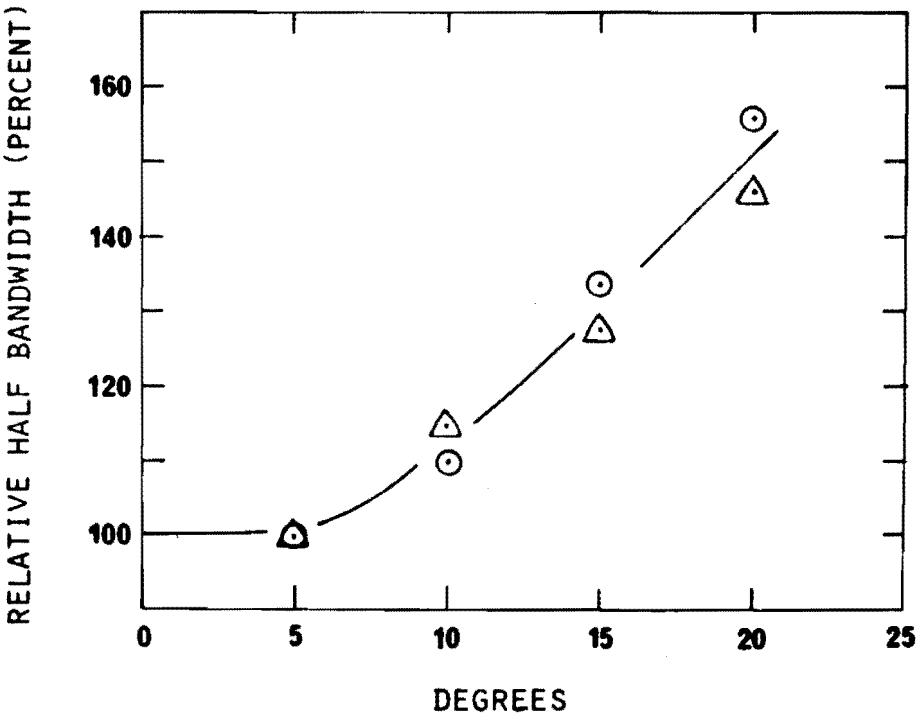

FIG.4.16 VARIATION OF FILTER HALF BANDWIDTH WITH RADIATION ANGLE OF INCIDENCE 305 nm FILTER ⊙, 311 nm FILTER △.

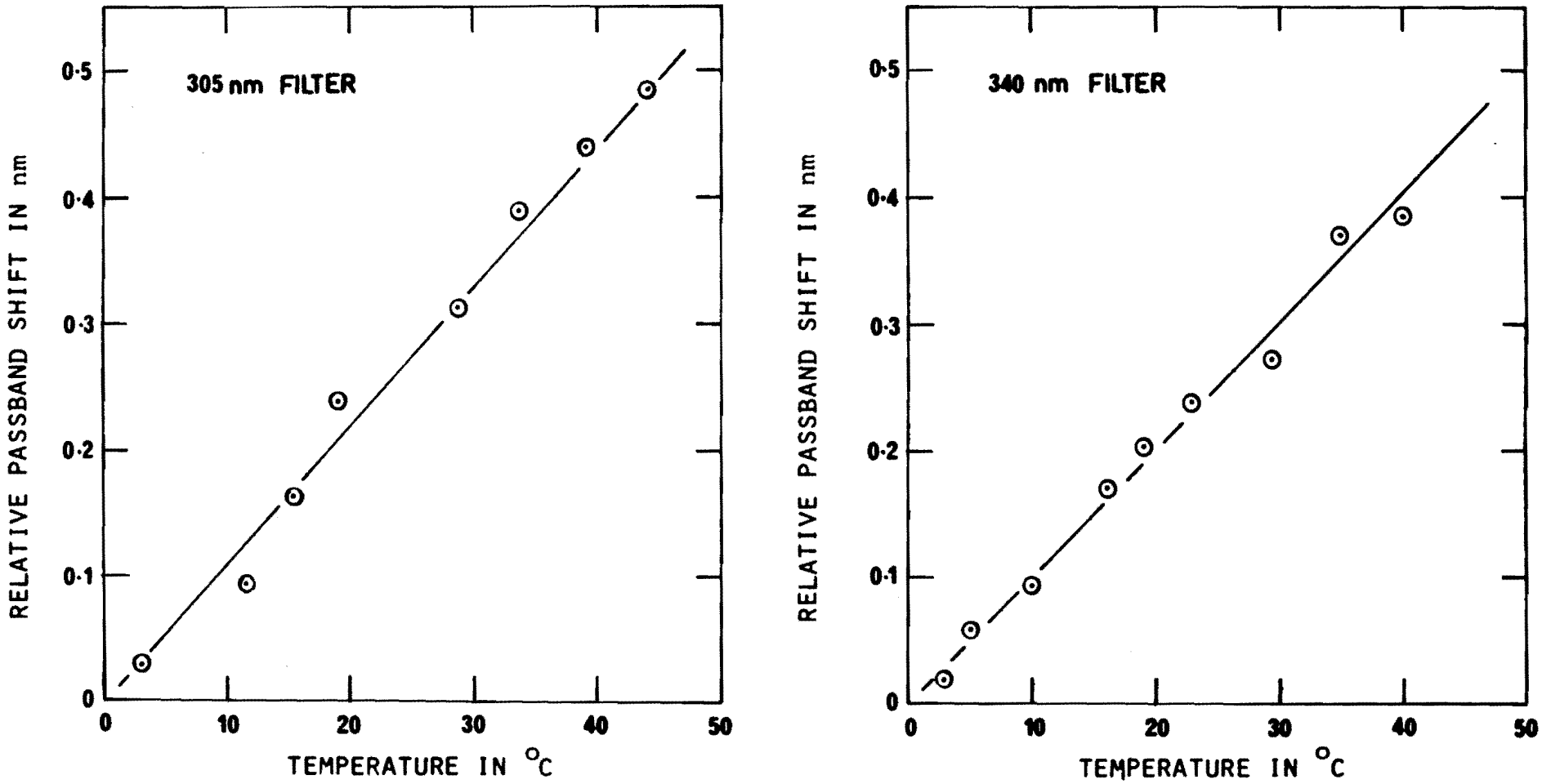

FIG.4.17. RELATIVE WAVELENGTH SHIFT OF FILTER PASSBANDS WITH TEMPERATURE

the centre wavelength depends on the square of the tilt angle, but is linear with temperature. A third alternative is to maintain the filter's temperature constant.

It may be possible to obtain filters which have especially low temperature coefficients of passband shift. The filters of Osherovich et al. (1969) are said to have a coefficient of 0.0015 nm/^{o}C, which is very small compared to that of our filters, at 0.0105 nm/^{o}C, and those of Blifford (1966), at 0.0100 to 0.0300 nm/^{o}C.

CHAPTER 5: PHOTOMULTIPLIERS

5.1 Introduction, General Description, Spectral Characteristics

The photomultiplier occupies a pivotal position in the instrument, determining, to some extent, the characters of both the optical and the electronic systems. It has many facets of behaviour which affect the total ozone measurement, and it is these which form the substance of this chapter.

A general description of photomultipliers is given in this section, 5.1, while in Section 5.2 their limitations relevant to the total ozone measurement are discussed. Lastly, in Section 5.3, a description is given of some evaluation tests carried out by the author on an experimental solar-blind photomultiplier specially offered by an English manufacturer.

The photomultiplier is the preferred detector for the ultraviolet spectrum (Hennes and Dunkelmann, 1966). The solid state devices which are now available are of little use as their main sensitivity bands lie in the red or infrared spectrum. Photomultipliers are valued for their extremely linear response, their sensitivity, stability, ease of use, and ready availability. They are therefore very suitable for the filter instrument.

Their main components are a semiconducting photoemissive cathode, which determines the tube's spectral response, and an array of electron-current multiplying electrodes, which (along with applied high voltage) determine its gain. These are sealed within an evacuated glass tube. Good accounts of the large numbers of tubes which are commercially available are

given in the manufacturers' handbooks, EMI (1970), RCA (1970), and Philips (1970). These manuals also contain a good deal of basic physical and theoretical information.

Despite the recent systematic study of photoemitters, promoted by semiconductor studies and space research, most photomultipliers still fall within the standard broadband spectral classes, e.g. S5, S11 etc., and are hence not able to isolate specified narrow bands (i.e. < 200 nm). Therefore, in the case of the filter instrument, it is more prudent to concentrate on the development of filters to isolate the desired narrow bands and to block sideband leakages. The suitability of photomultipliers is then judged more on other grounds, such as sensitivity and low dark current. Fortunately, very selective, well blocked filters are now available, such as the double filters described in Section 4.3.

Given the above approach, it is feasible to use the S5, S11 and S13 types of tube, which all have their main band of sensitivity, in or near the visible region, and sensitivity cut-offs at about 650 nm. Initially on the grounds of cost and availability, an S5 type RCA 1P28 tube was chosen, but since then a more suitable, though more expensive, S11 type EMI 9526S tube, of greater overall sensitivity and lower dark current, has been placed on order. Its qualities will make it well suited for zenith sky intensity measurements, and particularly Umkehr measurements (determination of ozone's distribution with height).

The final point of this section concerns two cautions to be borne in mind when comparing photomultipliers. Firstly, "overall sensitivity" is measured with respect to a standard 2857^{o}K tungsten lamp whose black-body radiation falls mainly in the infrared spectrum, and therefore this parameter is not a conclusive indicator of the relative ultraviolet performance of tubes whose spectral types are even slightly different. Secondly, the sensitivity and dark current of any individual tube may be up to plus or minus a power of ten different from the typical or average values listed by the tube's manufacturer.

5.2 Limits on Accurate Operation, Technical Means of Extending Operating Range

The following photomultiplier characteristics may give rise to error in the total ozone measurement. Cathode spectral sensitivity is dependent on temperature and on the cathode to first dynode voltage, and may vary spatially across the cathode. The gain is highly dependent on the high voltage supply stability, and the dynamic range is limited by the dark current, and by gain non-linearity at high anode currents. Each of these points is discussed below, in order, and generally with reference to the 1P28 photomultiplier.

In the spectral region 300 nm to 350 nm, the temperature dependence of caesium-antimony cathodes is 1.5 x 10^{-3} % (^{o}C nm)$^{-1}$ (RCA 1970). If this value is also typical of the 1P28 caesium-bismuth cathode, then, for example, the tube's relative spectral response for the A wavelength pair (i.e. the 325 nm and 305 nm bands) will change by +0.03%

per ^{o}C, which will appear as an increase in measured total ozone. The effect is small, however, and since the dependence is almost linear with wavelength, the error is largely eliminated by the use of double pairs of wavelength bands, such as the AD method. To help maintain a more stable photomultiplier temperature, the filter instrument photomultipliers' nearby voltage divider resistors have been mounted in heat-sinks.

The origin of the dependence of spectral sensitivity on the cathode to first dynode voltage is explained by Matthews (1971) who overcame the problem by maintaining the voltage constant with zener diodes. This solution is recommended in EMI (1970) and is used by the author.

The problem of spatial variation in cathode spectral response has been largely overcome in the instrument by using a fixed area of the cathode, defined by the rear aperture close to it, and ensuring that the aperture is always completely illuminated by the whole solar disc.

The dependence of a photomultiplier's gain on applied high voltage can be expressed using a simple, but realistic model (Philips 1970) as

$$G = \delta^N = (\kappa V)^N, \qquad (5.1)$$

where δ = mean gain per stage

N = number of tube stages

κ = constant, mean secondary emission factor

V = mean voltage per stage.

When differentiated, equation (5.1) becomes

$$dG/G = N\, dV/V \qquad (5.2)$$

which shows that variations in voltage will produce N-times greater variations in gain.

Hence, for the nine-stage 1P28 tube, the regulation of 0.02% (in one second) in the high voltage power supply yields a gain stability of 0.2%. Slow shifts in gain are unimportant since comparisons are made only between measurements taken within a single 400 ms cycle of the filter disc. However, the rapid spontaneous gain changes mentioned in Philips (1970) may cause error.

The dark current is the small current which flows from the anode when no light is incident on the photocathode. Since the dark current sets the lower limit of a photomultiplier's sensitivity, it is best kept as small as possible.

There are three principal causes of dark current: ohmic leakage, which depends on the cleanliness and resistivity of the tube materials, and is directly proportional to voltage; thermionic emission, which is dependent on gain and temperature, and is variable; and lastly regenerative effects which include less predictable phenomena such as internal fluorescence, residual gas ionisation, and ionic currents in the tube's glass walls (RCA 1970).

Refrigeration can drastically reduce the thermionic emission, which is believed to be the largest component of the dark current (EMI 1970), but this procedure is considered to be undesirably complicated for the filter instrument. The practice of holding the tube wall at cathode potential to

reduce the ionic current flow through the glass (RCA 1970) was adopted by the author, simply by wrapping it in metal foil and connecting the foil to the cathode.

The dark currents for the 1P28 photomultipliers used ranged from 2 nA to an unsatisfactorily large value of 100 nA at high voltages. Owing to special cathode processing, the EMI 95265 photomultiplier is considerably better with a reputed dark current of 0.2 nA to 2 nA. At these values, it is barely significant, even for low intensity zenith sky measurements.

The final topic to be considered is the gain non-linearity which occurs at high anode currents. It is explained as follows.

The electron current inside a photomultiplier is drawn from the bleeder current in the tube's resistive voltage divider, the bleeder current being divided between the nett dynode electron emission and the next resistor in the divider. If the electron emission increases, the resistor current must decrease, resulting in a simple Ohm's law reduction in the voltage on the next stage, and a consequent loss of gain. In this way, the gain on this stage, and hence the overall gain, become dependent on the internal current, which is itself dependent on the incident intensity. Therefore the tube's linearity of anode current with intensity is lost.

The effect first becomes apparent in the last stage, which carries the largest internal current, but only when the anode current is a significant proportion of the bleeder current. This is confirmed by the analysis described in Appendix F, which shows that the overall gain inaccuracy for the 1P28 photomultiplier is roughly equal to the ratio of anode to bleeder currents.

Calculations made in Appendix F, specifically for the filter instrument's 1P28 and power supply, show that in the voltage range of 500V to 750V, gain inaccuracies of less than 1.0% and 0.1% require upper anode current limits of 10 μA and 1 μA respectively. If these limits are unacceptably low, they may be increased by altering the designs of the high voltage supply and voltage divider to increase the bleeder current, as is explained in the appendix.

5.3 Experimental Evaluation of Developmental Solar Blind Photomultiplier

Even though filters with good blocking can be made (Section 4.3), it is still desirable to aid this blocking by using a solar-blind photomultiplier, i.e. one which is insensitive to visible and infrared radiation. Unfortunately, no suitable tubes are commercially available. One possibility, however, is to make a photocathode from the alkali tellurides CsTe and RbTe, whose middle ultraviolet responses have variable long wavelength cut-offs between 300 nm and 350 nm which might be extendible to cover the wavelength range of the filter instrument.

Recently, EMI Electron Tube and Microelectronics Division developed a suitable CsTe photocathode, and in response to correspondence initiated by Dr W.A. Matthews during his thesis study and continued by the author, loaned the author a photomultiplier for evaluation. The tube is labelled 9705QB, has eleven stages, and an end-on photocathode. Since it is experimental, no technical data were supplied. The aims of the evaluation were therefore to assess its relative spectral

sensitivity, its sensitivity near 300 nm and its dark current.

The relative spectral sensitivity was measured using a method devised by the author and described in Appendix A, section 4. It appears in figure 5.1 along with the standard S5 type response (RCA 1970) which represents the 1P28 tube. A comparison of the two curves clearly shows the good rejection of visible light (400 nm to 700 nm) by the 9705QB tube, whose 1% cutoff wavelength is 420 nm as against 640 nm for the 1P28 tube. Experiments made elsewhere on other 9705QB samples enabled the manufacturer to confirm that the author's "measurements agree very well with the sort of performance we would expect" (R.A. Stubberfield, in correspondence).

Direct comparison of the 9705QB with a 1P28 at the same applied voltage of 830V showed that although the dark currents were equal, the sensitivity of the new tube at 300 nm was 2.7 times that of the 1P28. In addition, since it has eleven stages, two more than the 1P28, it can be operated at a higher range of voltages and therefore at even greater sensitivities.

From these measurements the 9705QB appears to be very suitable for use in the filter instrument. However, when a second, production tube was acquired, and subjected to the same tests as the loaned tube, the performance was so disappointing that the tube had to be returned to the manufacturer. Its relative spectral sensitivity, which is compared in figure 5.2 with that of the first tube, has none of the visible light rejection of its predecessor, and to make matters worse, its sensitivity at 300 nm was down by a factor of about 100.

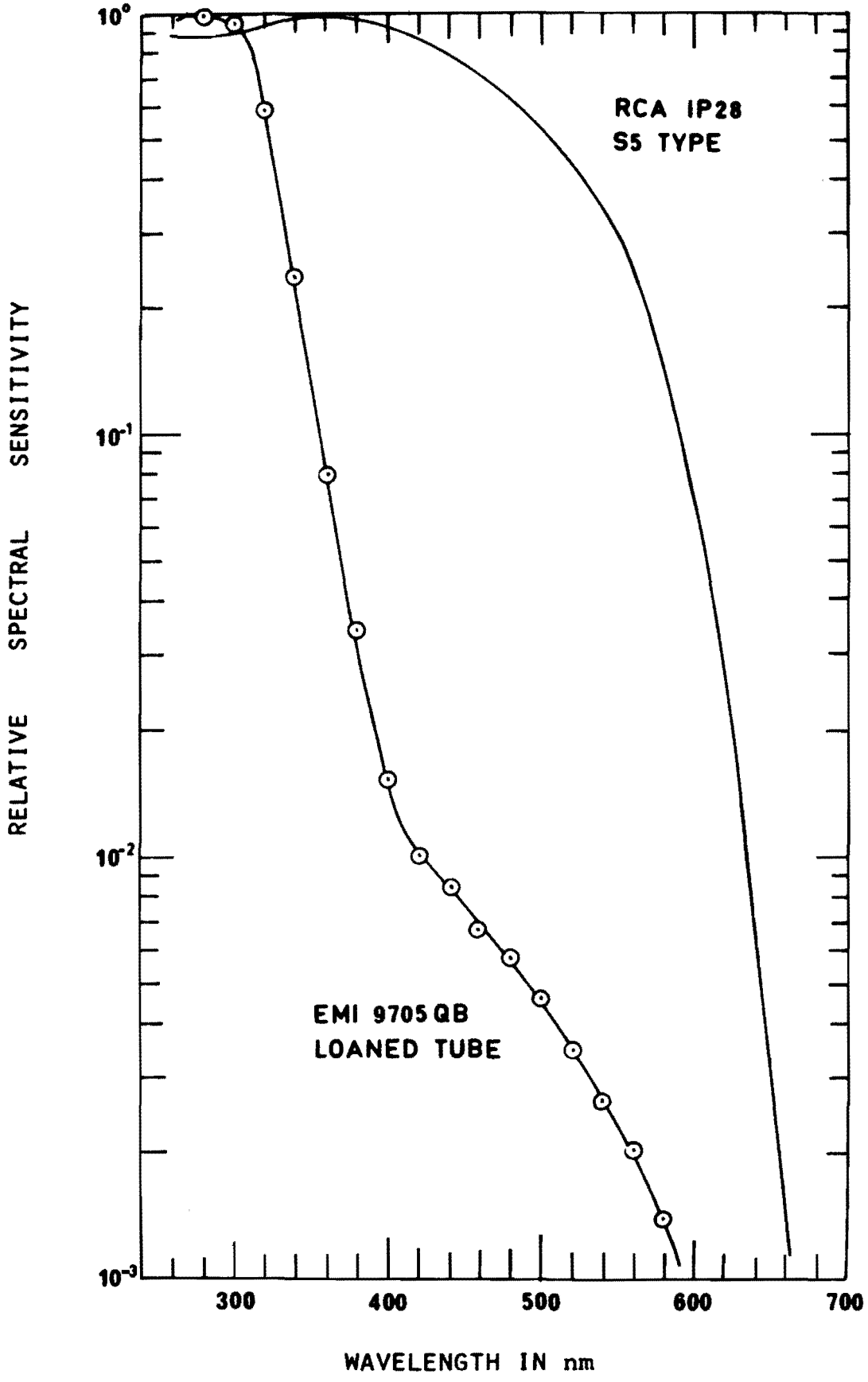

FIG.5.1 PHOTOMULTIPLIER RELATIVE SPECTRAL SENSITIVITY.

RCA 1P28 AND EXPERIMENTAL EMI 9705QB

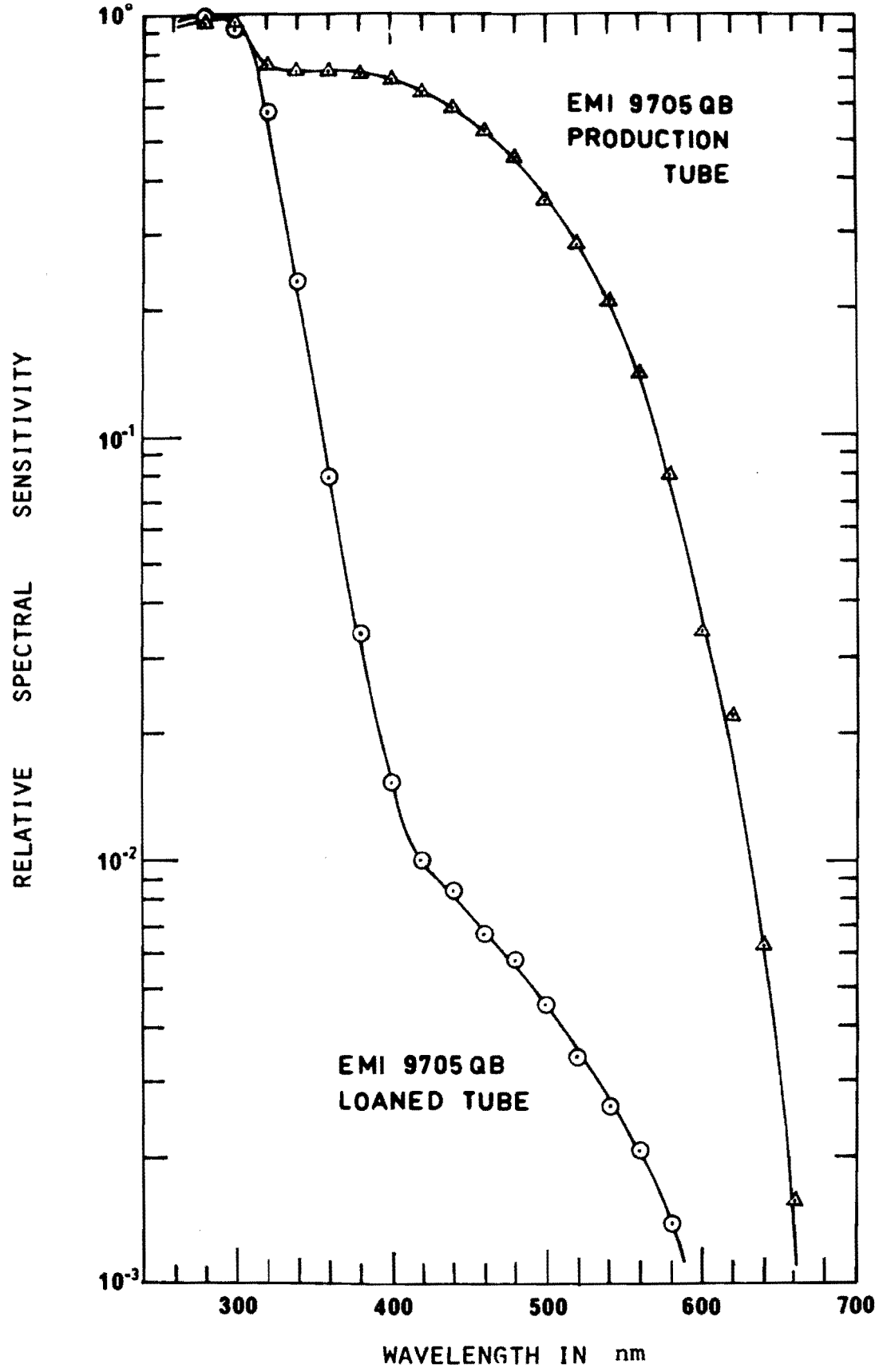

FIG.5.2 PHOTOMULTIPLIER RELATIVE SPECTRAL SENSITIVITY
EMI 9705QB, LOANED ⊙, PRODUCTION △.

The manufacturer, in reply, states that these results "do not entirely contradict our experience with this type of tube", and indicates that the spectral sensitivity is difficult to control. Substance is thus added to the point made in the introduction, that for the isolation of spectral bands, it is more worthwhile to concentrate on the development of good filters than on good photomultipliers.

CHAPTER 6: INSTRUMENT CALIBRATION AND ACCURACY

6.1 Calibration; Instruments' Linearity, Spectral Constancy, Coefficients and Constants

Instrument calibration involves:
(i) determining the ranges of operation in which the instrument's response is linear with intensity and spectrally constant, (ii) measuring the filter spectra and calculating their effective ozone absorption coefficients and Rayleigh scattering coefficients, (iii) experimentally determining the instrument's extraterrestrial constants. Each of these three aspects is considered in more detail below.

(i) The linearity and spectral constancy of the instrument depend on those of its constituent parts. The filters will be very linear, but, as explained in Sections 4.5, 4.6 and 4.7, will exhibit spectral response variations due to passband shifting. The errors due to the temperature-dependent shifting can be corrected with the aid of the correction tables which are given later in Section 8.4. Other shifts should be negligible, provided that a relatively constant area of each filter is used. Some variation in this area will occur as is explained in Section 4.4. The ±0.5% uncertainty in the electronically timed filter scan period will also produce a small apparent spectral response variation.

The photomultiplier response is linear over a large range which is limited only by the dark current at about 5 na and by the requirement that the anode current be significantly smaller than the bleeder current (Section 5.2). As shown by Matthews (1971), and discussed in Section 5.2, the tube's

spectral constancy with varying applied voltage and varying intensity levels is assured by using a constant area of the photocathode, and by stabilising the potential between the cathode and first two dynodes.

The rest of the system is spectrally independent. The current-controlled oscillator response (figure 3.5) is linear from at least 1 nA to 10 μA. The region beyond the upper limit can be used if suitable corrections are applied. The digital electronic system is of course linear in its response.

(ii) Specific difficulties in measuring the transmittance spectra of the interference filters are detailed in Appendix A. The spectra, when measured, are accurate to about ±0.05 nm in wavelength and 0.5% in transmittance, and are used as weighting functions to find the attenuation coefficients appropriate to their passbands. The coefficients are not easily calculated, however, as theyare not constant, but are dependent on the filters' temperature and bandwidth, and on the amount of atmospheric attenuation. The theory and calculations involved are discussed in detail in Part III.

(iii) The experimental method, given in Section 1.2, for finding the extraterrestrial constants requires sets of intensity measurements to be taken over as large a range of airmass as possible during which time the atmospheric attenuation should be constant. The method assumes that the filter passbands can be treated as monochromatic. The double filters can be treated this way (Section 9.2), but the filters of the prototype cannot (Section 1.3) and hence require the use of the broadband theory of Part III.

6.2 Accuracy, of Both the Basic Method Used and the Instrument

Uncertainty in the determined total ozone can arise from both the uncertainty in the basic experimental method, and the uncertainty of the instrument's measurements. Uncertainties in the basic method are common to filter, prism, and grating instruments and arise from the atmospheric attenuation coefficients, from the extraterrestrial constants, and from the effect of radiation scattered into the measured beam.

Published ozone absorption spectra are considered to be accurate to 1% to 2% in absorption and 0.1 nm in wavelength (Section G.4). Because the absorption changes with wavelength, this wavelength uncertainty will give a further 1% to 2% uncertainty in the absorption (Section 8.4). In addition, the absorption is temperature dependent. This point is considered in Appendix D, where it is shown that a 30^{o} range in stratospheric temperature will result in up to a 6% change in the ozone absorption coefficient.

The variation of the molecular scattering coefficient with air pressure of ±3%, described in Appendix H, gives rise to uncertainties of ±.002, ±.004 and ±.008 atm cm in total ozone determined by the A, C and D single wavelength pairs respectively. The double pair method uncertainties are negligible.

Unless accounted for, aerosol scattering will cause large errors in total ozone determined by the single pair method. For a 20 nm band separation within a pair, a maximum range of ±.0025 nm^{-1} in the linear aerosol scattering coefficient (Section G.4) will give errors of ±.030, ±.060 and ±.130 atm cm in total ozone determined by A, C and D pairs respectively.

The error for the double pair methods will be zero if the wavelength band separations are equal and the scattering is linear with wavelength. However, some non-linearity can be expected.

The extraterrestrial constants may be in error if the atmospheric attenuation changes during the period of their determination. The range in total ozone usually encountered during the type of day when determinations are made, will give a measure of the resulting error in total ozone.

The work of Thomas et al. (1974) shows that the effect of radiation scattered into the measurement beam by molecules and aerosols can be neglected for instrument fields of view of less than about 5^{o}.

It can be seen from the above that the total error in total ozone due solely to errors in the methods used is about ±5% to ±10% for the double pair method, and about ±20%, ±30% and ±50% for the A, C and D pair methods respectively.

Instrumental uncertainty will arise from uncertainty in the instrument's linearity, spectral constancy and ozone absorption coefficients. The first two items have been discussed in the previous section, 6.1, and should not cause total ozone errors of more than 1%.

The filter transmittance spectra used for the ozone absorption coefficient determinations are accurate to about .05 nm in wavelength and 0.5% in transmittance. The resulting uncertainties in the ozone absorption coefficients thus range from 0.5% to 1.0%. The linear corrections which account for the shift of the filter passbands with temperature are approximate (Section 8.4), and may result in a further 1% uncertainty in the coefficients depending on the particular

wavelength band, and the temperature range. The uncertainty in the bandwidth effect corrections is negligible.

The total instrumental uncertainty in total ozone determined by the AD double wavelength pair method is about 2%. This value will increase at extremes of airmass and temperature, while at very low light levels the uncertainty in the photomultiplier's dark current and the half integer uncertainty in the integer intensity measurements may become significant.

Experimental evidence of the instrument's accuracy and internal consistency is presented in Chapter 9, which describes a direct comparison of the filter spectrophotometer and a Dobson spectrophotometer.

6.3 Possible Improvements to the Instrument

The various steps toward improving the instrument's performance which are suggested throughout this and the preceding three chapters are brought together here, along with the sections in which they are mentioned.

Uncertainties due to optical non-uniformity across the filter surfaces (Section 4.4) can be reduced by placing the filters as close as possible to the photomultiplier, although this arrangement is less convenient mechanically than the present one. The same uncertainties can be further reduced by maintaining the speed of the filter-disc drive motor to within a few percent (Section 6.1).

A reduction of the field of view would reduce errors due to orientation effects (Section 4.5), but would require a corresponding improvement in the photometer's alignment accuracy, and would reduce its sensitivity for zenith sky

measurements.

Further investigation of the filters' long-term stability is needed (Section 4.6). Better filters may be available (Section 4.2) but are likely to be very expensive, and much the same is true of calibrating facilities. There is a need for a more accurate and detailed ozone absorption spectrum (Section 6.2).

Temperature control of the filters (Section 4.7) would remove the need for temperature corrections to total ozone. It might possibly be combined with refrigeration of the photomultiplier which would reduce the photomultiplier's dark current and stablise its cathode spectral sensitivity (Section 5.2), and thus improve the instrument's sensitivity, range and accuracy. It may be possible to devise a simple automatic mechanical system in which the effect of temperature on the filters is compensated for by a temperature-controlled tilting of the filters or filter disc (Section 4.7).

A high sensitivity, low dark current photomultiplier would improve the suitability of the instrument for zenith sky measurements and Umkehr measurements (Section 5.1). A seventh blanked filter channel to measure the dark current is suggested in Section 3.2, but might not be needed if a specially low dark current photomultiplier was used. Such tubes are available, although at higher cost (Section 5.1).

The photometer's range can be extended by modifying the photomultiplier's power supply to improve the photomultiplier linearity at high anode currents (Section 5.2). Lastly, the precision of the scan-period timing (Section 6.1) could be improved to advantage.

PART III: BANDWIDTH EFFECT

Preliminary Remarks

Part III is primarily a study of the so called 'Bandwidth Effect', using a mathematical model of the spectral characteristics of the total ozone measurement process.

The bandwidth effect results from a combination of two factors, firstly, the finite bandwidths which must be used for measuring the bands of solar radiation, and secondly, the variation in atmospheric attenuation across these bandwidths. It can be described as follows.

As the thickness of the attenuating atmosphere increases, i.e. as the airmass increases, the more strongly attenuated parts of the passband spectrum are selectively removed and the passband becomes more and more dominated by the less strongly attenuated parts. Hence the average attenuation coefficients for the filter passband must change with airmass, decreasing in favour of the less strongly absorbed radiation. If fixed coefficients are used, as is usual, the effect shows up as a reduction in total ozone with airmass.

The behaviour of the filter and its sideband leakage which is discussed in Chapter 2 falls within the above simple description, although in this case, the less attenuated part of the filter spectrum is actually the sideband leakage. Clearly the effect can be generalised beyond the simple idea of a finite bandwidth passband, and extended to any spectral transmittance function.

The mathematical theory for this is developed in Chapter 7, starting from the basic monochromatic attenuation equation,

equation 1.6. It applies specifically to direct sun measurements and does not include any account of the effects of radiation scattered into the measured beam, even though in some situations such effects may be large (Thomas et al., 1974).

The main aim of the theory is to define 'equivalent attenuation coefficients', $\bar{\alpha}$, $\bar{\beta}$ and $\bar{\delta}$, which can be used directly in an attenuation equation similar to the monochromatic form, equation 1.6. These new coefficients are not constant, however, but are functions of the spectral transmittance function used, and of the atmospheric airmass, total ozone, and aerosols. A feature of the theory is the treatment of the aerosol scattering coefficient as a linear function of wavelength.

After the bulk of the theory had been completed, the author became aware of a similar study by Vanier and Wardle (1969) in which the bandwidth effect on the Dobson instrument, a stellar spectrophotometer, and the broadband M83 filter instrument was evaluated. They define equivalent attenuation coefficients $\bar{\alpha}$ and $\bar{\beta}$ similar to those derived in Section 7.1 and come to much the same conclusions with respect to the Dobson instrument.

In contrast to Vanier and Wardle's work, the present study concentrates on the narrowband interference filters used by the author, and on the variation of the filters' full spectral characteristics. Also, an attempt is made here to account for aerosol scattering, which they omit, and an experimentally measured solar irradiance spectrum is used.

Chapter 8 presents the results of calculations which were made using a computer simulation based on the theory of Chapter 7. The main topics covered are: the variation of the filters' spectral characteristics; the variation of the equivalent attenuation coefficients; and the effect of pass-band shifting on the equivalent attenuation coefficients. Each is considered as a function of atmospheric attenuation.

The emphasis of the calculations is on relative variations of the filters' spectral characteristics and coefficients, rather than on absolute values. Attention is given in Appendix G to the accuracies of the model's various input data, which are adequate for these calculations, but for the calculation of absolute, or reference values, it would be desirable to try to improve the accuracies, especially that of the ozone absorption coefficient near the passbands.

CHAPTER 7: SPECTRAL MEASUREMENT THEORY

7.1 Derivation and Discussion of the Broad-Band Equivalent Attenuation Coefficients

The total electrical response, P, of the photometer for a measurement of direct sunlight, can be expressed as an integral over wavelength, λ, of $Q(\lambda)$, the spectral response function for that measurement. Hence

$$P = \int_{\lambda_a}^{\lambda_b} Q(\lambda)d\lambda \tag{7.1}$$

where λ_a and λ_b are limits outside of which the integral is negligible.

The spectral response function, $Q(\lambda)$, is the electrical response per unit wavelength, at wavelength λ, for the particular instrument and atmosphere. Following the monochromatic theory of Section 1.2, and of equation 1.6 in particular, $Q(\lambda)$ is defined as

$$Q(\lambda) = Q_\infty(\lambda)\exp -[\mu_h X\alpha(\lambda) + \mu_m\beta(\lambda) + \mu\delta(\lambda)] \tag{7.2}$$

where $Q_\infty(\lambda)$ is the spectral response function outside the atmosphere and hence is called the extraterrestrial spectral response function. The other terms are defined in Section 1.2, and account for atmosphere's attenuation at wavelength λ.

The extraterrestrial response can be written in terms of the spectral properties of the extraterrestrial solar radiation and the instrument's filters and detector. Thus

$$Q_\infty(\lambda) = qU(\lambda)F(\lambda)S(\lambda)D(\lambda) \tag{7.3}$$

where q = unknown factor accounting for non-spectral effects, e.g. aperture sizes, detector gain, etc.

$U(\lambda)$ = extraterrestrial solar irradiance at λ

$F(\lambda)$ = interference filter transmittance at λ

$S(\lambda)$ = blocking filter transmittance at λ

$D(\lambda)$ = detector (photomultiplier) relative spectral sensitivity at λ.

At this point, in order to simplify equations (7.1) and (7.2), wavelength independent "equivalent attenuation coefficients" are introduced to replace the spectral coefficients $\alpha(\lambda)$, $\beta(\lambda)$ and $\delta(\lambda)$. Combining equations (7.1) and (7.2) gives

$$P = \int_{\lambda_a}^{\lambda_b} Q_\infty(\lambda)\ \exp-[\mu_h X\alpha(\lambda) + \mu_m\beta(\lambda) + \mu\delta(\lambda)]d\lambda \tag{7.4}$$

which can be written as

$$P = \exp-(\mu_h X\bar{\alpha}) \int_{\lambda_a}^{\lambda_b} Q_\infty(\lambda)\exp-[\mu_m\beta(\lambda) + \mu\delta(\lambda)]d\lambda \tag{7.5}$$

to define $\bar{\alpha}$ the "equivalent ozone absorption coefficient".

Hence, by equating equations (7.4) and (7.5) $\bar{\alpha}$ can be expressed as

$$\bar{\alpha} = \frac{-1}{\mu_h X} \ln \frac{\int_{\lambda_a}^{\lambda_b} Q_\infty(\lambda)\exp-[\mu_h X\alpha(\lambda)+\mu_m\beta(\lambda)+\mu\delta(\lambda)]d\lambda}{\int_{\lambda_a}^{\lambda_b} Q_\infty(\lambda)\exp-[\mu_m\beta(\lambda)+\mu\delta(\lambda)]d\lambda} \tag{7.6}$$

Similarly, $\beta(\lambda)$ can be replaced by an "equivalent molecular scattering coefficient", $\bar{\beta}$, so that equation (7.5) becomes

$$P = \exp-(\mu_h X\bar{\alpha}+\mu_m\bar{\beta})\int_{\lambda_a}^{\lambda_b} Q_\infty(\lambda)\ \exp-[\mu\delta(\lambda)]\,d\lambda \qquad (7.7)$$

which, when equated with equation (7.5) yields

$$\bar{\beta} = \frac{-1}{\mu_m}\ln\frac{\int_{\lambda_a}^{\lambda_b} Q_\infty(\lambda)\exp-[\mu_m\beta(\lambda)+\mu\delta(\lambda)]\,d\lambda}{\int_{\lambda_a}^{\lambda_b} Q_\infty(\lambda)\exp-[\mu\delta(\lambda)]\,d\lambda} \qquad (7.8)$$

Lastly, $\delta(\lambda)$ can be replaced by an "equivalent aerosol scattering coefficient" $\bar{\delta}$, and thus equation (7.7) becomes

$$P = \exp-(\mu_h X\bar{\alpha} + \mu_m\bar{\beta} + \mu\bar{\delta})\int_{\lambda_a}^{\lambda_b} Q_\infty(\lambda)\,d\lambda \qquad (7.9)$$

Equating (7.7) and (7.9) gives

$$\bar{\delta} = \frac{-1}{\mu}\ln\frac{\int_{\lambda_a}^{\lambda_b} Q_\infty(\lambda)\ \exp-[\mu\delta(\lambda)]\,d\lambda}{\int_{\lambda_a}^{\lambda_b} Q_\infty(\lambda)\,d\lambda} \qquad (7.10)$$

The usefulness of these equivalent attenuation coefficients will be seen from consideration of equation (7.9). The integral term in this equation is just the value of P when $\mu_h = \mu_m = \mu = 0$, i.e. outside the atmosphere, and therefore can be written as

$$\int_{\lambda_a}^{\lambda_b} Q_\infty(\lambda)\,d\lambda = P_\infty \qquad (7.11)$$

where P_∞ is called the extraterrestrial total response (c.f. equation 7.1). Equation (7.9) thus becomes

$$P = P_{\infty} \exp-(\mu_h X\bar{\alpha} + \mu_m\bar{\beta} + \mu\bar{\delta}) \qquad (7.12)$$

This is the equation which describes the measurement P using any shape of filter, yet it is in the form of equation 1.6 which describes the monochromatic case. Therefore, provided the coefficients $\bar{\alpha}$, $\bar{\beta}$ and $\bar{\delta}$ are known, equation (7.12) can be used to determine the total ozone in just the same way as is equation (1.6).

The equivalent attenuation coefficients are averages for the filter passband specified by the transmittance spectrum $F(\lambda)$, and can be calculated from equations (7.6), (7.8) and (7.10). They are not simple means, however, and they are dependent on the airmass, total ozone and atmospheric aerosol content. The dependence on total ozone implies that, in order to use the coefficients for the determination of total ozone, it may be necessary to iteratively calculate the coefficients and the total ozone. Only one iteration is needed for the narrow transmittance bands of the filter and Dobson instruments.

Of all the constituents of the equations, only the aerosol scattering coefficient $\delta(\lambda)$ is difficult to determine. Consideration is given to this point in Section 7.2.

It should be noted that the coefficients $\bar{\alpha}$, $\bar{\beta}$ and $\bar{\delta}$ can be extracted from equation (7.4) in any order, and that consequently, each order will have a different set of equations to define its particular set of coefficients $\bar{\alpha}$, $\bar{\beta}$ and $\bar{\delta}$. For example, if $\bar{\delta}$ was extracted first, it would be defined by an equation similar to equation (7.6), and if $\bar{\alpha}$ was extracted last, it would be defined by an equation similar to (7.10).

The advantage of the present order of extraction is that the most rapidly varying component, $\alpha(\lambda)$, the ozone absorption coefficient, appears in only one expression, in equation (7.6) for $\bar{\alpha}$, and hence that variations due to the bandwidth effect are largely confined to this expression. It will be shown later (Section 8.3) that the variable aerosol scattering coefficient $\delta(\lambda)$ does not have a significant effect on $\bar{\alpha}$ and $\bar{\beta}$ as defined.

7.2 Spectrally Linear Aerosol Scattering, Application to Monochromatic Total Ozone Theory

Although in principle the aerosol scattering coefficient, $\delta(\lambda)$, can be calculated from the Mie theory, the necessary aerosol characteristics of composition, number and size distribution are highly variable and usually unknown. It is, however, believed that the coefficient is approximately linear with wavelength.

Recently, Rat'kov (1971) experimentally confirmed the linearity, which has long been a basic assumption of the Dobson total ozone formulation, and showed that the gradient of the scattering coefficient with wavelength can be determined from the standard Dobson spectrophotometer measurements, or their equivalent. A summary of his analysis follows.

He begins by separating the aerosol component of equation (1.7) into

$$X = X^* - \frac{\mu[\delta(\lambda_1)-\delta(\lambda_2)]}{\mu_h[\alpha(\lambda_1)-\alpha(\lambda_2)]} \qquad (7.13)$$

where

$$X^* = \frac{\ln[P_\infty(\lambda_1)/P_\infty(\lambda_2)] - \ln[P(\lambda_1)/P(\lambda_2)] - \mu_m[\beta(\lambda_1) - \beta(\lambda_2)]}{\mu_h[\alpha(\lambda_1) - \alpha(\lambda_2)]} \tag{7.14}$$

is the usual total ozone value calculated from a single pair of wavelength bands when the effects of aerosols are neglected.

If $\delta(\lambda)$ is linear with wavelength, then since the separations $\lambda_1 - \lambda_2$ are approximately equal for the standard slitband pairs of the Dobson spectrophotometer, the term $\delta(\lambda_1) - \delta(\lambda_2)$ should be a constant for these pairs. Hence, if measurements of X* are made with the pairs and plotted against $\alpha(\lambda_1) - \alpha(\lambda_2)$, a straight line should result. (The ratio μ/μ_h is set equal to 1.) In addition, the intercept of the line will give the true total ozone value X.

Rat'kov did this for the standard A, B, C and D wavelength pairs of a Dobson instrument and found that the points approximated straight lines to an excellent degree in 80% of the 1000 cases considered. This gives very good support to the linear aerosol scattering hypothesis, i.e. to

$$\delta(\lambda) = \delta_0 + g\lambda \tag{7.15}$$

in the spectral region of 300 nm to 340 nm, where δ_0 is a constant and g is the gradient of the aerosol scattering.

Although Rat'kov does not do so, it is possible to develop the mathematics a little further to produce correct expressions for both total ozone and the aerosol scattering gradient. Inserting equation (7.15) into equation (7.13) gives

$$X^* = X + \frac{g\mu[\lambda_1-\lambda_2]}{\mu_h[\alpha(\lambda_1)-\alpha(\lambda_2)]} \tag{7.16}$$

Since this is a straight line equation of X^* against $\mu[\lambda_1-\lambda_2]/\mu_h[\alpha(\lambda_1)-\alpha(\lambda_2)]$, its intercept X (the true total ozone) and gradient g (the aerosol scattering gradient) can be determined from just two points, i.e. from the measurements of X^* for two wavelength pairs.

To enable the expressions for X and g to be more concisely stated, the following commonly used notation is introduced. The parameters of one wavelength pair, A say, are written

$$\begin{aligned} L_{\infty A} &= \ln [P_\infty(\lambda_1)/P_\infty(\lambda_2)] \\ L_A &= \ln [P(\lambda_1)/P(\lambda_2)] \\ \Delta\alpha_A &= \alpha(\lambda_1) - \alpha(\lambda_2) \\ \Delta\beta_A &= \beta(\lambda_1) - \beta(\lambda_2) \\ \Delta\delta_A &= \delta(\lambda_1) - \delta(\lambda_2) \\ \Delta\lambda_A &= \lambda_1 - \lambda_2 \end{aligned} \tag{7.17}$$

For a second wavelength pair, D say, at wavelengths λ_3 and λ_4, similar expressions hold.

Equation (7.16) now becomes, for the A and D wavelength pairs,

$$X_A^* = X + \frac{g\mu\Delta\lambda_A}{\mu_h\Delta\alpha_A} \tag{7.18}$$

and

$$X_D^* = X + \frac{g\mu\Delta\lambda_D}{\mu_h\Delta\alpha_D} \tag{7.19}$$

Eliminating g from equations (7.18) and (7.19) gives

$$X = \left[\frac{\Delta\lambda_A}{\Delta\alpha_A} X_D^* - \frac{\Delta\lambda_D}{\Delta\alpha_D} X_A^*\right] / \left[\frac{\Delta\lambda_A}{\Delta\alpha_A} - \frac{\Delta\lambda_D}{\Delta\alpha_D}\right] \tag{7.20}$$

while eliminating X gives

$$g = \mu_h\left[X_A^* - X_D^*\right] / \mu\left[\frac{\Delta\lambda_A}{\Delta\alpha_A} - \frac{\Delta\lambda_D}{\Delta\alpha_D}\right] \tag{7.21}$$

Using equation (7.14) to express X_A^* and X_D^* yields

$$X = \frac{(L_{\infty A} - L_A - \mu_m\Delta\beta_A)/\Delta\lambda_A - (L_{\infty D} - L_D - \mu_m\Delta\beta_D)/\Delta\lambda_D}{\mu_h(\Delta\alpha_A/\Delta\lambda_A - \Delta\alpha_D/\Delta\lambda_D)} \tag{7.22}$$

and

$$g = \frac{(L_{\infty A} - L_A - \mu_m\Delta\beta_A)\Delta\alpha_D - (L_{\infty D} - L_D - \mu_m\Delta\beta_D)\Delta\alpha_A}{\mu(\Delta\lambda_A\Delta\alpha_D - \Delta\lambda_D\Delta\alpha_A)} \tag{7.23}$$

These expressions account for the assumption of a linear aerosol in the monochromatic passband theory. The assumption can be applied to the broad-passband theory as is shown in the next section.

7.3 Application of Linear Aerosol Scattering Hypothesis to the Broadband Theory

If the aerosol scattering coefficient is linear with wavelength, then the equivalent attenuation coefficients can be simplified and expressed in terms of the gradient of the aerosol scattering coefficient. Inserting equation (7.15) into equations (7.6), (7.8) and (7.10) gives, respectively,

$$\bar{\alpha} = \frac{-1}{\mu_h X} \ln \frac{\int_{\lambda_a}^{\lambda_b} Q_\infty(\lambda) \exp-[\mu_h X \alpha(\lambda) + \mu_m \beta(\lambda) + \mu g \lambda] d\lambda}{\int_{\lambda_a}^{\lambda_b} Q_\infty(\lambda) \exp-[\mu_m \beta(\lambda) + \mu g \lambda] d\lambda} \tag{7.24}$$

$$\bar{\beta} = \frac{-1}{\mu_m} \ln \frac{\int_{\lambda_a}^{\lambda_b} Q_\infty(\lambda) \exp-[\mu_m \beta(\lambda) + \mu g \lambda] d\lambda}{\int_{\lambda_a}^{\lambda_b} Q_\infty(\lambda) \exp-[\mu g \lambda] d\lambda} \tag{7.25}$$

$$\bar{\delta} = \delta_0 - \frac{1}{\mu} \ln \frac{\int_{\lambda_a}^{\lambda_b} Q_\infty(\lambda) \exp-[\mu g \lambda] d\lambda}{\int_{\lambda_a}^{\lambda_b} Q_\infty(\lambda) d\lambda} \tag{7.26}$$

The δ_0 term in equation (7.15) cancels out in equations (7.24) and (7.25), but remains in (7.26). It is not a problem there since it is eliminated in the total ozone determination where the difference of two coefficients is used.

The linearity of aerosol scattering can be extended to the equivalent aerosol scattering coefficient if the idea of a filter's "equivalent centre wavelength", $\bar{\lambda}$, is introduced. In

analogy with equation (7.15), $\bar{\lambda}$ is defined by

$$\bar{\delta} = \bar{\delta}_o + g\bar{\lambda} \tag{7.27}$$

where $\bar{\delta}_0$ is a constant at any time, and g is the same gradient as in equation (7.15). Therefore, for two filters, 1 and 2,

$$\bar{\delta}_1 - \bar{\delta}_2 = g(\bar{\lambda}_1 - \bar{\lambda}_2) \tag{7.28}$$

which implies that whatever bandwidth effect there is in the equivalent scattering coefficients, can be represented by the equivalent centre wavelength separation. The separation can be expressed in terms of equations (7.28) and (7.26) as

$$\bar{\lambda}_1 - \bar{\lambda}_2 = \frac{1}{\mu g} \ln \frac{\int_{\lambda_a}^{\lambda_b} Q_{\infty_2}(\lambda)\exp-[\mu g\lambda]d\lambda \int_{\lambda_a}^{\lambda_b} Q_{\infty_1}(\lambda)d\lambda}{\int_{\lambda_a}^{\lambda_b} Q_{\infty_2}(\lambda)d\lambda \int_{\lambda_a}^{\lambda_b} Q_{\infty_1}(\lambda)\exp-[\mu g\lambda]d\lambda} \tag{7.29}$$

As can be seen from this equation, the separation $\bar{\lambda}_1 - \bar{\lambda}_2$ does not include the effects of ozone absorption or molecular scattering. It therefore does not represent the separation of the mean centre wavelengths of the passbands' spectral response functions, $Q(\lambda)$.

The calculation of the equivalent attenuation coefficients, using equations (7.24), (7.25) and (7.26), and of the equivalent centre wavelength separation, using equation (7.29), is described in Section 8.3.

The expressions for total ozone, X, and aerosol scattering gradient, g, using this broadband filter theory,

can now be found by analogy with the monochromatic theory of the last section, Section 7.2.

The equation of a filter measurement, equation (7.12), can be written down for two filters and subtracted in the usual way to give

$$X = \frac{\ln[P_{\infty_1}/P_{\infty_2}] - \ln[P_1/P_2] - \mu_m[\bar{\beta}_1-\bar{\beta}_2] - \mu[\bar{\delta}_1-\bar{\delta}_2]}{\mu_h[\bar{\alpha}_1-\bar{\alpha}_2]} \quad (7.30)$$

where the subscripts refer to each of the two filters.

Equation (7.30) is identical in form to equation (1.7) for the monochromatic measurements, and hence can be split up, as is equation (1.7), to become similar to equations (7.13) and (7.14). The aerosol scattering linearity of equation (7.15) has its equivalent in equation (7.27). As in equation (7.17), a more compact notation can be introduced where

$$\begin{aligned} L_{\infty_A} &= \ln [P_{\infty_1}/P_{\infty_2}] \\ L_A &= \ln [P_1/P_2] \\ \Delta\bar{\alpha}_A &= \bar{\alpha}_1-\bar{\alpha}_2 \\ \Delta\bar{\beta}_A &= \bar{\beta}_1-\bar{\beta}_2 \\ \Delta\bar{\lambda}_A &= \bar{\lambda}_1-\bar{\lambda}_2 \end{aligned} \quad (7.31)$$

and where similar expressions can be written for a second wavelength pair, D, at λ_3 and λ_4.

Therefore, by purusing the method of Section 7.2, it is possible to arrive at the following expressions for total ozone, X, and aerosol scattering gradient, g, as determined

with double-pair broadband filter measurements

$$X = \frac{(L_{\infty_A} - L_A - \mu_m \Delta\bar{\beta}_A)/\Delta\bar{\lambda}_A - (L_{\infty_D} - L_D - \mu_m \Delta\bar{\beta}_D)/\Delta\bar{\lambda}_D}{\mu_h(\Delta\bar{\alpha}_A/\Delta\bar{\alpha}_A - \Delta\bar{\alpha}_D/\Delta\bar{\lambda}_D)} \tag{7.32}$$

$$g = \frac{(L_{\infty_A} - L_A - \mu_m \Delta\bar{\beta}_A)\Delta\bar{\alpha}_D - (L_{\infty D} - L_D - \mu_m \Delta\bar{\beta}_D)\Delta\bar{\alpha}_A}{\mu(\Delta\bar{\lambda}_A \Delta\bar{\alpha}_D - \Delta\bar{\lambda}_D \Delta\bar{\alpha}_A)} \tag{7.33}$$

These are the final expressions for X and g and account for both the bandwidth effect and the linear aerosol scattering assumption. However, there are several more points about this theory which bear mentioning.

The extraterrestrial constants (e.g. $L_{\infty_A} = \ln[P_{\infty_1}/P_{\infty_2}]$), are usually determined experimentally (see Section 1.2), but can in fact by calculated directly from equations (7.3) and (7.11). If they are determined experimentally, the raw intensity data must be corrected to account for the changing equivalent attenuation coefficients in equation (7.30).

The reason for initially taking a pair of filters (or slitbands, as in the case of the Dobson instrument) is made clear from a consideration of the extraterrestrial constant. The use of a single filter would require that P_∞ (in equation (7.12)) be known, but from its definition, equations (7.11) and (7.3), it can be seen to contain a factor q which is usually unknown. However, since q is common to all filter passbands, it can be eliminated in the ratio $P_{\infty_1}/P_{\infty_2}$ when two passbands are used.

This method of comparative photometry is built into the Dobson instrument through its null measurement system. The filter instrument, on the other hand, measures individual

intensities, and so with suitable calibration to find q, it could be used to find individual passband attenuations, and therefore the aerosol scattering constant $\bar{\delta}_0$ in equation (7.27).

The final point is that the theory need not be restricted to the standard wavelength pairs used with the Dobson instrument. The reduction of total ozone and aerosol scattering gradient requires measurements on either three or four wavelength bands, and the bands can have any wavelength separation.

7.4 Relationship of Broadband Theory and Dobson Instrument Total Ozone Theory

The bandwidth theory of the preceding sections can be applied to the Dobson instrument, provided equation (7.3) is restated in terms of the instrument's slitbands, blocking filters, and detector. Hence its equivalent attenuation coefficients can be calculated.

The usual total ozone formulation for the Dobson instrument is an approximation to this theory. For example, the attenuation coefficients usually used are means of the spectral coefficients weighted by the slitband transmittance functions, as in

$$\alpha_0 = \frac{\int_{\lambda_a}^{\lambda_b} F(\lambda)\alpha(\lambda)d\lambda}{\int_{\lambda_a}^{\lambda_b} F(\lambda)d\lambda} \qquad (7.34)$$

These means would be more accurate if weighted by the extra-

terrestrial response function, $Q_\infty(\lambda) = qU(\lambda)F(\lambda)S(\lambda)D(\lambda)$, i.e.

$$\alpha_0 = \frac{\int_{\lambda_a}^{\lambda_b} Q_\infty(\lambda)\alpha(\lambda)d\lambda}{\int_{\lambda_a}^{\lambda_b} Q_\infty(\lambda)d\lambda} \qquad (7.35)$$

But it is shown in Appendix I that α_0 is simply the limit of $\bar{\alpha}$, the equivalent attenuation coefficient, when the airmass tends to zero. The coefficients α_0 and β_0 are therefore called "extraterrestrial attenuation coefficients".

The assumption that the scattering coefficient difference, $\delta_i - \delta_j$, is equal for all the standard pairs of wavelengths, necessary for the double pair method of total-ozone determination, only approximates the aerosol linearity, equation (7.15), since it also implies that the band separations, $\lambda_i - \lambda_j$, are equal for all the pairs.

The usual expression for total ozone determined from the A and D wavelength pairs

$$X = \frac{(L_{\infty_A} - L_A - \mu_m \Delta\beta_A) - (L_{\infty_D} - L_D - \mu_m \Delta\beta_D)}{\mu_h(\Delta\alpha_A - \Delta\alpha_D)} \qquad (7.36)$$

is just the simplification of equation (7.32) when the wavelength separations $\Delta\lambda_A$ and $\Delta\lambda_D$ are assumed equal, and the extraterrestrial attenuation coefficients are used.

The difference between the Dobson instrument's extraterrestrial attenuation coefficients, e.g. α_0, and equivalent attenuation coefficients, e.g. $\bar{\alpha}$, are calculated in Section 8.3. The error in total ozone caused by assuming $\Delta\lambda_A$ and $\Delta\lambda_D$

to be equal can be assessed in the following manner.

Equation (7.16) can be written for the A and D wavelength pairs as

$$\Delta\alpha_A X_A^* = \Delta\alpha_A X + \mu g \Delta\lambda_A / \mu_h \tag{7.37}$$

$$\Delta\alpha_D X_D^* = \Delta\alpha_D X + \mu g \Delta\lambda_D / \mu_h \tag{7.38}$$

Subtracting and solving for X gives

$$X = \frac{\Delta\alpha_A X_A^* - \Delta\alpha_D X_D^*}{\Delta\alpha_A - \Delta\alpha_D} - \frac{\mu g (\Delta\lambda_A - \Delta\lambda_D)}{\mu_h (\Delta\alpha_A - \Delta\alpha_D)} \tag{7.39}$$

If $\Delta\lambda_A$ and $\Delta\lambda_D$ are assumed equal, the last term of equation (7.39) disappears. But the remaining first term is simply the usual expression for total ozone, equation (7.36) (for definition of X*, see equation (7.14)). The second term is therefore the error in total ozone caused by assuming $\Delta\lambda_A$ and $\Delta\lambda_D$ to be equal. Note that the error is essentially independent of airmass.

From Rat'kov (1971) the aerosol gradient can be found to range between ± 0.0025 nm^{-1}, and from the Dobson instrument handbook (1957) $\Delta\lambda_A - \Delta\lambda_D = -2.3$ nm, and $\Delta\alpha_A - \Delta\alpha_D = 1.385$ (atm cm)$^{-1}$. Hence the maximum likely range of error in total ozone is ± 0.004 atm cm. This is equivalent to about $\pm 1\%$ to 2% of usual total ozone values.

CHAPTER 8: MEASUREMENT SIMULATION

8.1 Computer Model and Input Data

A computer model was set up to simulate the measurement process described in Chapter 7. This section contains only a general outline of the model but detailed consideration is given to the sources and accuracies of the model's components in Appendix G.

Calculations have been made for single filters, doubled filters, and for the Dobson spectrophotometer slitbands. Section 8.2 describes their spectral characteristics for various atmospheric conditions, while Section 8.3 discusses their equivalent attenuation coefficients. Section 8.4 is devoted to the effects of the passband shifting mentioned in Chapter 4, and Section 8.5 contains concluding remarks on this and the preceding chapter.

Each of the spectral variables in equations (7.2) and (7.3) is converted to equal interval spectra of 500, 0.2 nm spaced points, bounded by λ_a = 290 nm and λ_b = 390 nm. The 0.2 nm wavelength interval, $d\lambda$, is smaller than the characteristic detail of the ozone absorption spectrum, which largely controls the bandwidth effect, although it is large compared to the very fine detail in the solar irradiance spectrum.

Experimental determinations of the solar irradiance, $U(\lambda)$, and the ozone absorption, $\alpha(\lambda)$, as reported in the literature, are used, and are accurate to about 10% and 1% respectively. The interference filter and blocking filter transmittance spectra, $F(\lambda)$ and $S(\lambda)$, were measured by the

author (see Appendix A), and are accurate to about 1% in the important spectral regions. The detector sensitivity, $D(\lambda)$, and the molecular scattering coefficient, $\beta(\lambda)$, both of which are smooth and vary relatively slowly in the integration domain, are described by analytic functions. The aerosol scattering coefficient, $\delta(\lambda)$, is approximated by the linear function, equation (7.15). Unless otherwise indicated, the ratios μ_h, μ_m and μ are set equal and are collectively called the airmass, μ.

Graphs of the spectra are to be found as follows: $U(\lambda)$ figure 8.1, $\alpha(\lambda)$ figure 8.3, $F(\lambda)$ figures 4.1 to 4.6, $S(\lambda)$ figure 4.10, $D(\lambda)$ and $\beta(\lambda)$ figure 8.2.

Although a great deal of time was used in measuring the filter spectra and producing the equal interval spectra, the calculations themselves required little computer time. The fifteen or so separate programmes that were completed consumed, in total, less than 1500 seconds of Burroughs B6700 central processor time.

8.2 Filter and Slitband Spectral Characteristics, Variation with Atmospheric Attenuation

A very good qualitative understanding of the bandwidth effect, and the measurement process in general, can be gained from a study of the spectral response of the sun-atmosphere-photometer system. To this end, figures 8.4 to 8.10 are presented, in which the spectral responses of the 305 nm and 340 nm filters, and of the Dobson instrument slitbands, under various conditions are shown.

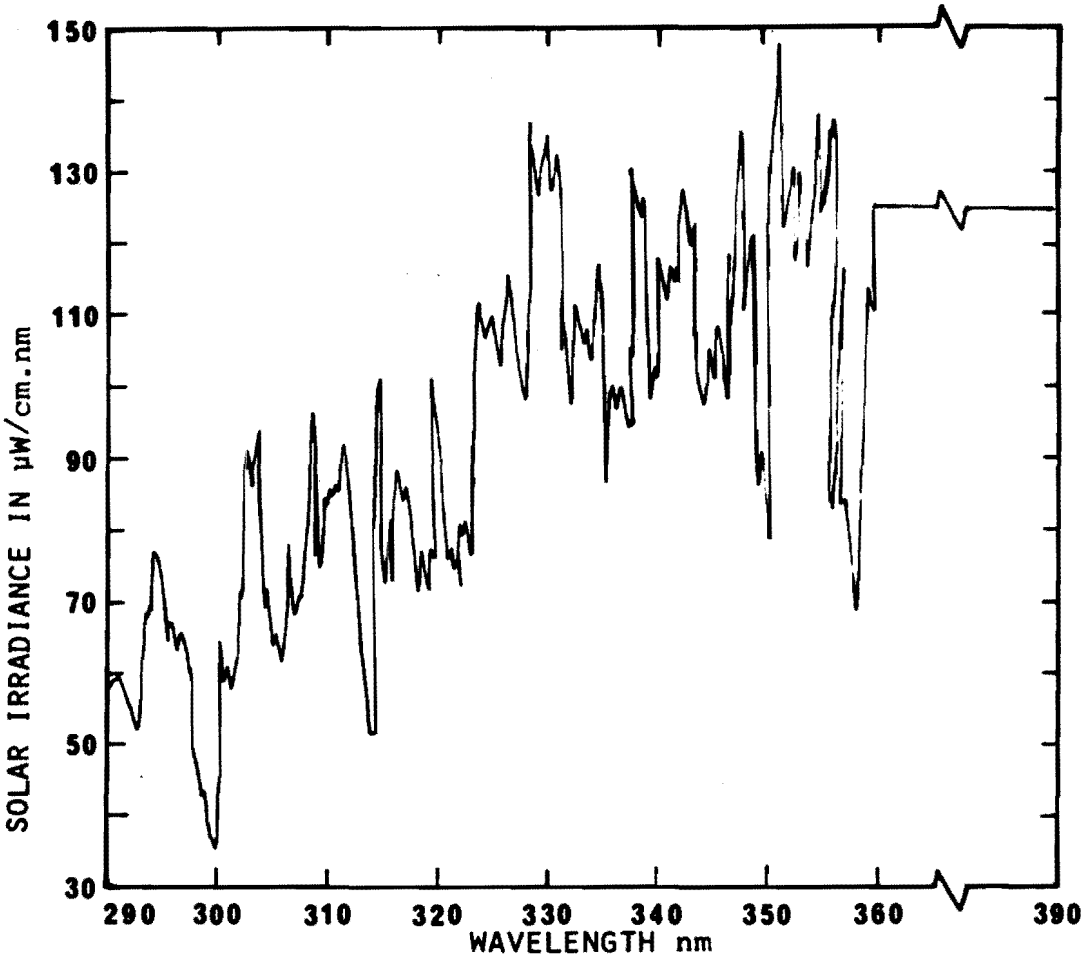

FIG.8.1 SMOOTHED SOLAR IRRADIANCE SPECTRUM, U(λ)

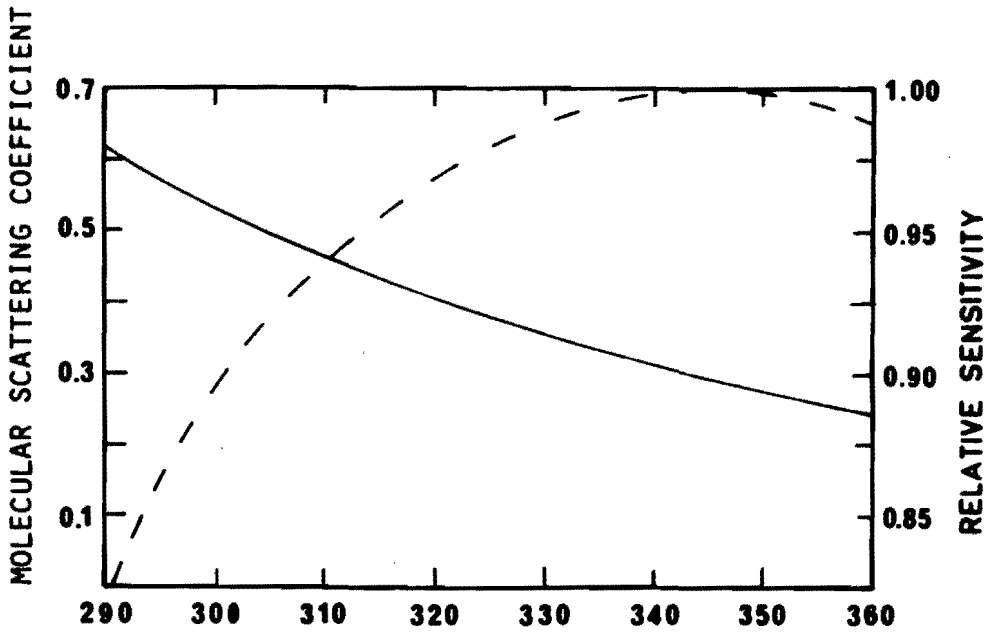

FIG.8.2 MOLECULAR SCATTERING COEFFICIENT SPECTRUM, β(λ), ——

PHOTOMULTIPLIER RELATIVE SENSITIVITY SPECTRUM, D(λ), --

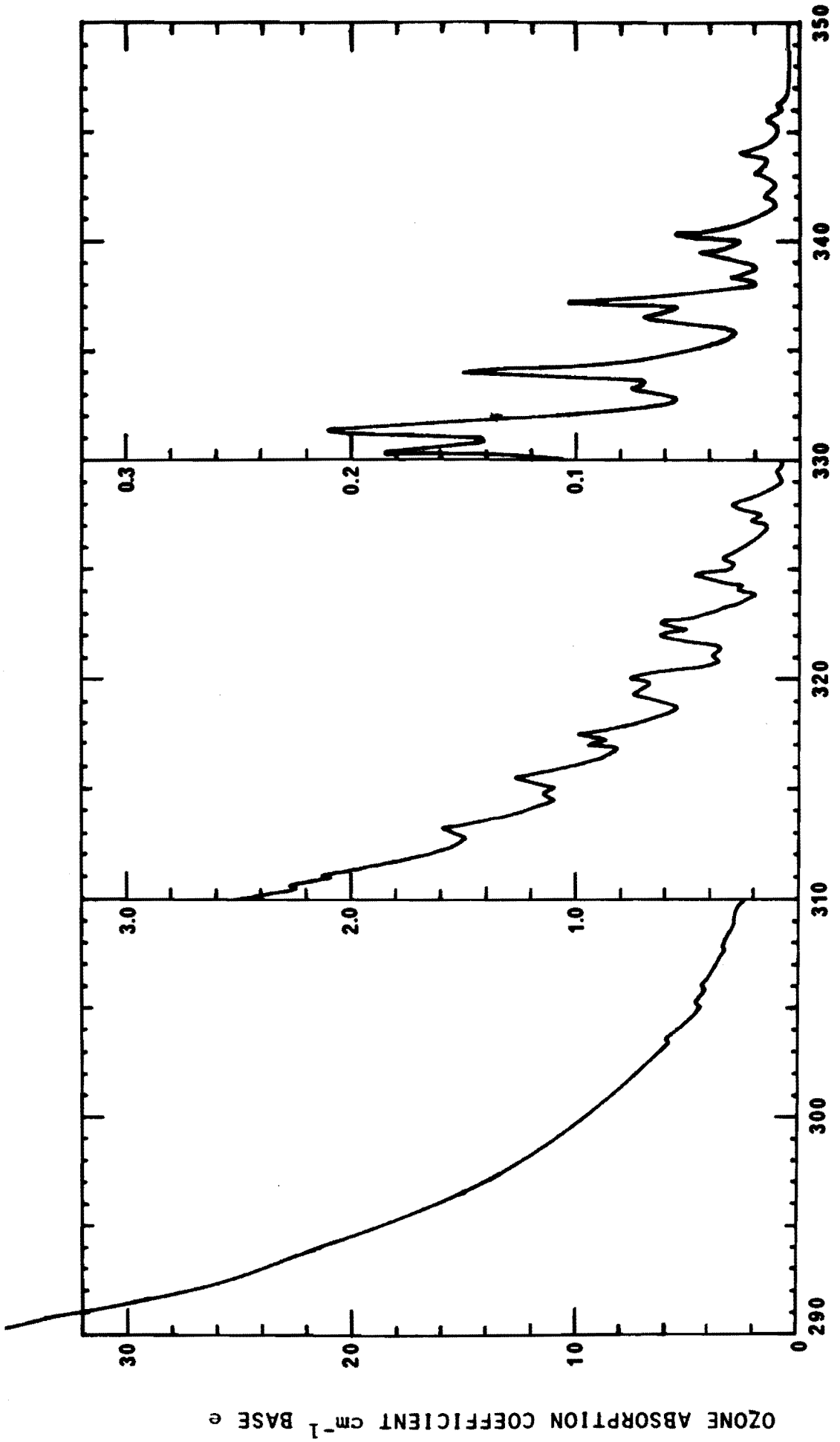

FIG.8.3 ABSORPTION SPECTRUM FOR OZONE, $\alpha(\lambda)$, AT 229°K

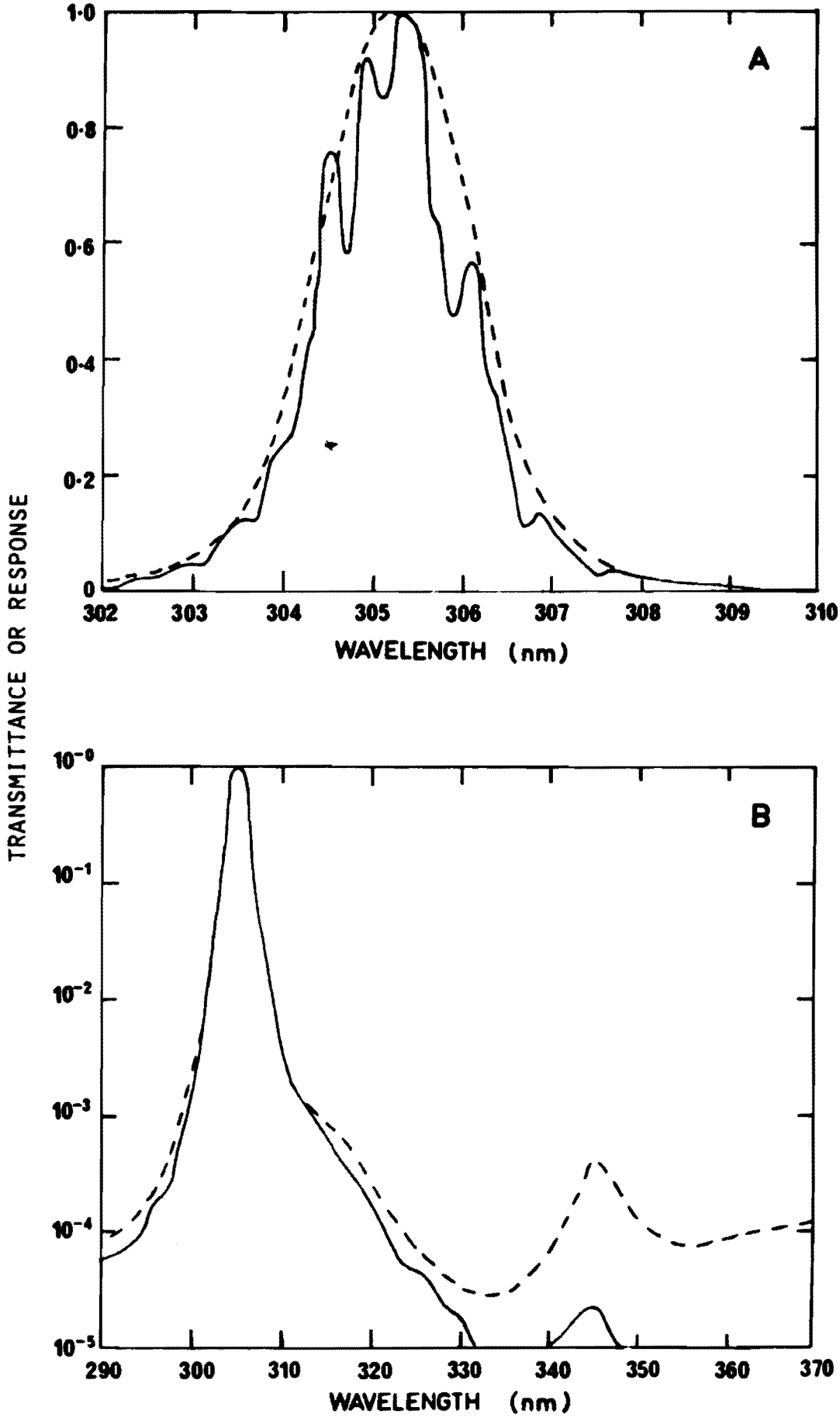

FIG. 8·4 305 nm SINGLE FILTER
NORMALISED SPECTRA OF TRANSMITTANCE, $F(\lambda)$---,
AND EXTRATERRESTRIAL RESPONSE, $Q^{\infty}(\lambda)$ ——

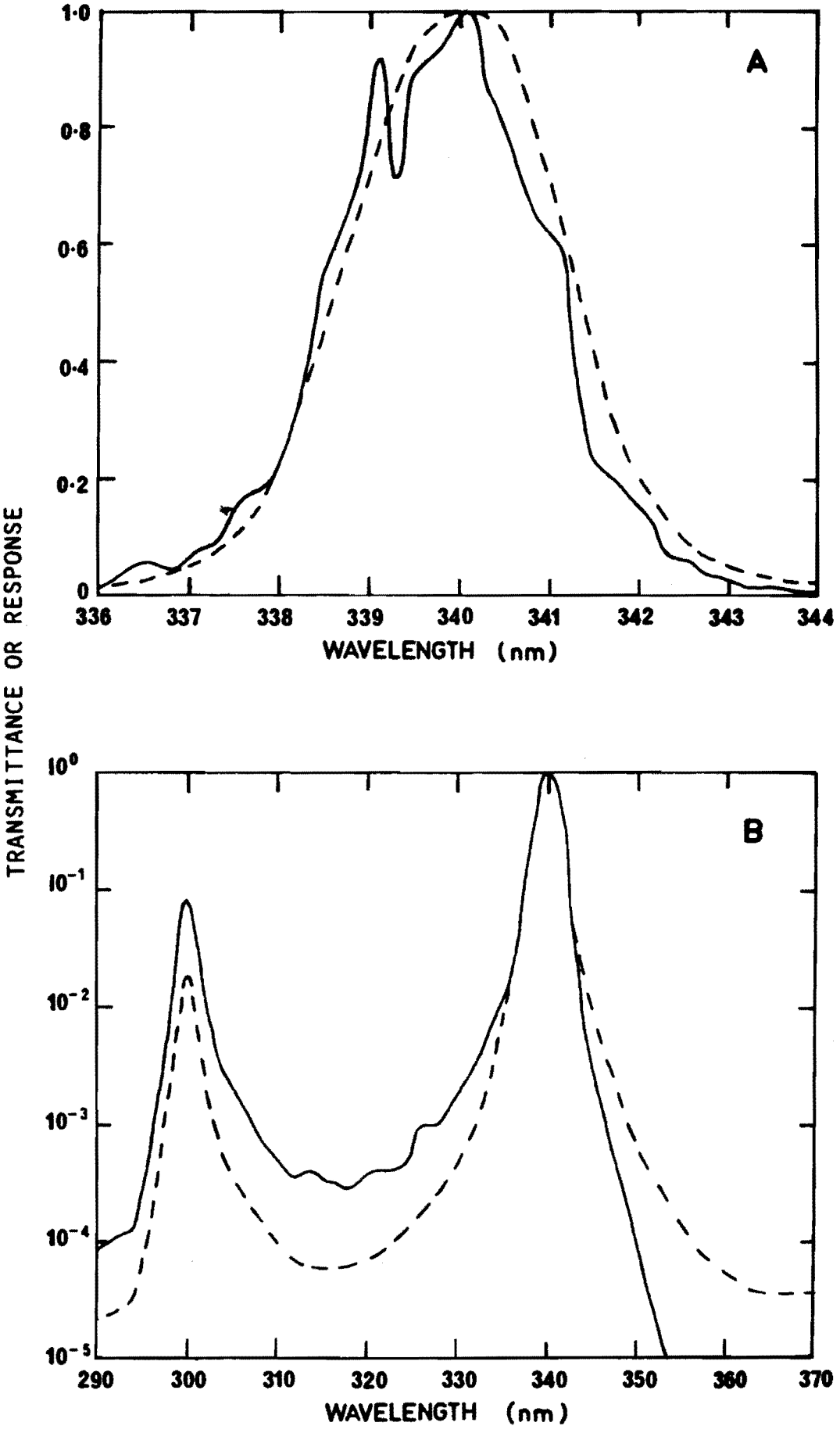

FIG. 8·5 340 nm SINGLE FILTER
NORMALISED SPECTRA OF TRANSMITTANCE, $F(\lambda)$---,
AND EXTRATERRESTRIAL RESPONSE, $Q^{\infty}(\lambda)$ ——

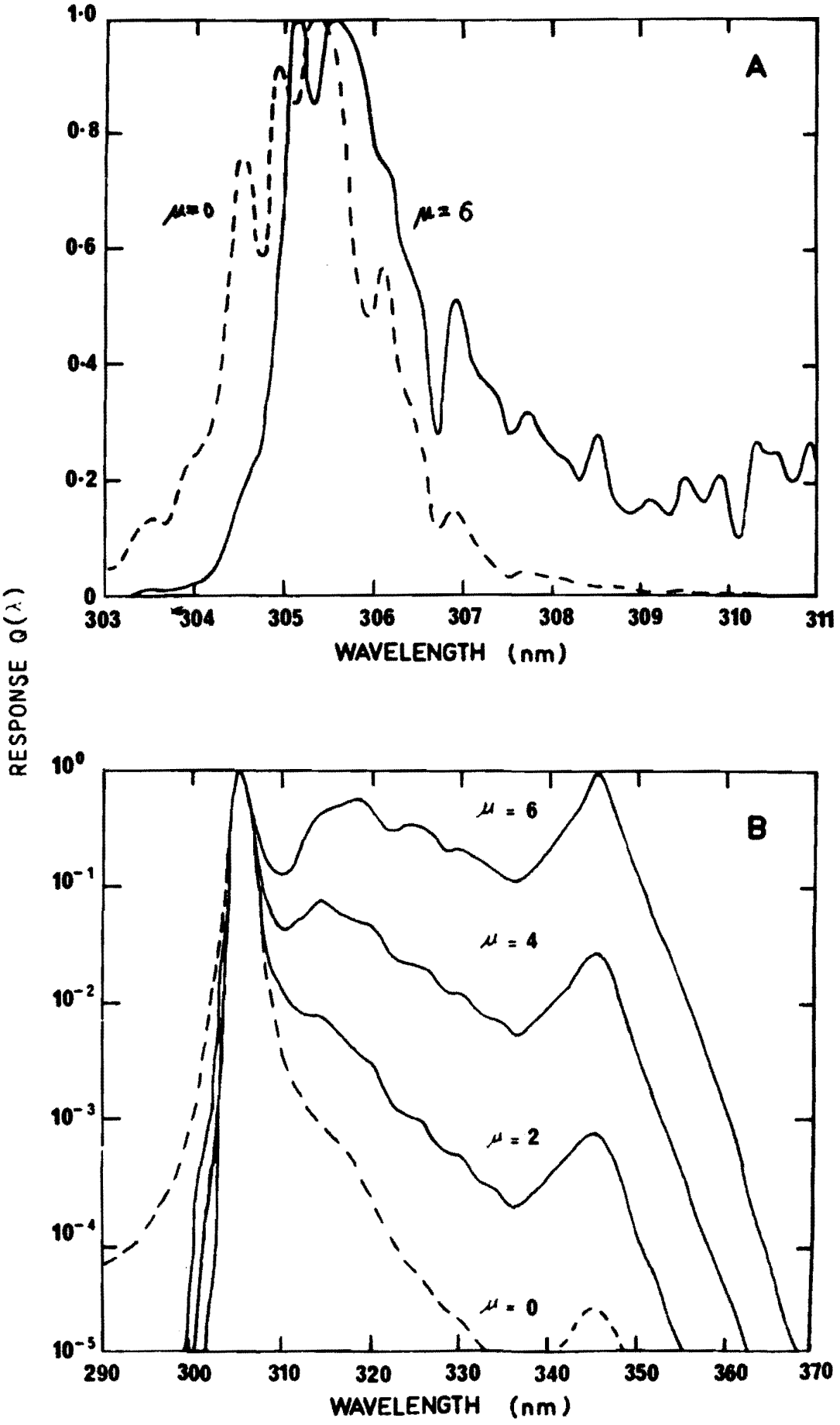

FIG. 8·6 305 nm SINGLE FILTER,
NORMALISED SPECTRA OF RESPONSE
FUNCTION Q(λ) AT AIR MASSES μ

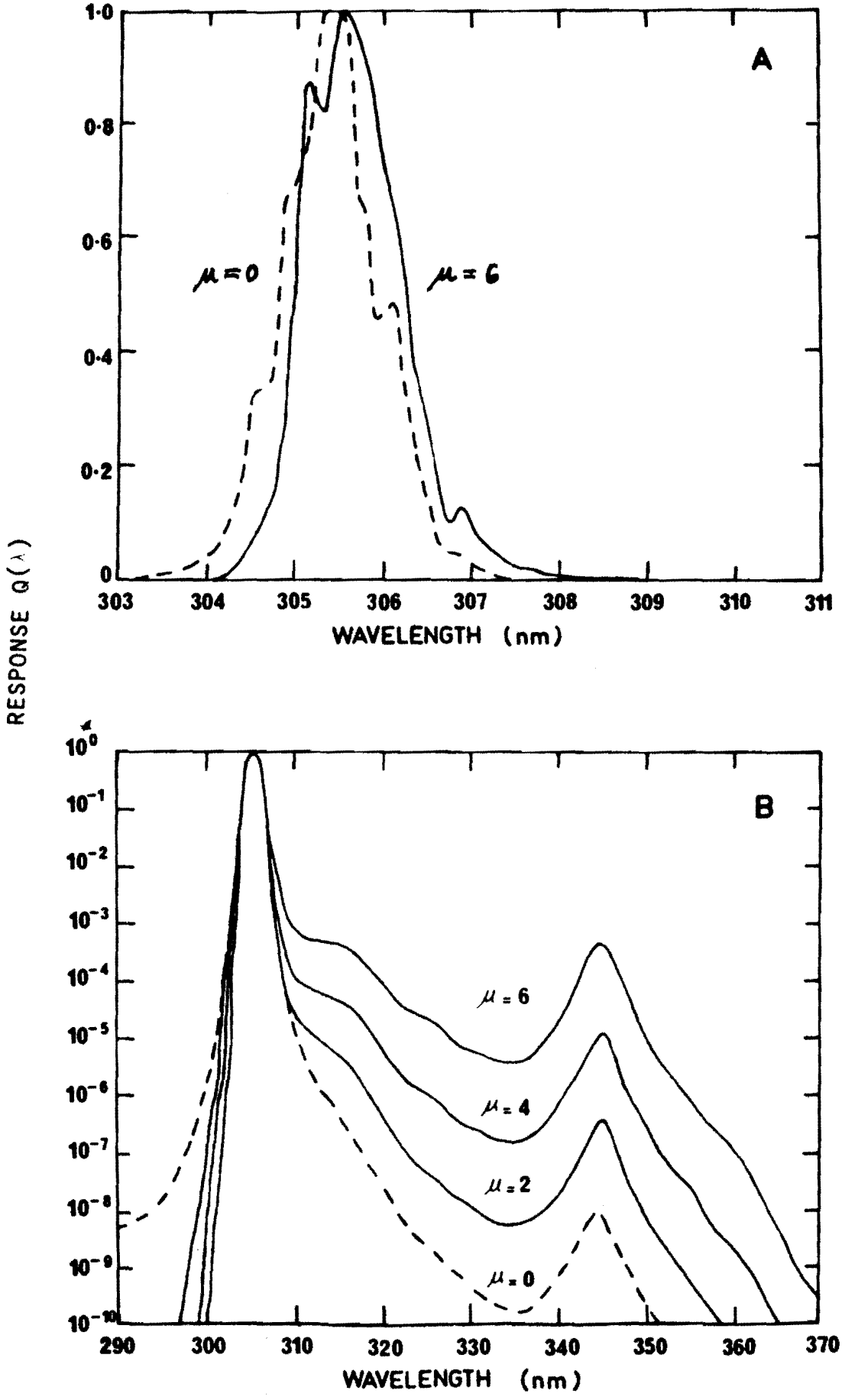

FIG. 8·7 305 nm DOUBLE FILTER,
NORMALISED SPECTRA OF RESPONSE
FUNCTION Q(λ) AT AIR MASSES μ

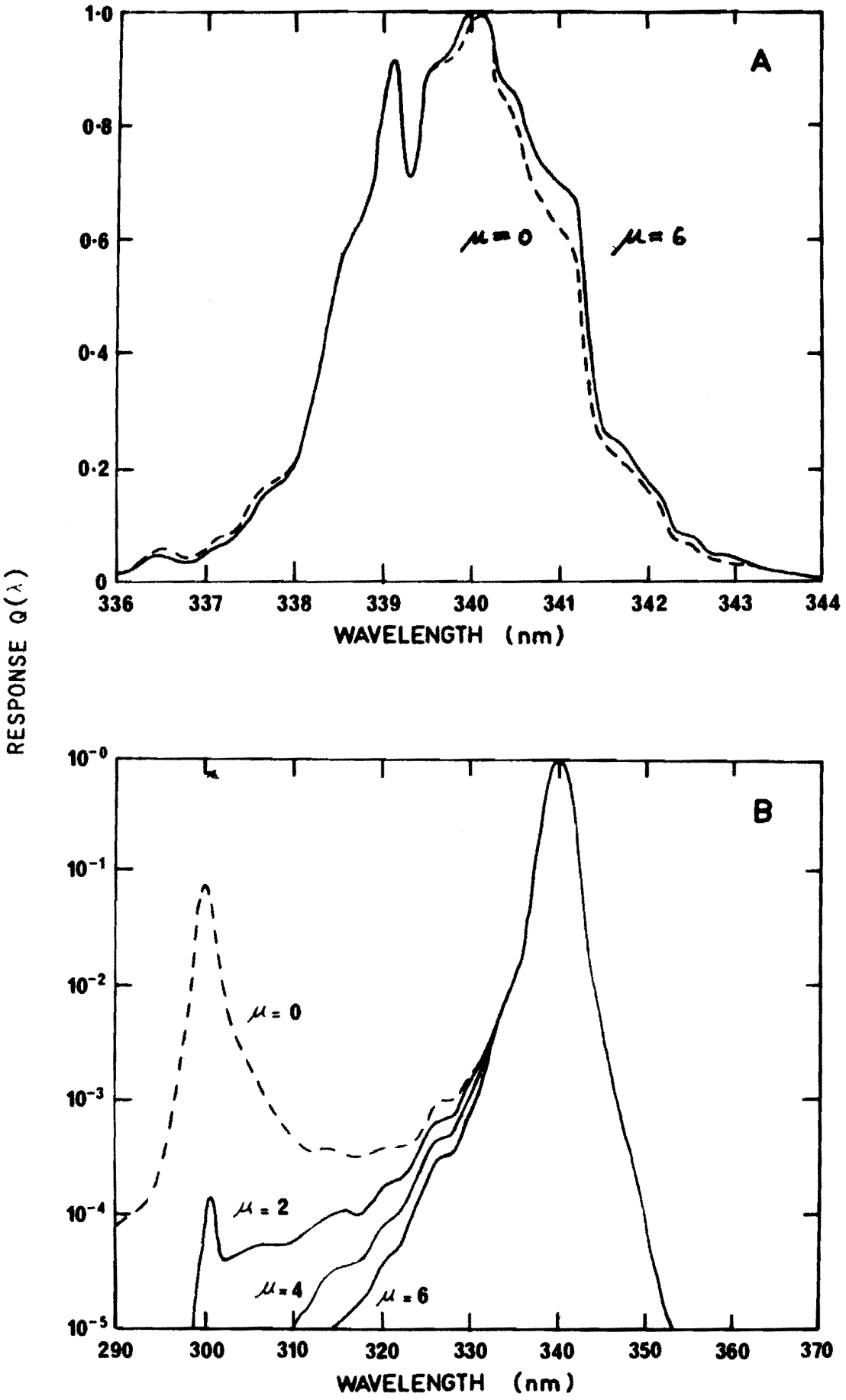

FIG. 8·8 340 nm SINGLE FILTER,
NORMALISED SPECTRA OF RESPONSE
FUNCTION Q(λ) AT AIR MASSES μ

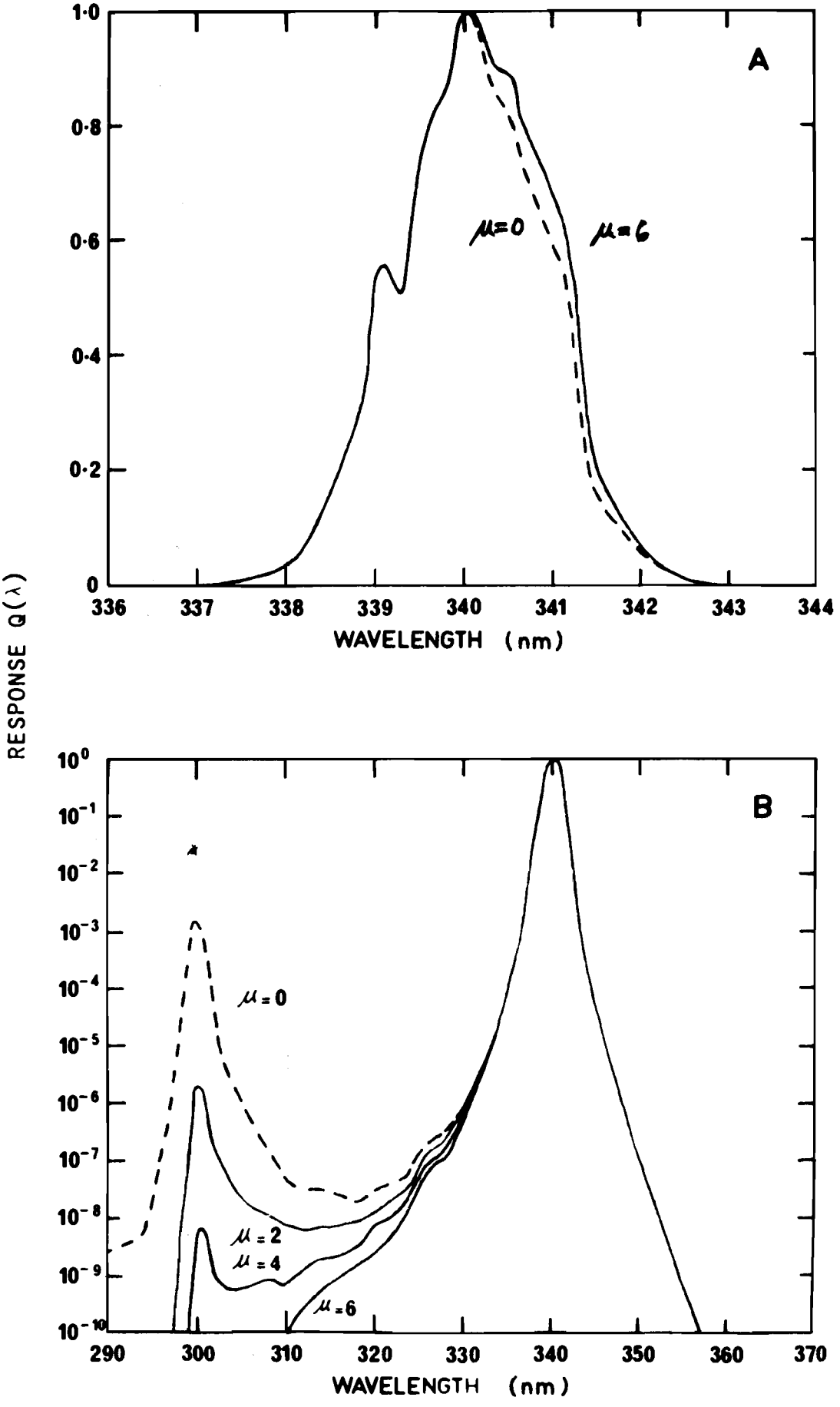

FIG. 8.9 340 nm DOUBLE FILTER,
NORMALISED SPECTRA OF RESPONSE
FUNCTION Q(λ) AT AIR MASSES μ

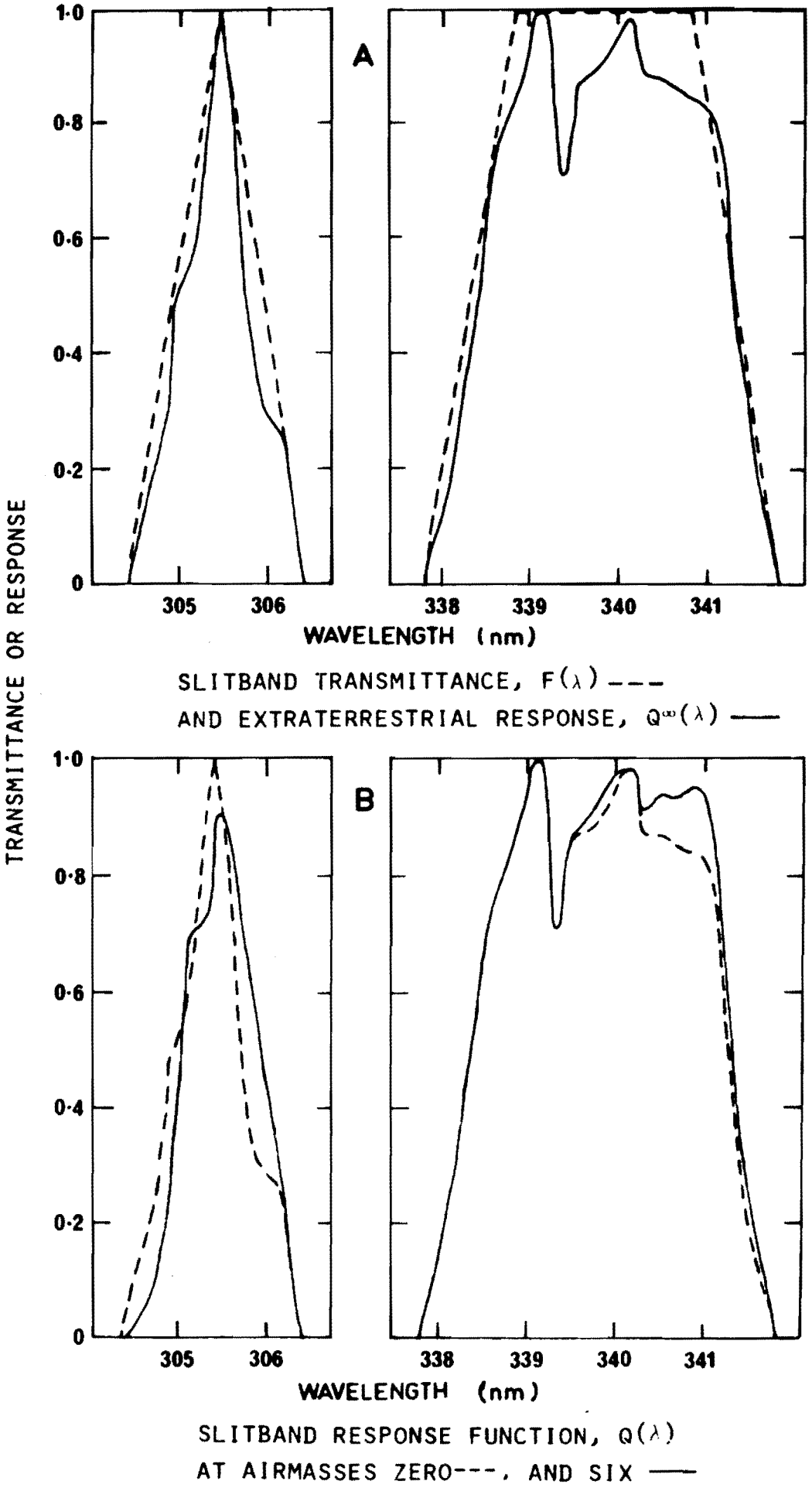

FIG. 8·10 DOBSON 305.4 nm AND 339.8 nm SLITBANDS, NORMALISED SPECTRA

Excepting figure 8.10, all the figures contain two graphs of the particular filter, the top, or A-graph, being a linear graph of the passband region and the lower, or B-graph, being a logarithmic graph of the whole near ultraviolet region. All the spectra are normalised to their peak values so that the trends are more easily seen. Because the graphs' source data are spaced 0.2 nm apart in wavelength, interpolation is necessary to provide smooth passband A-graphs, but results in unrealistic 0.2 nm period fluctuations. The true $Q(\lambda)$ spectra are in fact riddled with extremely variable, fine detail which comes from the solar irradiance (compare figures G.1, G.2 and 8.1). The 0.2 nm sized detail, seen in the A-graphs, is further smoothed for the logarithmic B-graphs.

Figures 8.4 and 8.5 show the marked differences between a filter's transmittance $F(\lambda)$ and its extraterrestrial response function $Q_{\infty}(\lambda)$ (defined in equation 7.3). Similar graphs for the Dobson instrument slits are given in figure 8.10-A. The significant, small scale detail, seen in the A-graphs, is caused by the highly variable solar irradiance term $U(\lambda)$ in $Q_{\infty}(\lambda)$.

The solar irradiance (see figure 8.1) also produces a general reduction of $Q_{\infty}(\lambda)$ for wavelengths shorter than 320 nm. This second effect is somewhat obscured, however, by the blocking filter transmittance term, $S(\lambda)$ (see figure 4.10), which progressively reduces $Q_{\infty}(\lambda)$ toward longer wavelengths and provides the sharp cut-offs at about 350 nm. This has the unfortunate effect of enhancing the transmittance region on the short wavelength side of a passband, and in particular, of enhancing the large leakage in the 340 nm filter, as in figure 8.5. The detector sensitivity, $D(\lambda)$, of the 1P28 photo-

multiplier has no noticeable effect on the spectra.

The effect of atmospheric attenuation on the response function, $Q(\lambda)$ (defined in equation (7.2)) is to be seen in figures 8.6 to 8.9 where $Q(\lambda)$ is plotted for different values of airmass μ, but with total ozone fixed at .300 atm cm and no aerosol scattering included. With increasing airmass, the general trend, shown in all the graphs, both A and B, is a progressive shifting in the balance of $Q(\lambda)$ in favour of the longer wavelengths.

This is simply the result of the increasing atmospheric attenuation of shorter wavelength radiation due to both ozone absorption (figure 8.3) and molecular scattering (figure 8.2).

The effect on the filter passbands, A-graphs, is an increase in their effective centre wavelengths. For example the 305 nm single and double filters, figures 8.6-A and 8.7-A, shift quite noticeably to longer wavelengths with airmass. The size of the shift depends on the gradient of attenuation across the passband, and hence for the longer wavelength filters, for example figures 8.8-A and 8.9-A, the shift is very small. Similar behaviour is shown in figure 8.10-B for the Dobson instrument's 305.4 nm and 339.8 nm slitbands.

The logarithmic B-graphs (figures 8.6 to 8.9) show the significant changes with airmass in the filters' underlying sideband regions of the response function. The rapid, real attenuation with airmass of the shorter wavelength radiation, ensures an equally rapid relative enhancement of the 305 nm filters' longer wavelength regions (figures 8.6-B and 8.7-B) but, on the other hand, ensures an equally rapid attenuation of the 340 nm filters' large, short wavelength leakages

(figures 8.8-B and 8.9-B). The importance, therefore, of a leakage band depends on the range of airmass encountered; short wavelength leakages have importance at low airmasses, while long wavelength leakages have importance at high airmasses.

Because the atmospheric attenuation changes rapidly with wavelength, the accuracy of the filter photometer's spectral measurements depends on the extent to which the response function is concentrated at the passbands. In this respect, the double filters (figures 8.7 and 8.9) are clearly superior to the single filters (figures 8.6 and 8.8) both in reducing the response contributions of sidebands, and in confining the passband transmission to a narrower wavelength range. (Note that the transmittance range of the double filters is extended to 10^{-10}).

The improvement in doubling the 305 nm filter is particularly marked, owing to the more rapid rate of change of attenuation on the short wavelength side of 310 nm. A doubled filter spectrum at airmass = 6 is better than the single filter spectrum at airmass = 2. Stacking filters is by far a better method for effectively blocking the spectral regions close to the passband than the use of absorption blocking filters such as nickel sulphate hexahydrate.

In addition to the overall changes with airmass described above, there are small scale changes due to the impression of the ozone absorption band structure on the response function spectra. This can be seen in figures 8.6-A and 8.7-A where, in going from airmass = 0 to airmass = 6, some old detail is destroyed and new detail is created. The consequent removal from the passband of the more strongly attenuated radiation

reduces the filters' equivalent absorption coefficient in exactly the same way as the other larger scale effects.

The small scale structure in the ozone absorption spectra (figure 8.3) is greatest in the Huggins bands, from about 310 to 340 nm, and will therefore most affect the filters in this region. However, owing to the rapid average decrease in ozone absorption with wavelength, molecular scattering becomes the dominant attenuation process beyond 310 nm, and since it is monotonic over the whole region, it tends to obscure the ozone absorption structure.

8.3 Equivalent Attenuation Coefficients, Variation with Atmospheric Attenuation

The equivalent attenuation coefficients are given by equations (7.24), (7.25) and (7.26), and are used in equation (7.12) as part of the total ozone determination. The significance of the coefficients is that they are not constant, but are dependent on airmass, total ozone and atmospheric aerosols. Whereas the spectra in the previous section gave a qualitative description of the bandwidth effect, the equivalent attenuation coefficients give a quantitative description of the effect on the total ozone measurement. This section will concentrate on the equivalent ozone absorption coefficient as it is the most variable.

As is shown in Appendix I, in the limit of zero airmass, the equivalent attenuation coefficients become equal to the extraterrestrial attenuation coefficients (equation 7.35). These are listed in table 8.1 and illustrate three points.

TABLE 8.1: Extraterrestrial Attenuation Coefficients for Single Filters, Double Filters and Dobson Slitbands.

Band	305	311	317	325	332	340	nm
Filter instrument, single filter							
α_0	1.930	.869	.403	.154	.062	.260	
β_0	.490	.452	.420	.382	.352	.325	
Filter instrument, double filter							
α_0	1.941	.879	.397	.138	.060	.018	
β_0	.491	.452	.420	.382	.351	.311	
Dobson instrument, with solar irradiance term							
α_0	1.924	.871	.381	.120	.049	.013	
β_0	.491	.452	.416	.374	.343	.312	
Dobson instrument, without solar term							
α_0	1.916	.867	.378	.121	.049	.013	
Dobson instrument, standard values (Dobson 1957)							
α_0	1.882	.912	.391	.120	.047	.017	

Firstly, all the filter instrument coefficients appear to be of the expected size, except the ozone absorption coefficient of the 340 nm single filter. This coefficient is actually correct, its large size being due to the large, short wavelength leakage component in the filter's extraterrestrial response $Q_\infty(\lambda)$, as shown in figure 8.5-B. Fortunately, the leakage's influence declines very rapidly with airmass, as will be seen later. A similar but considerably smaller effect is observed for the scattering coefficient.

Secondly, the usual exclusion of the solar irradiance term $U(\lambda)$ from $Q_\infty(\lambda)$ (see equations (7.34) and (7.35)), when calculating the Dobson instrument's ozone absorption coefficients, results in decreases of up to 0.9% in the coefficient. Quite fortuitously, the decrease tends to match that needed to account for the instruments' bandwidth effect.

Thirdly, there are differences of up to 5% between the coefficients calculated by the author, and the standard coefficients. These may be due to differences in the shape and positions of the model slitbands used, but if they are due to interpolation errors in the ozone absorption spectrum, then the filter coefficients may also be in error by similar amounts. Such errors would give a fixed percentage error in determined total ozone, but would not affect the conclusions of this chapter.

The variation of the equivalent ozone absorption coefficients, $\bar{\alpha}$, of the single and doubled filters relative to their extraterrestrial coefficients, α_0, is shown in figure 8.11 as a function of airmass, and in figure 8.12 as a function of total ozone. No aerosol scattering was included in the calculations. The coefficients show the expected general decrease with increasing absorption, with the variation in the single filter coefficients being up to seven times larger than the variation on the double filter coefficients.

The coefficient variations are approximately linear with total ozone and airmass, with the exception of the 305 nm and 340 nm filter variations which show the effects of their transmittance leakages. As mentioned earlier, the 305 nm

filter has a leakage region on the long wavelength side of the passband which introduces significant variation at high airmass, while the 340 nm filter has a leakage band on the short wavelength side of the passband which only produces significant variation at low airmass.

The very large percentage variation in the 340 nm filter coefficient is not of great consequence, since the actual coefficient is very small compared to the coefficients of the other filters used, and therefore it can contribute only minor errors to the determined total ozone. To enable the reader to compare the variations in actual coefficients, the change, $\Delta\alpha$, represented by each graph's full scale, is given below the graphs. In figures 8.11 and 8.12, for the 340 filter, $\Delta\alpha'$ refers to the single filter and $\Delta\alpha$ refers to the double filter.

Figure 8.13 compares the performances of the double filters and the Dobson instrument slitbands. The most noteworthy point is that, for the 305 nm and 311 nm bands, which contribute the largest proportion of variation to the calculated total ozone, the variation in the filter coefficients is only twice that of the slitband coefficients. Of the remaining bands, only the 332 nm and 340 nm bands show large differences. The difference between the 340 nm bands is due to the leakage in the filter, while the difference between the 332 nm bands is probably due to the difference in centre wavelength of the slitband and filter passband. In any case, the variations of the 332 nm and 340 nm bands have an extremely small effect on the calculated total ozone.

From an operational point of view, it is only the variation in the coefficients over the usually encountered ranges of airmass and total ozone which is important, and

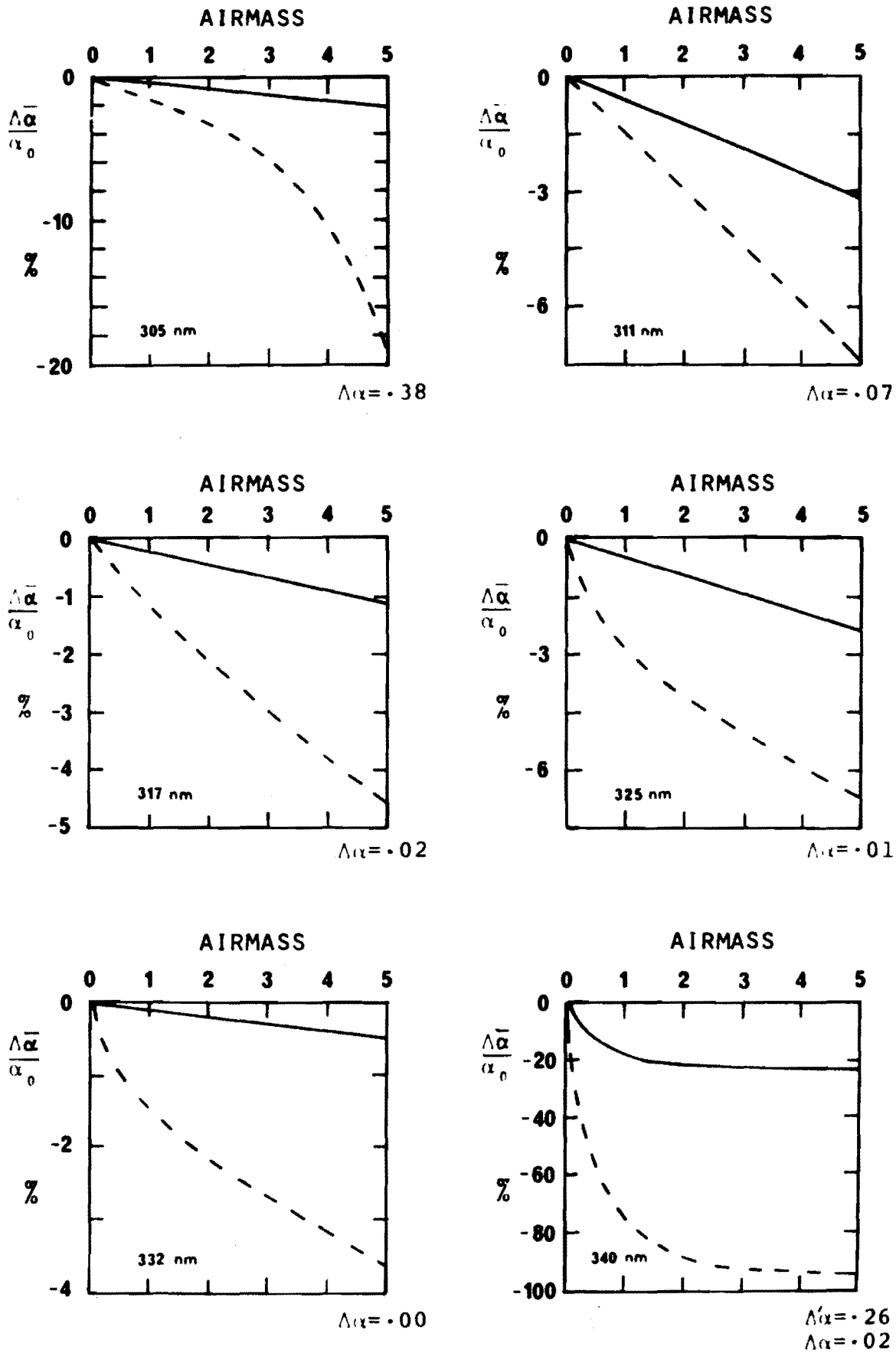

FIG. 8·11 VARIATION OF EQUIVALENT OZONE ABSORPTION COEFFICIENT $\bar{\alpha}$ WITH AIRMASS FOR TOTAL OZONE X =·300 atm cm. SINGLE FILTERS (--), DOUBLE FILTERS (—) .

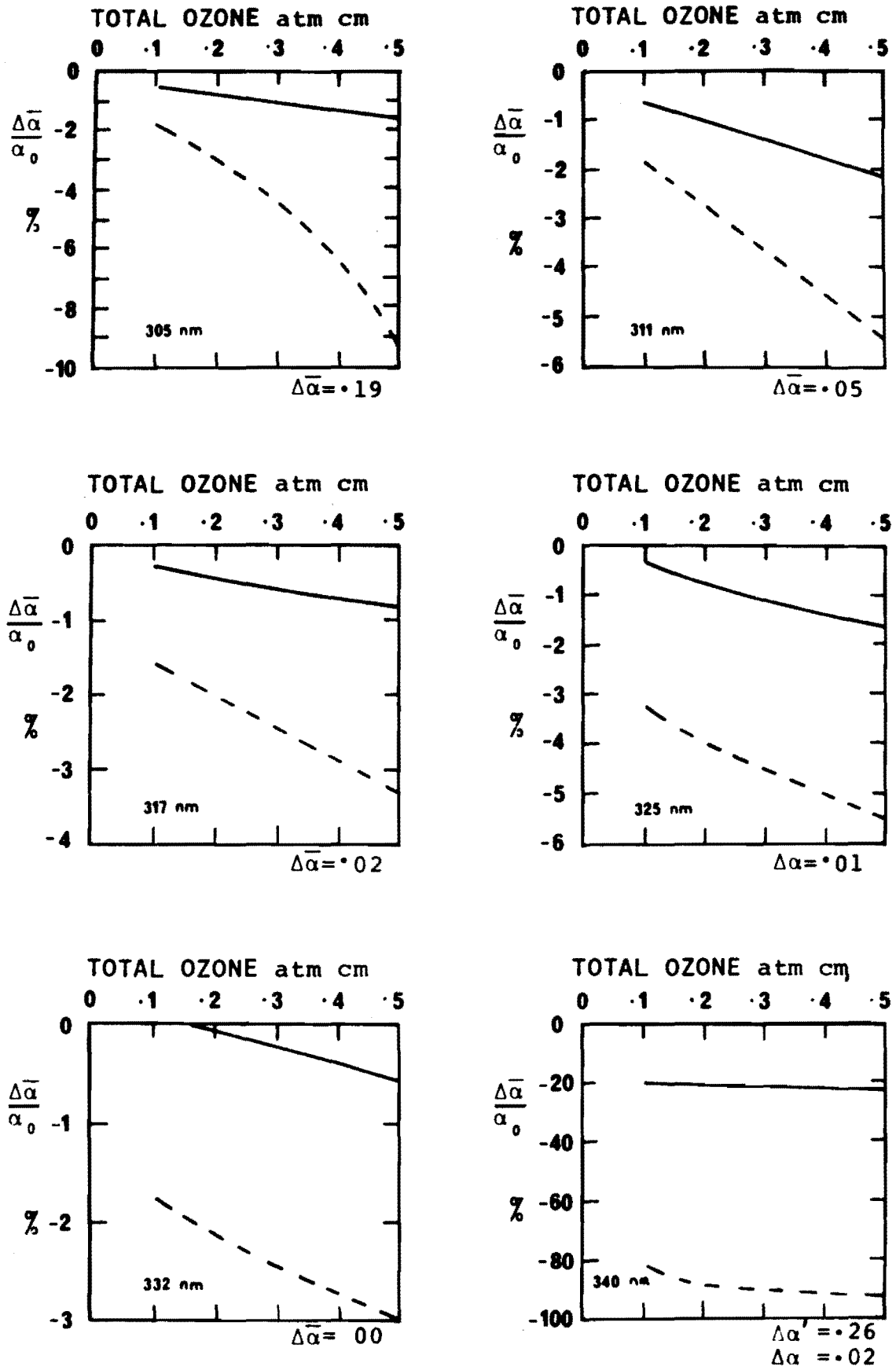

FIG. 8·12 VARIATION OF EQUIVALENT OZONE ABSORPTION COEFFICIENT $\bar{\alpha}$ WITH TOTAL OZONE, FOR AIRMASS=2·5 SINGLE FILTERS (--), DOUBLE FILTERS (——)

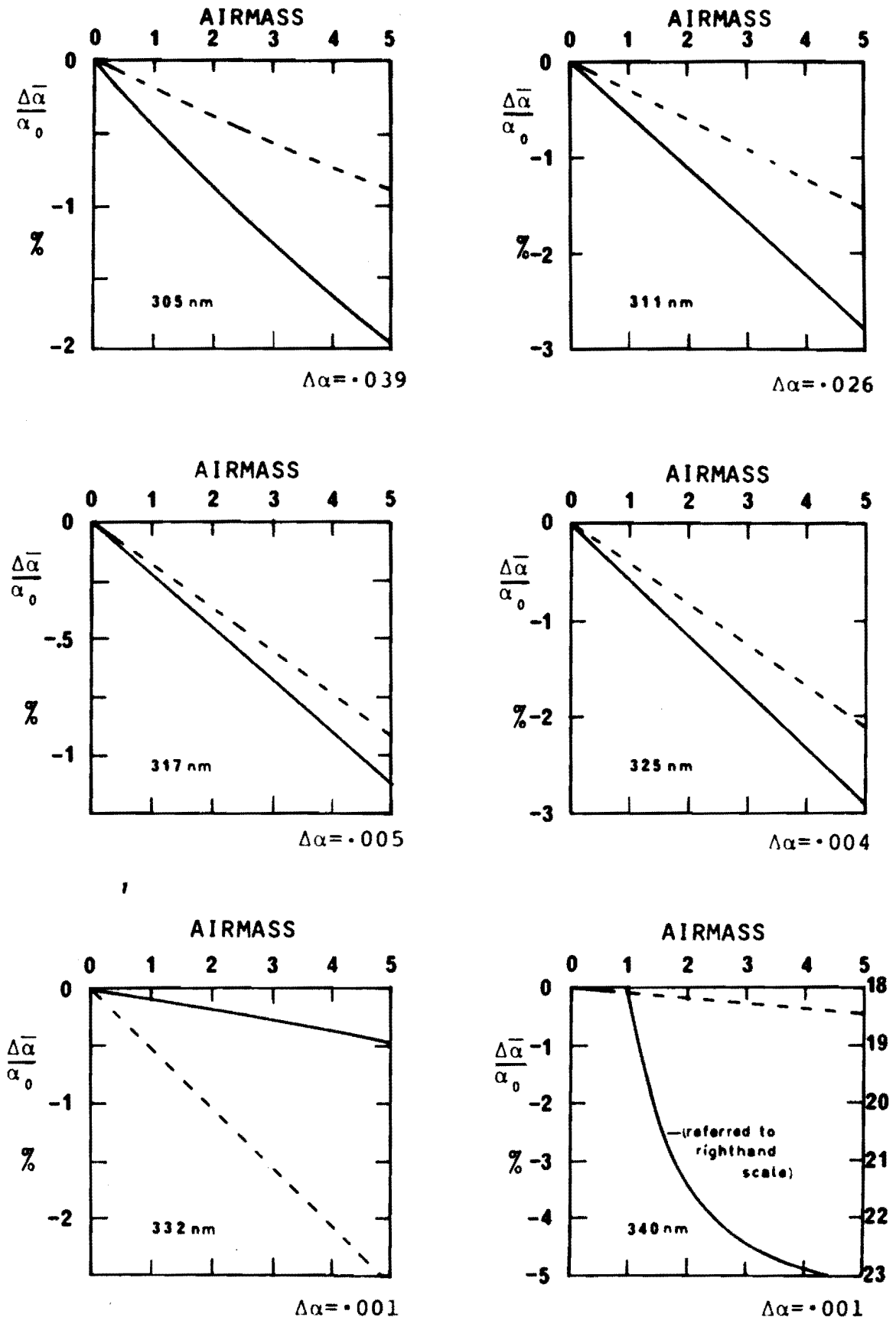

FIG. 8·13 VARIATION OF EQUIVALENT OZONE ABSORPTION $\bar{\alpha}$ WITH AIRMASS FOR TOTAL OZONE X = ·300 atm cm. COMPARISON OF (DOUBLED FILTER) INSTRUMENT (——) WITH DOBSON INSTRUMENT (--)

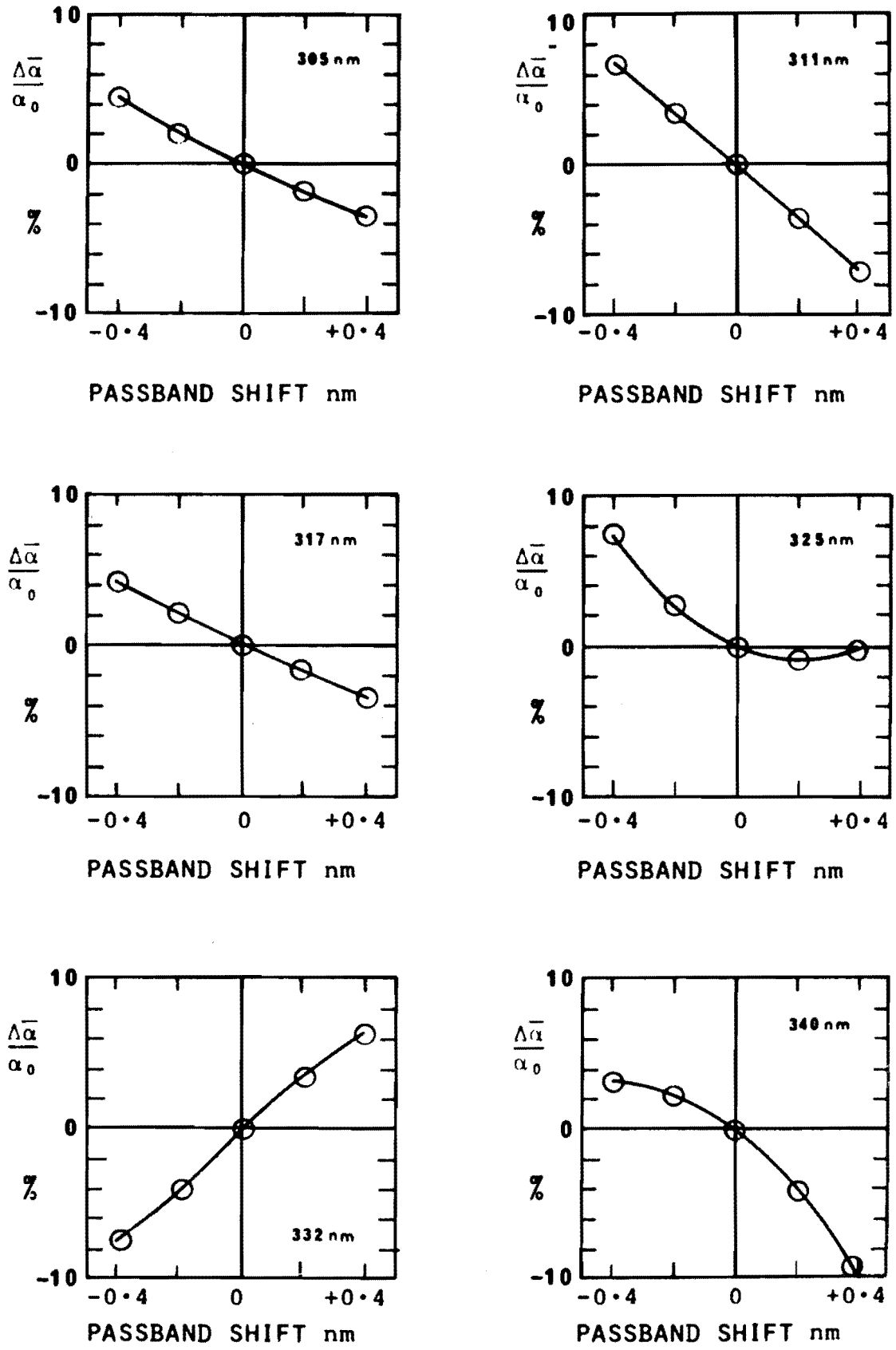

FIG. 8-14. VARIATION OF THE DOUBLED FILTERS' EQUIVALENT OZONE ABSORPTION COEFFICIENTS, $\bar{\alpha}$, WITH PASSBAND CENTRE WAVELENGTH, AT AIRMASS = 3·0, TOTAL OZONE = 0·300 atm cm.

hence it is desirable to consider the variation only within these ranges, about some suitable average, or reference coefficient. Such reference coefficients can be derived from table 8.1 and figures 8.11, 8.12 and 8.13 for given ranges of airmass and total ozone. For an operating range of $1 < \text{airmass} < 4$ and $.2 < \text{total ozone} < .4$ atm cm, table 8.2 lists suitable reference coefficients, α_a, along with their appropriate maximum variations.

TABLE 8.2: Reference Absorption Coefficients, α_a, and Corresponding Ranges of Variation, for Single Filters, Double Filters, and Dobson Slitbands

Band	305	311	317	325	332	340 nm
Filter instrument, single filters						
α_a	1.741	.832	.392	.147	.061	.051
$\pm\Delta\alpha_a$	.166	.029	.007	.003	.001	.035
$\pm(\Delta\alpha_a/\alpha_a)$%	9.5	3.5	1.8	2.1	1.1	69%
Filter instrument, double filters						
α_a	1.918	.865	.394	.136	.060	.014
$\pm\Delta\alpha_a$	.016	.011	.002	.001	.000	.001
$\pm(\Delta\alpha_a/\alpha_a)$%	0.8	1.2	0.5	0.9	0.3	3.3%
Dobson instrument						
α_a	1.914	.863	.379	.118	.048	.013
$\pm\Delta\alpha_a$	.008	.006	.002	.001	.001	.000
$\pm(\Delta\alpha_a/\alpha_a)$%	0.4	0.7	0.4	1.2	1.0	0.2%

The following points are confirmed by table 8.2:

(i) The single filters have from three to ten times more variation in their coefficients than the double filters (the 340 nm filter excepted).

(ii) The 305 nm and 311 nm double filters have in their coefficients only about twice the variation of the corresponding Dobson slitbands.

(iii) Items (i) and (ii) above suggest that the filters' performance is more critically dependent on effective blocking than on half-bandwidth.

(iv) Most of the variation in calculated total ozone will come from the 305 nm and 311 nm bands' variation, $\Delta\alpha_a$.

(v) It would be desirable to reduce the variation in the 340 nm single filter by blocking its leakage.

The equivalent molecular scattering coefficient, equation (7.25), depends on airmass, but not on total ozone. As expected, its variation is small, being generally less than ±0.013% for the double filters and the Dobson slitbands, and less than ±0.04% for the single filters. The exception is the 340 nm band whose double filter variation is ±0.03% and whose single filter variation is ±1.3%. These larger variations are again due to the 340 nm filters' leakages. It is clear that the variation in the molecular scattering coefficient with airmass is insignificant compared with the variation in the ozone absorption coefficient.

Where an instrument's bandwidth effect is small (this might well include the case of the single filter photometer), the most practical solution to the effect is a tabulation of the corrections to total ozone needed for various conditions, such as is given as table 8.3. The tabulations, which reflect changes relative to a set of reference attenuation coefficients, will remain accurate even if subsequent calibration changes are made to the coefficients. As

TABLE 8.3: Double Filter Bandwidth Effect Corrections to Total Ozone, for Standard Methods of Total Ozone Determination

Total Ozone 10^{-3} atm cm	Airmass	Corrections to Total Ozone 10^{-3} atm cm Method: A	C	D	AD	CD
200	1.0	-1.7	-2.5	-0.5	-2.0	-4.2
	2.0	-1.1	-1.6	-0.5	-1.2	-2.5
	3.0	-0.5	-0.7	-0.3	-0.5	-1.1
	4.0	0.1	0.2	-0.0	0.1	0.3
	5.0	0.6	1.1	0.3	0.7	1.8
250	1.0	-1.9	-2.9	-0.7	-2.3	-4.9
	2.0	-1.0	-1.6	-0.6	-1.1	-2.5
	3.0	-0.2	-0.3	-0.2	-0.2	-0.4
	4.0	0.6	1.0	0.2	0.7	1.7
	5.0	1.4	2.4	0.7	1.6	3.9
300	1.0	-2.1	-3.3	-0.8	-2.5	-5.4
	2.0	-0.9	-1.5	-0.6	-1.0	-2.2
	3.0	0.3	0.3	-0.0	0.4	0.7
	4.0	1.4	2.2	0.6	1.6	3.7
	5.0	2.4	4.1	1.2	2.8	6.7
400	1.0	-2.3	-3.7	-1.1	-2.7	-6.0
	2.0	-0.3	-0.7	-0.4	-0.2	-0.9
	3.0	1.6	2.4	0.5	1.9	4.1
	4.0	3.4	5.6	1.6	3.9	9.2
	5.0	5.3	8.8	2.7	6.0	14.5
350	1.0	-2.3	-3.5	-1.0	-2.6	-5.8
	2.0	-0.6	-1.2	-0.5	-0.7	-1.7
	3.0	0.9	1.3	0.2	1.1	2.2
	4.0	2.3	3.7	1.0	2.6	6.2
	5.0	3.7	6.2	1.9	4.2	10.2
450	1.0	-2.4	-3.8	-1.2	-2.7	-6.2
	2.0	0.2	-0.1	-0.3	0.3	0.1
	3.0	2.5	3.8	1.0	2.9	6.4
	4.0	4.7	7.8	2.3	5.4	12.9
	5.0	7.4	11.9	3.6	8.4	19.5

mentioned by Vanier and Wardle (1969), an iterative correction procedure is needed where the effect is large.

The effect of the aerosol scattering gradient, g, in equations (7.24), (7.25) and (7.26), is most conveniently considered in relation to the bandwidth effects already described. A negative aerosol scattering gradient (more aerosol scattering at short wavelengths) is spectrally similar to the average gradients of ozone absorption and molecular scattering and will therefore tend to accentuate the bandwidth effect of those two processes. Conversely, a positive aerosol scattering gradient will tend to reduce their bandwidth effect.

Calculations on the double filters show that g has a negligibly small effect on the equivalent attenuation coefficients. The maximum range in g of ±0.025 (see Appendix G) produces maximum changes of about ±0.2% in the equivalent ozone absorption coefficients, and of about ±0.02% in the equivalent molecular scattering coefficients, for the ranges $1 < \text{airmass} < 4$, $0.2 <$ total ozone < 0.4 atm cm. Resulting errors in total ozone calculated by the standard A, C, AD and CD methods are less than 0.2%.

The bandwidth effect on the equivalent aerosol scattering coefficient, $\bar{\delta}$, is encompassed by the related equivalent centre wavelengths, $\bar{\lambda}$, which are defined in equation (7.27). As explained in Section 7.3, only differences of coefficients need be considered.

The separation, $\bar{\lambda}_j - \bar{\lambda}_i$, of equivalent centre wavelengths was calculated for all possible combinations of the six double filters, for ranges of ±0.025 in g and from 1 to 4 in airmass μ. For the consequent maximum range of ±0.1 in the product μg,

the filter separations are essentially constant, i.e. within ±0.01%, except those for pairs which include the 340 nm filter. The leakage in the 340 nm filter gives rise to a variation of ±.03 nm, equivalent to ±0.1 to 0.2%, in the separation of these pairs.

The effect of these variations on the total ozone and aerosol scattering gradient calculated from equations (7.32) and (7.33) is negligible.

8.4 Passband Shifting, Effect on Equivalent Attenuation Coefficients and on Total Ozone

In Chapter 4, it was explained how interference filter passbands can shift in wavelength, at different positions across the filter surface, and with varying filter orientation, age and temperature. It is possible to calculate the effect of this shifting on the attenuation coefficients and the determined total ozone, since the variables of the measurement model used here consist of sets of data points at 0.2 nm spacings, and therefore the filter spectra may be "shifted" in integer multiples of 0.2 nm.

Although this topic is not related to the bandwidth effect, it is included here as it uses the same measurement model.

The effect on the equivalent ozone absorption coefficients of the double filters can be seen in figure 8.14. The variation shown for each filter reflects the variation of the ozone absorption spectrum (figure 8.3) in the vicinity of its passband, and hence is linear and negative for the three shorter wavelength filters, and is uncertain for the three

longer wavelength filters. Of these, the passband of the nominal 332 nm filter is actually centred on 330.5 nm, which puts it just to the short wavelength side of the ozone absorption band at 331 nm, and hence in a region of positive absorption gradient. The variation of this filter's equivalent coefficient is thus also positive.

The variation is dependent on the conditions of airmass and total ozone, but in the range of 1 < airmass < 4 and 0.2 < total ozone < 0.4 atm cm, the differences amount to less than ±0.5% for the ±0.4 nm shifts.

Change in filter temperature is the most likely source of passband shifting. The maximum expected shift, for a temperature range of ±20^{o}C centred on +20^{o}C, is ±0.2 nm, which is found using the temperature coefficient of passband shift of 0.01 nm/^{o}C given in Section 4.7. These values hold for all the filters, and result in a maximum variation of ±4% in the equivalent ozone absorption coefficients.

Table 8.4 lists the average variations of the coefficients for the ±0.2 nm range of passband shift and usual ranges of airmass and total ozone, while table 8.5 lists the average variations in total ozone determined by the standard methods, as functions of passband shift and of filter temperature, for the same ranges.

One can conclude from table 8.5 that the effect of filter temperature on total ozone is significant and should be corrected for. As an example, a 10^{o}C temperature change will alter the AD and CD method total ozone by about 1% and 3% respectively.

TABLE 8.4: Average variation, with passband shift, of the equivalent ozone absorption coefficient, for ranges of ±0.2 nm in shift, 1 to 4 in airmass, and 0.2 to 0.4 atm cm in total ozone.

Nominal wavelength	305	311	317	325	332	340	nm
Actual wavelength	305.4	311.3	316.4	323.9	330.5	340.3	nm
Coefficient variation	-10.1	-17.4	-9.5	-9.1	+19.2	-15.1	%/nm
Uncertainty ±	1.6	0.7	1.0	5.9	0.8	5.2	%/nm

TABLE 8.5: Average variation in total ozone with passband shift and filter temperature, for standard methods of total ozone determination, and for ranges of ±0.2 nm in shift, 1 to 4 in airmass, and 0.2 to 0.4 atm cm in total ozone.

Standard method	A	C	D	AD	CD	
Total ozone variation	-8.6	-19.4	-5.4	-10.2	-30.3	%/nm
Uncertainty ±	1.3	1.4	3.9	1.3	4.2	%/nm
Temperature variation	- .086	- .194	- .054	- .102	- .303	$\%/^{\circ}C$

Since the given uncertainties, which account for non-linearity in the coefficients of variation, are generally small, the listed coefficients may be applied directly as correction coefficients for the filter set used.

The data of tables 8.4 and 8.5 can be applied, with caution, to filter sets other than the set used in the calculation of the data. This is possible since the variations in the 305 nm and 311 nm filter coefficients, which are responsible for most

of the variation in total ozone, are relatively independent of the filters' centre wavelengths. In contrast, the coefficient variations of the longer wavelength filters are highly dependent on their centre wavelengths, as is shown in figure 8.14, and may not readily be used with other filter sets.

Since the molecular scattering coefficient, β, is proportional to the inverse fourth power of wavelength, its variation with wavelength, λ, is just $\Delta\beta/\beta = -4\Delta\lambda/\lambda$. For ± 0.2 nm passband shifts, this has the negligibly small variation of $\pm 0.3\%$.

There are no changes in filter centre-wavelength separations, $\bar{\lambda}_j - \bar{\lambda}_i$, as all the filter passbands experience essentially the same shifts.

It should be noted that tables 8.4 and 8.5 can be used to find the uncertainty in the ozone absorption coefficients and the determined total ozone due to the original wavelength uncertainty in the filter transmittance spectra. For example, the wavelength uncertainty of 0.05 nm, given in Appendix A, yields a 0.5% uncertainty in the AD method total ozone.

8.5 Summary and Conclusions

The foregoing analysis of the bandwidth effect shows conclusively that the effect does not prevent the use of interference filters for measurement of total ozone. In particular, it is shown that, for the range of airmass and total ozone usually encountered, the bandwidth effect error in the doubled filters' ozone absorption coefficients is, at 1%, only twice that of the Dobson instrument slitbands.

A very significant point is the superior performance of the double filters compared to that of the single filters. It is clear that, for total ozone measurement, it is more important to have the rapidly attenuated passband skirts of the double filters than to have merely a smaller half bandwidth single filter. The comparable performance of the double filters and Dobson slitbands suggests that there is little need for triple filters.

For a given filter set it is possible to calculate a table of corrections to total ozone, such as in table 8.3. These tables could well be represented by some form of nomagram for regular use. The corrections for the double filters and the Dobson slitbands are so small that they cannot be readily tested, but the same is not true of the single filter corrections. No corrections have been calculated for the prototype filter set described in Chapter 2.

The other major source of error in using interference filters for total ozone determination, that of passband shifting, has also been reduced by model calculations to simple, total ozone correction factors, table 8.5. As with the bandwidth correction factors, these factors are calculated for only the author's set of doubled filters, but may, with greater uncertainty, be applied to other similar sets.

The large short wavelength leakage in the 340 nm filters is retained for the calculations in order to illustrate the large effects that leakages in general, and short wavelength leakages in particular, can have on a filter's attenuation coefficients. The leakage is of course easily blocked (Section 4.3), and has little effect on the total ozone measured with the double filters. The bandwidth effect error

in total ozone is dominated by the larger coefficients of the shorter wavelength filters.

Although the calculated bandwidth effect for the Dobson slitbands is very small, it should be remembered that the calculations use idealised transmittance spectra (figure 8.10-A) for the slits. It is probable that the slits in fact transmit minute quantities of radiation internally scattered in the instrument which have wavelengths outside those defined by the slits. If so, the slitband spectra would be more like that of a double filter, and would consequently give rise to larger bandwidth errors than those calculated here.

As indicated in the introduction to Part III, the accuracy of the model's reference attenuation coefficients can be improved by increasing the accuracy of the input data. The need for this is pointed up by the differences, shown in table 8.1, between the Dobson standard ozone absorption coefficients and those calculated from the model. Further improvement would accrue from the use of a smaller integration interval, say 0.05 nm.

The model could be modified to examine zenith sky measurements, and hence Umkehr measurements. However, judging by the results of Vanier and Wardle (1969), the effects are likely to be somewhat smaller than those for the direct sun measurements.

PART IV: CONCLUSION

Preliminary Remarks

This final part contains a description of a direct comparison of the filter spectrophotometer with a Dobson spectrophotometer, in Chapter 9, and a brief overall conclusion to the thesis in Chapter 10.

The comparison shows that the measurements of the two instruments compare rather well, and shows the new filter instrument to be greatly improved over the prototype instrument.

The overall conclusion reviews the thesis' main findings, and indicates some further areas of study.

CHAPTER 9

DIRECT COMPARISON OF FILTER SPECTROPHOTOMETER AND DOBSON SPECTROPHOTOMETER

9.1 Introduction, Calibration, Experimental Arrangements

The performance of the new filter spectrophotometer could be tested by comparing its total ozone measurements, over a long period, with existing measurements to see whether the same daily and seasonal patterns occur. However, because of the great variability in total ozone, it is more desirable to directly compare the instrument with the internationally accepted standard total-ozone instrument, the Dobson spectrophotometer.

This chapter describes a brief, direct comparison made during six days in May (late Autumn) 1974 between the semi-automatic mobile filter instrument, shown in figure 1.1, and the Dobson instrument, No. 17, operated by the New Zealand Meteorological Service at their station at Invercargill ($46^{o}25'S$, $168^{o}20'E$).

A comparison of the old prototype instrument has been described by Matthews (1972). Despite the relatively broad filters used, and the leakage band in the 305 nm filter, the instruments were found to agree to within 5% to 10% over a range of 0.255 to 0.300 atm cm in total ozone, and 1.2 to 2.8 in airmass.

The calibration of the new filter instrument is described in Section 6.1, and mainly involves finding attenuation coefficients for the filter bands, and extraterrestrial constants for pairs of bands. All the coefficients and

constants were calculated with the aid of the model described in Chapters 7 and 8, using equations (7.24) and (7.26) (with zero aerosol scattering gradient) for the attenuation coefficients, and equations (7.3) and (7.11) for the extra-terrestrial constants.

The only conveniently available filter spectral transmittance data were those used in the calculations of Chapter 8, but which belonged to the Physics Department's filter set. Even though the two sets are cut from the same filter plates, small differences may exist between their spectra and therefore between their coefficients and constants. The adequacy of the calculated attenuation coefficients is verified by the subsequent total ozone measurements, but the extraterrestrial constants were discarded in favour of experimental values determined on May 1. The small bandwidth and temperature corrections (Sections 8.3 and 8.4) were not included in this preliminary comparison.

The Dobson spectrophotometer was calibrated independently by the New Zealand Meteorological Service. The instrument is described by Dobson (1957), and Matthews (1971) discusses the essential differences between it and the prototype filter instrument.

The sturdiness of the filter instrument is demonstrated by its survival of the 500 km rail freighting from Christchurch to Invercargill. No special precautions were taken, yet within an hour of arrival at the site, it was assembled and operating, just a few metres from the Dobson instrument.

Invercargill is a cloudy site, being host to continual south-westerly storms which blow in from the adjacent South Tasman Sea. During the seven days of the comparison, very few

completely clear periods were experienced, and, owing to the development of a moist westerly airstream, the cloud gradually increased. On 5 May, no measurements could be made. Although this therefore restricted the number of measurements taken, it did give the opportunity to assess the effects of cloud on the filter instrument.

All the total ozone data presented here were determined from direct-sun measurements using the double A and D wavelength pair method. Zenith sky intensity measurements were taken, but the filter instrument's values were found to be comparable with the dark noise of the instrument's particularly noisy photomultiplier, and are therefore not discussed. The dark noise also limited the direct-sun measurements of the 305 nm band, and consequently the measurement of AD total ozone, to an airmass of 4.1. At this point, the intensity and the dark noise were about equal.

9.2 Experimental Results, Airmass Independence, Effects of Cloud

The total ozone data determined by the two instruments are shown in figure 9.1 as functions of New Zealand Standard Time (NZST) and airmass. NZST precedes local time by about 45 minutes. All the data from the comparison are plotted, including those affected by cloud.

The greater number of filter instrument data points corresponds to its greater speed in taking measurements. Each measurement was easily completed in one minute, even though it represented the average of twenty independent

measurements of each wavelength band, and required the manual recording of six, five digit numbers. Each Dobson instrument measurement represents an average of three A pair and two D pair measurements, and takes about five minutes to complete.

The large amount of filter instrument data in figure 9.1 also illustrates the instrument's excellent short term internal consistency. There are many instances of five or more separate total ozone determinations being within ±0.0005 atm cm of each other; for example, over the five minutes near 1435 hours on 30 April. At times this consistency, of about ±0.2%, is maintained despite significant intensity changes caused by cloud. For example, during the periods of the data groups at both 1435 hours on 30 April, and at 1140 on 1 May, the raw intensities varied by 20%.

The total ozone data presented shows that for most of the time the two instruments are in very good agreement, their measurements being well within their experimental uncertainties of ±2%, over the encountered range of 0.020 atm cm, or 7%, in total ozone. All the instances of disagreement amount to less than 8% of the Dobson instrument values (±1% is equivalent to the height of the date characters in figure 9.1).

The differences shown on 1 May are due to airmass dependence of the Dobson instrument measurements. The effect is due to the increasing proportion of skylight to sunlight with airmass, and can be avoided by using the standard focussed-image technique. This point is well illustrated in figure 9.2, in which the 1 May total ozone data are plotted against airmass.

The scatter in the filter instrument data points of 3 May is caused by rapidly varying cloud whose presence can be clearly seen in the raw intensity measurements of all the bands. There was, however, a seven minute cloudless interval beginning at 11.38, during which the total ozone measurements were consistent to within 0.3% of each other and to within 1% of the single Dobson instrument value. The availability of the individual intensity measurements of the filter instrument is a distinct advantage in assessing the effects of cloud.

On 4 May, after an hour of very good agreement, the filter instrument data decrease and become about 7% lower than the relatively constant Dobson instrument values. The corresponding increase in cloud which was observed may have been the cause of the discrepancy, although the constancy of the Dobson instrument data places some doubt on this reason.

The only remaining disagreement, of about 8%, occurs on the first day of the comparison, 30 April, and may be due to either or both instruments. Increasing high cloud during the last hour of measurement halved the intensity levels, but appears to have had little effect on the total ozone values. Incorrect alignment or operation of the filter instrument are possible causes, since the instrument's assembly and adjustment were rather hurried in order to obtain measurements this day.

It is interesting to note that the reduction in the Dobson instrument's total ozone data with airmass, shown in figure 9.2, is not symmetrical about local noon, but is greatest in the morning. The first two groups of filter instrument data show a similar, though smaller effect. This

suggests that the increasing skylight/sunlight ratio, which causes the reduction, was being enhanced in the morning by the radiance of haze or cloud within the instruments' viewing cones.

The total ozone error produced in this way will be approximately proportional to the instruments' fields of view. The filter instrument's field of view, at 2.3^{o}, is somewhat smaller than that of the Dobson instrument, and hence will give rise to smaller errors. The effect may be larger with the Dobson instrument owing to the internal scattering and subsequent transmission through the slits of longer wavelength radiation which has been scattered from the haze or cloud. It is possible that the differences in determined total ozone observed on 30 April and 4 May are partly due to these effects.

The relative constancy of the 1 May filter instrument data enables its use for determining the extraterrestrial constants, $\ln[P_{\infty}(\lambda_1)/P_{\infty}(\lambda_2)]$. The method is outlined in Section 1.2, and involves plotting a graph of $\ln[P(\lambda_1)/P(\lambda_2)]$ against airmass, as is done in figure 9.3. For constant atmospheric attenuation, equation (1.9) predicts straight lines with extraterrestrial constants as intercepts. Figure 9.3 shows the filter instrument to be independent of airmass up to an airmass of at least 4.0.

The superiority of this filter instrument over the prototype instrument is obvious from a comparison of figure 9.3 with figure 1.2. The nonlinearity of figure 1.2, which is largely due to the bandwidth effect on the 305 nm filter, has been almost completely eliminated by the narrower and steeper-sided filters of the new instrument. The 305 nm filter spectra can be compared from figures 2.2 and 8.7.

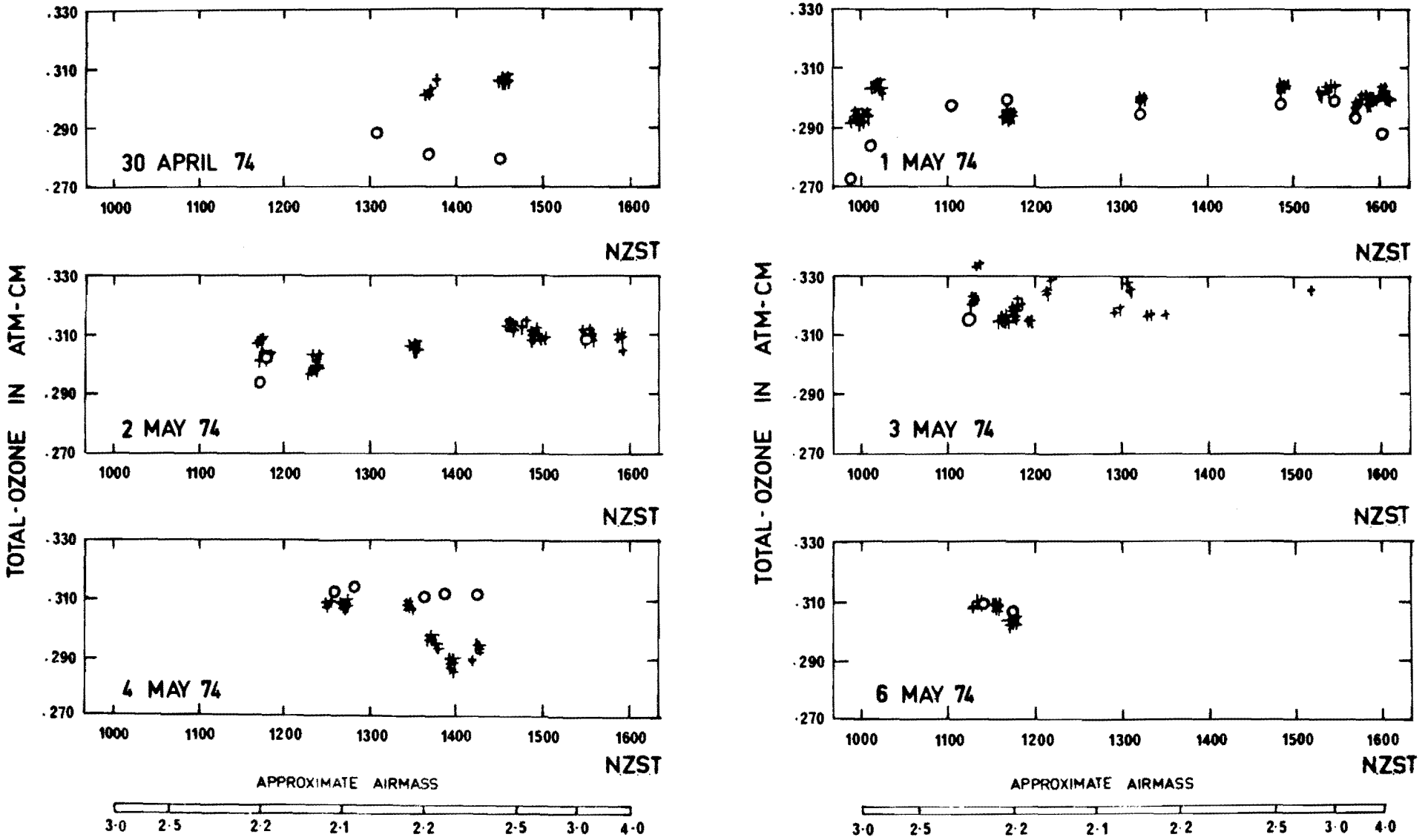

Fig 9 -1 MEASURED TOTAL-OZONE IN ATM-CM WITH NEW ZEALAND STANDARD TIME AND AIRMASS. COMPARISON OF FILTER INSTRUMENT (+) AND DOBSON INSTRUMENT (o) AT INVERCARGILL N.Z.

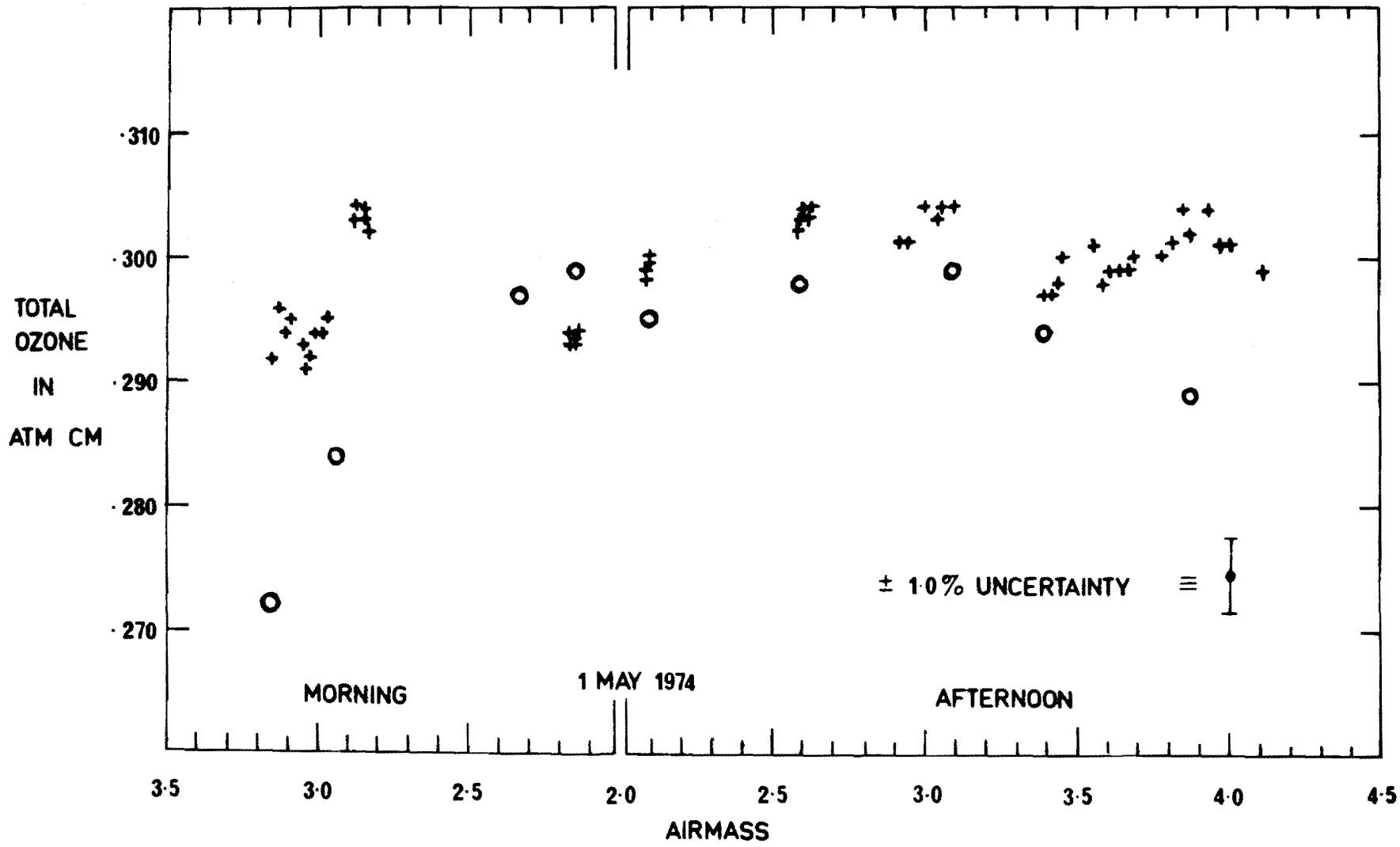

Fig 9-2 MEASURED TOTAL-OZONE WITH AIRMASS AT INVERCARGILL N.Z.
COMPARISON OF FILTER INSTRUMENT (✚) AND DOBSON INSTRUMENT (O)

FIG. 9.3
LOG RESPONSE DIFFERENCE VERSUS AIRMASS FOR A, C AND D PAIRS

EXTRATERRESTRIAL CONSTANTS

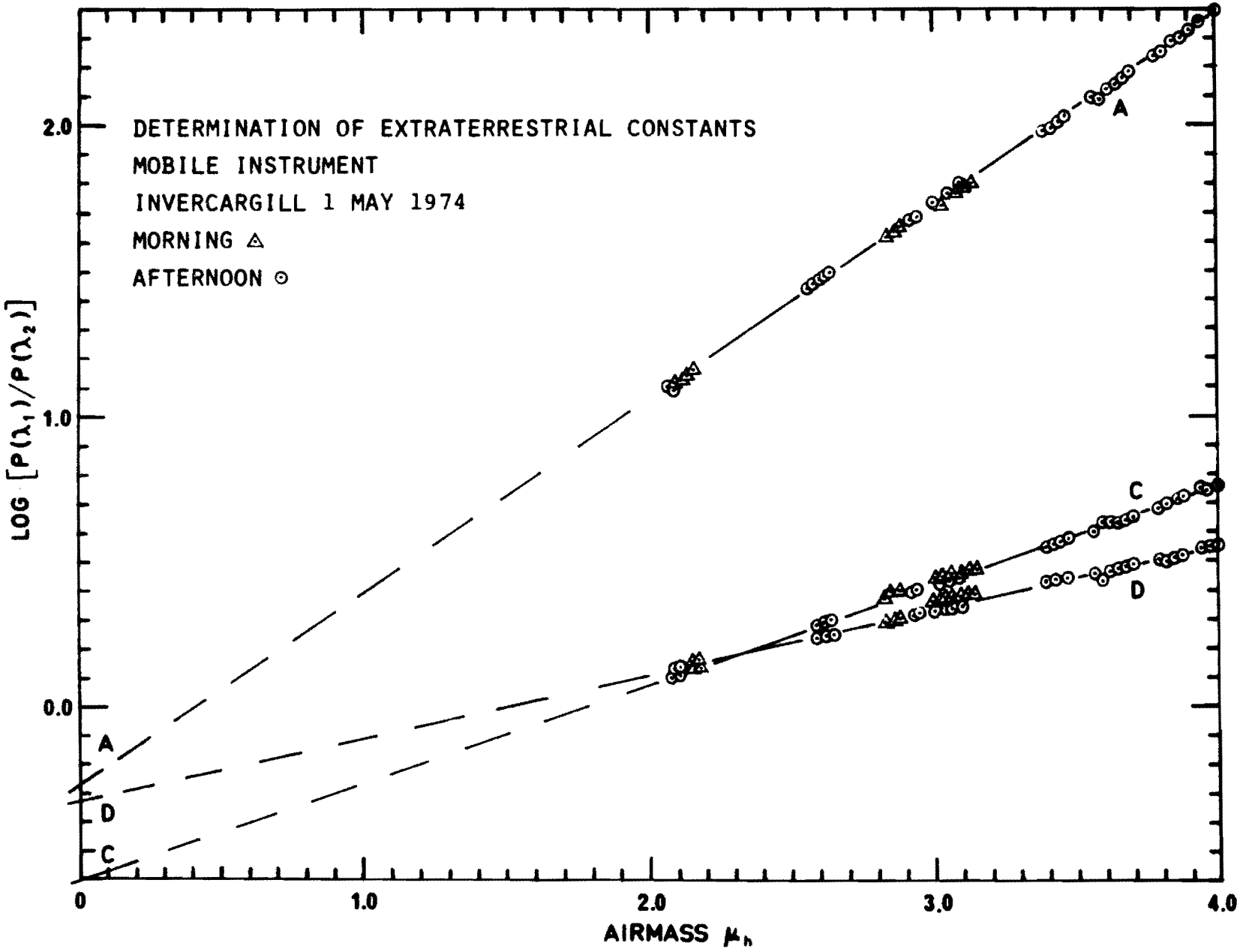

9.3 Summary and Conclusion

Most of the total ozone data determined by the two instruments agree to within ±1% over a 7% range in total ozone. This is not surprising, since the methods used are essentially the same, and the instruments' passbands, shown in figure 4.12, are very similar.

There are, however, two instances, on 30 April and 4 May, of 8% disagreements, which indicate the possibility of a design or operation fault in the filter instrument. The source of the disagreement should be found during the longer term comparison being conducted at present by the New Zealand Meteorological Service.

The filter instrument total ozone data shows no evidence of airmass dependence up to an airmass of 4.0. This performance is much better than that of the Dobson instrument and is partly due to the filter instrument's smaller field of view. It also depends on the narrowness of the filter pass-bands which minimises the errors due to the bandwidth effect. The filter instrument compares more than favourably with the standard Russian total ozone instrument, the M83 filter spectrophotometer, whose 6^{o} field of view and 25 nm filter half bandwidths result in total ozone errors of more than 30% at airmasses greater than 3.0 (Bojkov 1969, Asherovich et al., 1969).

The internal consistency of the filter instrument is excellent over periods of several minutes, but little can be said about its long term consistency, or about its accuracy over large ranges of total ozone. It is hoped that these questions will be resolved by the present evaluations of the instrument.

Despite the brevity of the comparison, the small range of total ozone encountered, and the uncertain effects of cloud, the filter instrument appears to have an accuracy comparable with that of the Dobson instrument.

The author is particularly grateful to Edith Farkas of the New Zealand Meteorological Service for her help in calibrating and operating the Dobson instrument and for analysing its raw measurements.

CHAPTER 10: OVERALL SUMMARY AND CONCLUSIONS

The aims of the project given in Section 1.3 have been largely met. The problem of the persistent systematic error of the prototype total ozone filter spectrophotometer, described in Section 1.3, has been solved, and a greatly improved instrument (figure 1.1) has been built as a result.

Detailed analyses of the characteristics of the instrument's filters and photomultiplier are made in Chapters 4 and 5 respectively, with a view to increasing the instrument's accuracy, and a full investigation of the filters' bandwidth effect, using a computer model of the measurement process, is described in Chapters 7 and 8.

The studies show that well designed interference filters are very suitable for use in the spectrophotometric determination of total ozone, and that the total ozone errors which result from the effect of temperature and from the bandwidth effect are small and can be easily corrected. Correction factors have been calculated and are listed for the filter set presently used.

The accuracy of the instrument has been partly verified by a direct comparison with a Dobson spectrophotometer as is reported in Chapter 9. Because the instrument was constructed prior to the completion of the studies of it, some aspects of its design are a little unsatisfactory. Suitable design changes are recommended in Chapter 6.

A summary of the instrument's design, from Chapter 3, and of the direct comparison of it and the Dobson instrument,

from Chapter 9, has been accepted for publication in Pure and Applied Geophysics early in 1975. However, before the instrument can be fully accepted, it will need to be evaluated over a period of at least a year, and over a wide range of atmospheric conditions. An effort in this direction is being planned.

The application of the filter instrument to zenith sky and Umkehr measurements also needs to be studied. It appears to be ideally suited to Umkehr measurements by virtue of its automation and the rapidity and simultaneity of its measurements. The bandwidth effect for this case can be calculated with the aid of the measurement model, but will be smaller than that for direct sun measurements.

Lastly, the instrument has the potential to investigate atmospheric aerosols through measurement of the aerosol gradient (equation 7.33). Its automation is clearly an advantage for following the relatively rapid changes in aerosol transmittance characteristics.

APPENDIX A

USE OF CARY 14 RECORDING SPECTROPHOTOMETER

A.1 Introduction

Much of the work of this thesis is heavily dependent on the spectral measurements made with the Physics Department's Cary 14 Recording Spectrophotometer. This Appendix describes some techniques developed by the author for measuring the low transmittance parts of interference filter spectra (Sections A.2 and A.3), the spectral sensitivity of photomultipliers, (Section A.4), and the effects of temperature on filter spectra (Section A.5). To provide a basis for these sections, a brief general description of the Cary 14 is given.

The instrument uses the comparative photometry principle. A light beam is passed alternately through a reference chamber and a sample chamber, and the ratio of the transmitted intensities determines the sample's transmittance. A double monochromator, consisting of a quartz prism and an echelette grating, is driven to provide a linear scan of the wavelength spectrum, and the resulting transmittance spectrum is recorded on linear chart paper by a servo-driven pen.

Transmittance calibration is made by electronically scaling the transmittance reading to 100% when no sample is present. An accuracy of from 0.2% to 2.0%, depending on transmittance, is possible in the available 10% and 100% full-scale ranges. Wavelength calibration is achieved by comparing the measured centre wavelengths of the emission lines of a mercury vapour lamp with standard values (Cary). A wavelength accuracy of about 0.05 nm can be attained.

Various combinations of two radiation sources and three detectors enable measurements from 186 nm to 2600 nm. Further details of the instrument can be found in the manufacturers handbook (Cary).

A.2 Low Transmittance Measurements

Low transmittance (<0.1%) regions in the spectrum of an interference filter can contribute a sizeable proportion of the filter's total transmitted radiation when the filter is used for measurement of direct solar ultraviolet radiation, especially if the regions are on the long wavelength side of the filter passband. The consequences for total ozone measurement using interference filters are discussed, initially in Section 2.2, and more fully in Part III.

As already indicated, in the Cary a filter's transmittance at any wavelength is proportional to the ratio of transmitted sample path and reference path intensities. A very low transmittance therefore gives rise to a very small ratio. However, if the ratio is too small to be recorded on the instrument's 10% scale, it may be increased by inserting a suitable attenuator into the reference path. In particular, if a neutral density filter of optical density 1.0 is introduced, the ratio increases ten times and may become measurable. (An optical density of x is equivalent to an attenuation of 10^x.) The effect is to change the full scale readings from 10% and 100% to 1% and 10%.

The author has found it possible to introduce up to four such neutral density filters having a combined optical density

of 4.0 and thus to provide a full scale transmittance of 0.001%. Transmittances of 0.00001% or 10^{-7} can then, in principle, be detected. For the measurement of a complete spectrum it may be necessary to periodically change the number of neutral density filters used.

An example of the technique is to be seen in figure A.1, which traces the transmittance spectrum for the 340 nm filter. The logarithmic spectrum of figure 4.6 is derived from this spectrum. Two neutral density filters, each of optical density 2.0, are used in conjunction with the instrument's 10% and 100% scales. They are made from crossed stainless steel gauze, and are spectrally flat to 2% within the near ultra-violet spectrum.

The lowest transmittance measurable is determined by the signal to noise (D.C. and A.C.) ratio and spectral resolution required. Progressively decreasing transmittance eventually reduces the radiation flux at the instrument's detector to a level which is insignificant compared to the instrument's internal noise level. The noise limit for the spectrum of figure A.1 can be read off as equivalent to a transmittance of about 10^{-7} at 400 nm and 10^{-6} at 290 nm, and is largely due to radiation scattered within the instrument, and to the dark current of the instrument's photo-detector. The signal to noise ratio can be increased by opening up the optical slits since this increases the radiation flux at the detector, but the increased width results in decreased resolution.

A feature of the Cary is a servo system which continually adjusts the slit widths to maintain a constant detector output for the reference path beam. This results in an approximately constant signal to noise ratio and in normal operation

compensates for changes in the source intensity and detector sensitivity with wavelength. It can be seen that with the introduction of a neutral density filter into the reference path, the servo system will widen the slits in order to increase the radiation flux at the detector to its previous level. As a result, the resolution decreases.

At low transmittances, the resolution can be improved in the following three ways.

(1) A smaller signal to noise ratio can be set by adjusting the slit servo amplifier. This gives smaller slit widths and therefore better resolution, but the transmittance accuracy is less, owing to the increased D.C. component of the noise, and the pen response is noisier, owing to the increased A.C. component.

(2) Increasing the source lamp voltage increases the source intensity, particularly in the ultraviolet spectrum. The slit servo system compensates for the increased detector signal by setting smaller slit widths.

(3) Increasing the photomultiplier's supply voltage increases its gain and therefore its output signal, and, as with (2) above, results in smaller slit widths. Its D.C. and A.C. noise also increase, but at lesser rates.

The following approximate expression for the spectral resolution, $\Delta\lambda$, within the spectral range 300 nm to 400 nm, can be derived from information given in the instrument's handbook.

$$\Delta\lambda = 4.5W + 0.3 \text{ nm} \qquad \text{(A.1)}$$

where W is the slit width in mm, displayed on the instrument. The 0.03 constant is the resolution limit due to diffraction and slit curvature mismatch. The resolutions for the 340 nm filter are listed in figure A.1.

At the sides of interference filter passbands, where the transmittance changes rapidly with wavelength, it is necessary to maintain a good resolution for accurate measurements. The following section describes a quantitative method for determining the resolution required.

A.3 The Error Due to Low Resolution of an Exponential Transmittance Spectrum

Because the spectral transmittance of a filter is generally not linear with wavelength (e.g. figure A.1), its measurement using a finite wavelength band will be in error. However, it is possible to derive an expression for this transmittance error if the spectrum around the band is approximated by an exponential function. It is reasonable to do this for the interference filters, since their logarithmic spectra, figures 4.1 to 4.6, are approximately linear over small wavelength intervals.

Figure A.2 represents a measurement of an exponential transmittance

$$F = e^{a\lambda+c} \qquad (A.2)$$

where a is the exponential gradient and c is a constant appropriate to the wavelength interval of width $\Delta\lambda$ and centred on λ_c. $\Delta\lambda$ represents the spectral resolution of the measurement.

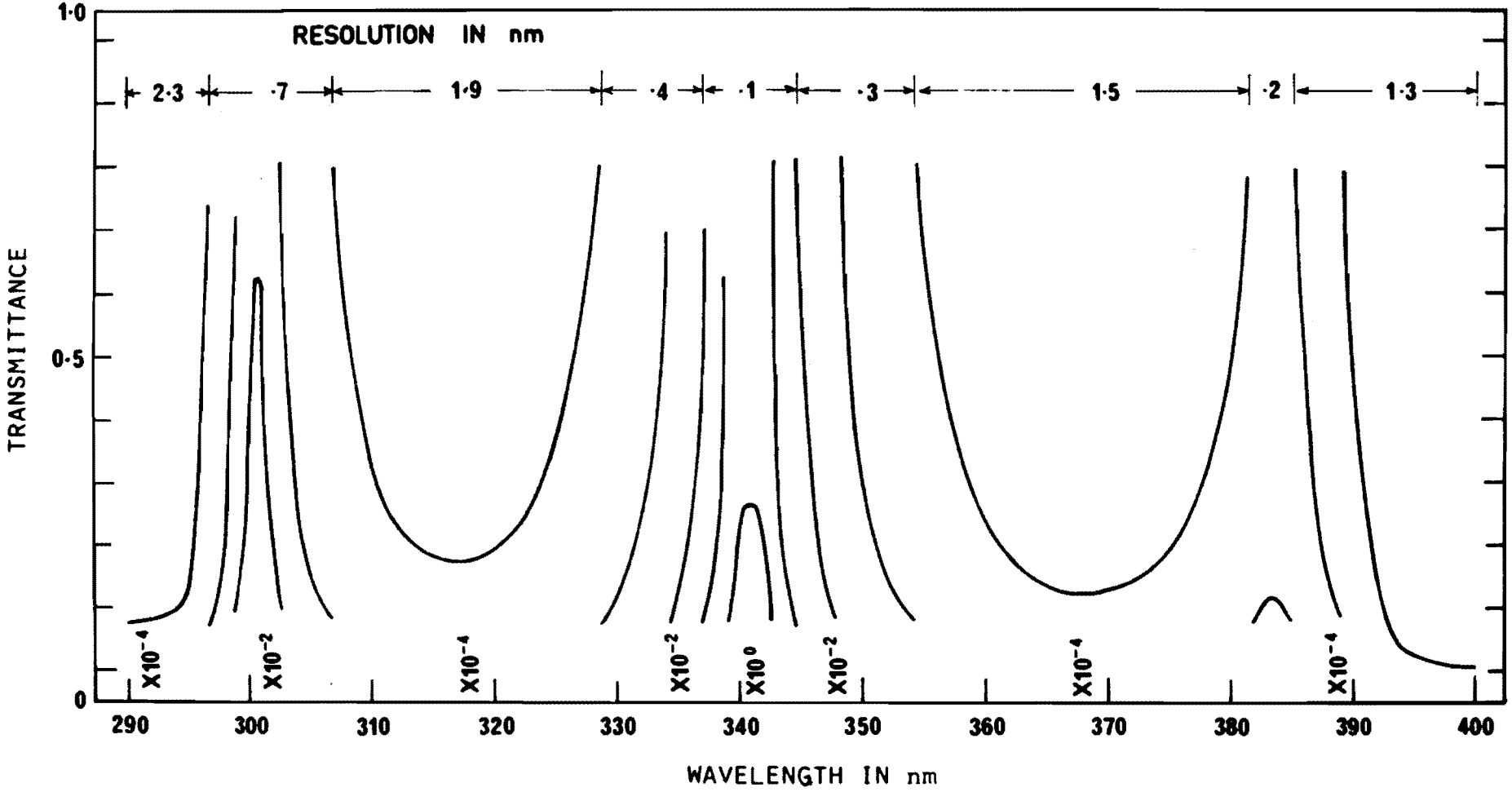

FIG. A.1 COPY OF CARY 14 TRANSMITTANCE CHART RECORD FOR 340nm FILTER SHOWING PERIODIC 10X SCALE CHANGES AND WAVELENGTH RESOLUTION.

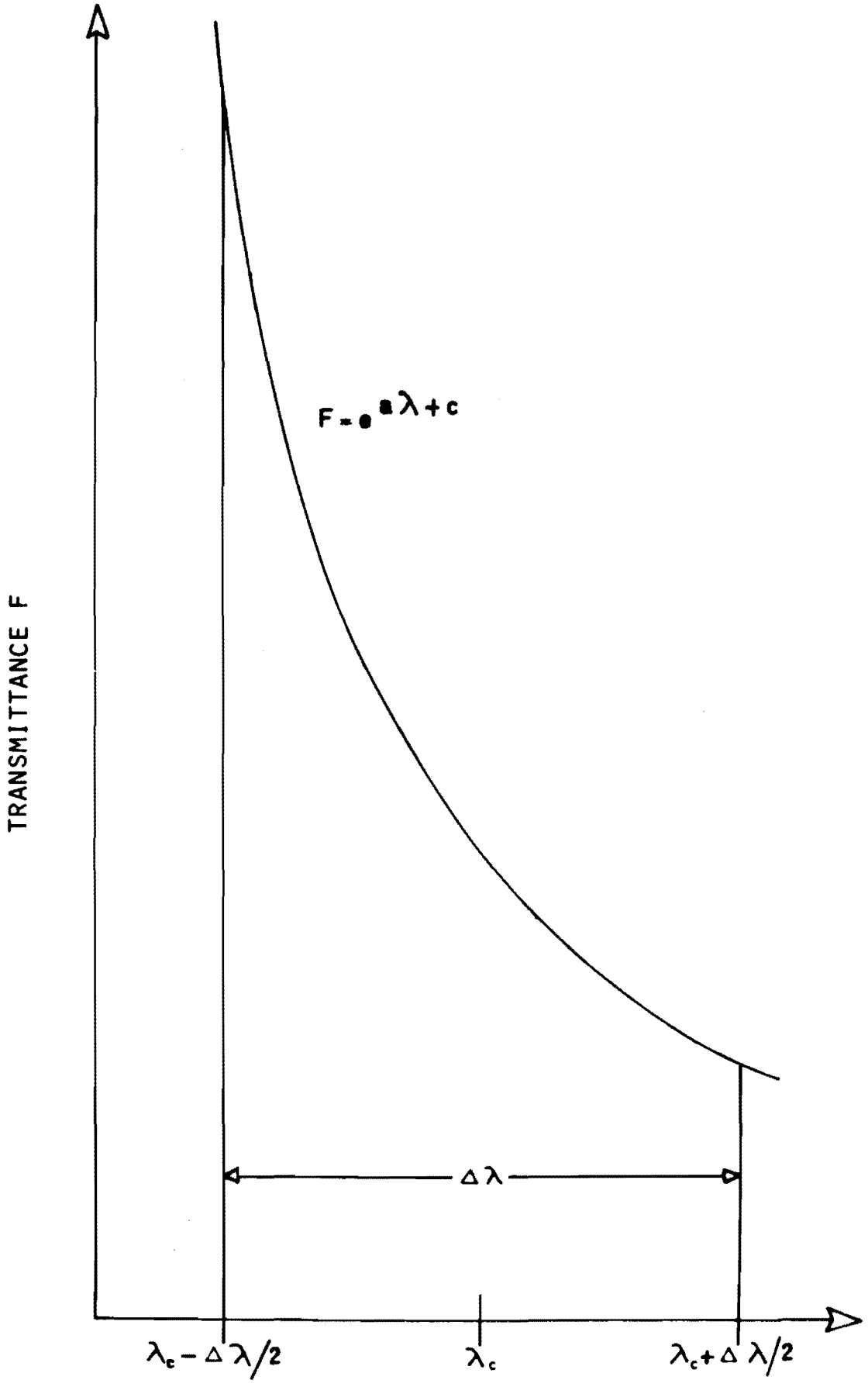

FIG. A.2 FINITE RESOLUTION OF AN EXPONENTIAL TRANSMITTANCE.

The result of the measurement, F_m, is the average of the transmittance over the interval, i.e.

$$F_m = \frac{1}{\Delta\lambda} \int_{\lambda_c-\Delta\lambda/2}^{\lambda_c+\Delta\lambda/2} e^{a\lambda+c}\, d\lambda \qquad (A.3)$$

$$= \frac{1}{a\Delta\lambda}\, e^{a\lambda_c+c}\, (e^{a\Delta\lambda/2} - e^{-a\Delta\lambda/2}) \qquad (A.4)$$

which can be expressed as

$$F_m = F_c \frac{\sinh y}{y} \qquad (A.5)$$

where F_c = actual transmittance at λ_c

and $y = a\Delta\lambda/2$ (A.6)

The error in the measurement, E_r, due to the finite resolution, is then

$$E_r = F_m - F_c = \frac{\sinh y}{y} - 1 \qquad (A.7)$$

As $y \to 0$, the error $E_r \to 0$. This corresponds to either a very shallow gradient, or a very narrow resolution.

Figure A.1 provides a good example for the use of equation (A.7); the resolution, $\Delta\lambda$, is given, and the gradient, a, can be determined, and hence y is known. (Note that a can also be found from figures 4.1 to 4.6). For instance, near the passband, the resolution is 0.1 nm, and since the transmittance changes by a factor of 10 in 1.5 nm, the exponential gradient must be 1.54. The data of table A.1 is found in a similar

fashion, and shows that the resolution error is small, increases with decreasing transmittance, and in the high transmittance regions is negligible.

TABLE A.1: Resolution Error for the 340 nm Filter

Wavelength Region	340	350	360	nm
Gradient a	1.5	0.7	0.4	nm^{-1}
Resolution $\Delta\lambda$	0.1	0.3	1.5	nm
Error E_r	0.1	0.2	2.0	%

In practice, equations (A.6) and (A.7) were used to find the resolution required to keep the error to an acceptable level. Section A.2 lists the three steps that can be made to improve the resolution. When the neutral density 4.0 filters were being used it was necessary to invoke all three steps to their maximum extent.

A.4 Photodetector Spectral Sensitivity Measurements

It has been found possible to use the Cary to measure the relative spectral sensitivity of certain photodetectors to an accuracy of about ±5% over a sensitivity range of three decades. The key to the method is the slit servo system, described in Section A.2, which adjusts the widths of the optical slits to maintain a constant detector output for the reference path beam.

This constant output is proportional to the detector's spectral sensitivity, $D_0(\lambda)$, and to the reference path beam flux. This flux is, in turn, proportional to the source intensity, $I_0(\lambda)$, and to the square of the slit width, $d(\lambda)$.

The slit width is squared because there are two active slits, each with width $d(\lambda)$. Hence the product

$$D_0(\lambda)I_0(\lambda)d^2(\lambda) = \text{constant.} \qquad (A.8)$$

Now the flux in the sample path, $W_s(\lambda)$, is also controlled by the slits, and is therefore proportional to the square of the slit width as well as the source intensity. That is,

$$W_s(\lambda) \propto I_0(\lambda)d^2(\lambda) \qquad (A.9)$$

Combining equations (A.8) and (A.9) eliminates both $I_0(\lambda)$ and $d(\lambda)$ to give

$$W_s(\lambda) \propto (D_0(\lambda))^{-1} \qquad (A.10)$$

Thus the sample path flux is inversely proportional to the spectral sensitivity of the instrument's detector. In the case of the 1P28 photomultiplier which is used in the near-ultraviolet and visible spectral regions, this spectral sensitivity is reasonably well known (type S5 in RCA 1970). Hence the Cary provides a beam of radiation whose wavelength, resolution and relative spectral intensity is known, and which therefore can be used to calibrate the relative sensitivities of other detectors.

If an external detector is placed in the sample chamber, its electrical output, $P_s(\lambda)$, will be proportional to its own spectral sensitivity, $D_s(\lambda)$, and to the sample path flux, $W_s(\lambda)$. Hence by equation (A.10),

$$P_s(\lambda) \simeq D_s(\lambda)/D_0(\lambda) \quad (A.11)$$

$$\text{or} \quad P_s(\lambda) = kD_s(\lambda)/D_0(\lambda) \quad (A.12)$$

where k is a constant.

Since $P_s(\lambda)$ can be measured experimentally and $D_0(\lambda)$ is known, the relative spectral response, $kD_s(\lambda)$, of the external detector can be found.

The above method was used to measure the spectral sensitivities of the two experimental photomultipliers described in Section 5.4. In the experiment, the photomultiplier output current, $P_s(\lambda)$, is converted by a logarithmic amplifier to a voltage which is recorded on a chart recorder. By adding the appropriate values of log $D_0(\lambda)$ to the charted values of log $P_s(\lambda)$, a graph of relative spectral sensitivity, kD_s, is produced.

The method requires that:

(i) the photosensitive area of the external detector is of constant sensitivity across its whole area, so that the detector's output is strictly proportional to the square of the slit widths;

(ii) the spectral sensitivity of the instrument's detector is the same as that published, in particular, that the Cary's 1P28 photomultiplier is well described by the standard S5 type response shown in RCA 1970;

(iii) the external and instrument photodetectors have their main band of sensitivity in approximately the same spectral region;

(iv) the slit servo system is sufficiently precise.

It is possible to check the first requirement by measuring the external detector's response for various known slit widths. The second requirement was partially verified by testing another 1P28 photomultiplier as the external detector. If its relative spectral sensitivity is the same as that of the instrument's 1P28, then by equation (A.12), its electrical output will be spectrally constant.

The test showed this to be the case. The relative spectral sensitivities were found to be equal to within ±5% over the full response range, from 300 nm to 700 nm, and to within ±2.0% over any 50 nm within this range. This equivalence suggests that the relative spectral sensitivities of 1P28 photomultipliers do fall within a well defined class and are hence well described by the standard S5 type response. In support of this, there is no indication from the manufacturer (RCA 1970) of significant variation in spectral response from the standard.

The above test also shows that the slit servo system is accurate to at least ±5%, since within the spectral range there are regions of both increasing and decreasing slit widths.

A.5 Measurement of the Effect of Temperature on Interference Filters

The various effects of temperature on interference filters are discussed in Section 4.7. The most significant of these is the small, positive, and linear shift in centre wavelength with temperature. It is measured in the following manner.

The filter perimeter is surrounded by a 0.3 litre water jacket which is connected by a pump and hoses to a 6.0 litre constant temperature water bath. The filter temperature is measured by a fine copper-constantan thermocouple mounted in the centre of the filter's face. The filter and jacket are placed in the Cary's sample chamber and when temperature equilibrium is reached, a passband transmittance spectrum is recorded, using the lowest scanning rate. Each spectrum is overlaid by a reference spectrum, taken at some reference temperature, to find the relative shifts of the start and finish wavelength marks.

Figure 4.17 shows the relative shift in centre wavelength of two filters for the temperature range of $0^{o}C$ to $40^{o}C$. Because the shifts are small, i.e. at 0.01 nm/^{o}C, great care is needed to minimise the errors due to slackness in the gear transmissions of the wavelength and chart drive systems. It is also very important to maintain the filter in a fixed orientation relative to the sample radiation beam, since the passband will shift with angle of incidence, as is described in Section 4.5. A 2^{o} change from normal incidence will cause a 0.1 nm shift in centre wavelength. This is equivalent to the shift caused by a $10^{o}C$ temperature change.

APPENDIX B

ASSESSMENT OF THE TOTAL OZONE ERROR CAUSED BY A MONOCHROMATIC LEAKAGE BAND IN A FILTER

The spectral transmittances of a filter's leakage band and passband can be approximated by triangular functions which have the same peak transmittances and bandwidths as the original bands. The ratio of the areas of the triangles then represents a measure of the relative contribution of the leakage band to the photometer's total electrical output for the filter.

This ratio, R, is called the Power Ratio by the author, and is defined as

$$R = \frac{(\text{leakage peak transmittance})(\text{leakage half bandwidth})}{(\text{passband peak transmittance})(\text{passband half bandwidth})} \qquad (B.1)$$

The power ratio can be summed for more than one leakage band, but usually only one band is of importance for the interference filters used. It should not be confused with the Rejection Ratio which is used by most manufacturers to specify their products, and which is the ratio of only the peak transmittances. The rejection ratio excludes the ratio of leakage half-bandwidth to passband half-bandwidth, which typically ranges from 2 to 15, and therefore does not describe the relative power contributions of the bands.

The error in total ozone caused by a leakage band can be assessed as a function of the power ratio. Following equation (1.6), the photometer's electrical response P_i, due to a narrow filter band at wavelength λ_i can be very well approximated by

$$P_i = P_{\infty i}\, e^{-\mu(X\alpha_i+\beta_i+\delta_i)} \tag{B.2}$$

where μ is the airmass, $P_{\infty i}$ the photometer's response at $\mu = 0$, X the total ozone, and α_i, β_i and δ_i the coefficients of ozone absorption, molecular scattering and aerosol scattering respectively at wavelength λ_i. Thus, the response to a filter passband at λ_1 is

$$P_1 = P_{\infty 1}\, e^{-\mu(X\alpha_1+\beta_1+\delta_1)} \tag{B.3}$$

A small error ΔP_1 in P_1 will therefore cause an error ΔX in total ozone X, where

$$\Delta X = \frac{-\Delta P_1}{\mu\alpha_1 P_1} \tag{B.4}$$

If the error ΔP_1 is caused by a small leakage band in the filter at λ_2, then one may write that

$$\Delta P_1 = P_2 = P_{\infty 2}\, e^{-\mu(X\alpha_2+\beta_2+\delta_2)}. \tag{B.5}$$

Combining equations (B.3), (B.4) and (B.5) results in

$$\Delta X = \frac{-1}{\mu\alpha_1}\frac{P_{\infty 2}}{P_{\infty 1}}\, e^{-\mu(X(\alpha_2-\alpha_1)+\beta_2-\beta_1+\delta_2-\delta_1)} \tag{B.6}$$

which can be simplified by the following approximations.

(i) The photometer's detector sensitivity and the solar irradiance are approximated as spectrally flat. This means that the ratio of $P_{\infty 2}$ to $P_{\infty 1}$ is just the ratio of the integrals of the bands' transmittance which in turn is

approximated by the power ratio, R.

(ii) Since the ozone absorption coefficient at the usual wavelengths of the leakage bands (350 nm to 370 nm) is small, the coefficient α_2 is set to zero.

(iii) The difference in aerosol scattering, $\delta_2-\delta_1$, is unknown, but is believed to be small, so is set to zero.

Hence,

$$\Delta X = \frac{-R}{\mu\alpha_1} e^{\mu(X\alpha_1+\beta_1-\beta_2)} \qquad (B.7)$$

Equation (B.7) can be used to find the approximate error in total ozone caused by a filter leakage band, or conversely, to specify a filter's maximum allowable power ratio for a given performance criterion.

The criterion used in specifying the maximum power ratios for the new set of filters described in Chapter 4, was that the total ozone error due to a leakage band at 40 nm beyond the passband, and at an airmass of 4 and total ozone value of 0.400 atm cm , be less than 1%. The calculated power ratios are listed in table B.1 below.

TABLE B.1: Maximum Power Ratios for Standard Wavelength Filters

Wavelength	305	311	317	325	332	340	nm
Power ratio	5×10^{-6}	10^{-4}	3×10^{-4}	3×10^{-4}	2×10^{-4}	10^{-4}	

APPENDIX C

DATA ACQUISITION BY MINI-COMPUTER

A PDP-8 mini-computer, used as part of the fully automatic ozone spectrophotometer, controls the acquisition, storage and subsequent output of data by a combination of external timing pulses, internal programmes, and keyboard commands. The task is complicated by the fact that it shares its time, and its rather small 4K words of memory, among two other experiments and a monitor control programme. Careful, compact programming, in assembler language, is needed in order to provide a good sized data storage space as well as accurate counting and flexible operation which are well protected against external electronic failure.

The programme, written by the author, uses the PDP-8 real-time clock to provide accurate sampling rates and time-of-sample information. As with the mobile spectrophotometer, the filter channel counts are integrated over a chosen number of disc cycles during each sample. The resulting six, double precision (.'. 24 bit) words are stored along with the number of integrations made and the time when the record was made.

The user initialises and controls the system with simple keyboard commands and switch-register settings. In this way the programme is engaged into and out of the monitor programme, the data areas are cleared, and the date, the starting time, the sample rate and the integration number are set. Initialising takes no more than five minutes, and the sample rate and integration number can be changed at any time.

The printing/punching data output programme has two options. One writes out all the accumulated data for permanent storage, while the other writes just the last two records taken along with the time interval before the next record, to enable checking of the measurements. All data is converted to decimal form before writing, and the sample times are in New Zealand Standard Time. The paper tape copy of the accumulated data is processed in a larger computing facility to provide total-ozone values. The arithmetic involved in simple, however, and could be carried out in an unshared mini-computer.

The programmes occupy 0.4K words leaving 1.4K words for data storage. At 14 words per record this allows 100 records. At one record every six minutes, ten hours sampling is possible. By adjusting the sampling rate during the day, the density of measurements can be varied to suit the experimental requirements.

If the time required to complete a chosen number of integrations is greater than the interval between samples, the programme prematurely terminates the integrating in time for the next record, and stores only the data actually accumulated. For example, a sample interval of one minute will allow only about 150 0.4 sec. cycle integrations, irrespective of how large a number is chosen. When the allocated data storage areas are full, the programme stops all sampling.

A feature of both the controlling and the printing programmes is their ability to automatically cope with filter discs which have less than the usual six filter channels. The necessary information on the position and number of channels is derived from the position of the photoswitch mirrors carried

by each filter disc around its perimeter. Filter discs can therefore be readily interchanged for instrumental comparison, and individual filter channels excluded by taping their mirrors. There is also the possibility of using the photometer and programmes for quite different spectral measurements.

APPENDIX D

TEMPERATURE DEPENDENCE OF OZONE ABSORPTION

In the determination of total ozone, as described in Section 1.2, it is assumed that the ozone absorption coefficient is constant and independent of the stratospheric conditions of pressure and temperature. In fact, this is not so. The coefficient, although independent of pressure (Vigroux 1953, Hearn 1961) is quite dependent on temperature, as is clearly shown by Vigroux' (1953) experiments. The purpose of this Appendix is to briefly examine the nature of the dependence and its effect on the total ozone determination.

Ozone's near-ultraviolet absorption is due to the long wavelength wing of a broad band of electronic-vibrational-rotational lines which extend up from 200 nm. The band is very strong, having a peak absorption coefficient, at 260 nm, of about 250 cm^{-1}, and consists of a multitude of transitions between the combined electronic and vibrational-rotational energy levels of the triatomic molecule.

Vigroux's (1953) measurements of this spectrum were made at nine temperatures, ranging from 181^{o}K to 393^{o}K, and detailed the maxima and minima. Figure 8.3 shows a spectrum reconstructed from the data taken at 229^{o}K.

The effect of temperature is generally to increase the coefficient, the change being greatest for the minima, and therefore tending to smear out the detail. The principal minima increase steadily over the whole temperature range by as much as 0.7% per ^{o}K, whereas the principal maxima show a turning pattern, at first slowly decreasing, by about 0.1% per

^{o}K from 181^{o} to 198^{o}K, then remaining constant until 229^{o}K, beyond which they slowly increase.

This behaviour can be simply interpreted as temperature broadening of the many individual absorption lines whose wings overlap to form the observed spectrum. In this case, each line spreads out with temperature, its bandwidth increasing and correspondingly, its height decreasing.

The temperature dependence of the absorption at a particular wavelength will depend on the strength and proximity of the surrounding lines. With increasing temperature, the decrease in the maxima, by their own broadening, will be opposed by the increase due to the broadened wings of adjacent lines, and the resulting sum may increase or decrease. On the other hand, the minima can only increase with temperature. The greater strength and density of lines at shorter wavelengths ensures a general increase in absorption with temperature in the region of interest, 290 nm to 370 nm.

At first sight, it might appear that the effect of the temperature dependence could be minimised by choosing the instrument slits or filter bands to lie on the absorption maxima, since, over the 200^{o}K to 250^{o}K stratospheric temperature range, these only vary by about 2% whereas the minima vary by up to 30%.

However, the total ozone, as determined by the usual equations (see equation (1.7), Section 1.2), is inversely proportional to the difference of the absorption coefficients for two wavelength bands, and therefore only changes in this difference need be minimised. This can be achieved by choosing the smaller absorption coefficient to be more temperature-dependent than the larger one.

An example of this method can be found in Brewer's (1973) spectrophotometer. One band of a pair, at 310.4 nm, has an absorption coefficient of 2.3 cm^{-1} whose temperature dependence is about 0.1% per ^{o}K, while the other band, in a minima at 323.9 nm, has a smaller absorption coefficient of 0.22 cm^{-1} whose temperature dependence is larger, at about 0.7% per ^{o}K. The temperature dependence of the difference of these two absorption coefficients is therefore

$$(2.3 \times .001 - 0.22 \times .007) = .08 \text{ cm}^{-1} \text{ per } ^{o}K,$$

$$= .04 \% \text{ per } ^{o}K.$$

This value, which also represents the temperature dependence of the derived total ozone, is markedly smaller than both the original band dependences.

Unfortunately, the detail in the absorption spectra is such that only very narrow bands, less than 0.2 nm in bandwidth, can be completely sited on maxima or minima. The larger 1 nm to 3 nm bands of the filter instrument and Dobson instrument can only be approximately sited, so as to include as many or as few maxima and minima as required. Because of this, the temperature dependence of both the absorption coefficients of a pair of bands will be similar.

Since the larger coefficient is usually about ten times the smaller coefficient, the temperature dependence of the difference will be essentially that of the larger coefficient. This being so, the temperature dependence of the difference of the absorption coefficients, and therefore of the total-ozone, is about 0.1% to 0.2% per ^{o}K. The maximum range of

stratospheric temperature, 30^{o} say, will result in, at most, a 6% range in total ozone.

These values are similar to those of Walshaw et al. (1971) who, along with Powell (1971), give detailed consideration to the effect of temperature on the determination and use of ozone absorption coefficients for the Dobson instrument.

APPENDIX E

COMPOSITE BLOCKING FILTER CONSTRUCTION

This Appendix describes the construction of the blocking filter used in the filter photometer. The main task is to grow a large, blemish free, nickel sulphate hexahydrate crystal.

To do this, an aqueous salt solution, held at constant temperature ($\pm 0.5^{o}C$), is seeded, and then is slowly evaporated to maintain a steady solution saturation while the crystal grows. The solution temperature must be above $32^{o}C$ or else the undesired heptahydrate crystal forms in preference.

As the crystal increases in size, it may become necessary to remove it to replenish the solution. Cleanliness, and care in maintaining the correct temperature and saturation are necessary during this process, and also during the initial seeding, in order to produce a clear regular crystal. A growing period of a month may be needed for a large crystal of, say, 4 cm diameter.

An alternative method of growing the crystal, used and described by Matthews (1971), is to maintain the solution's saturation by a stepped reduction in its temperature. This method is less preferred since, firstly, it requires a more sophisticated temperature controlled bath, and more attention during crystal growth, and secondly, because the temperature, and therefore saturation, is discontinuous, a less perfect crystal is likely to result.

A 4 cm crystal, produced by the author using the first method, was cleaved, and a 4 mm thick slice sandwiched between two pieces of Corning CS 7-54 glass. To prevent hydrolysis of the crystal, and mechanical damage, the edges of the composite blocking filter were sealed with a hard setting glue (Araldite). The filter's size was about 1 cm cubed. Its transmittance spectrum is given in figure 4.10.

APPENDIX F

PHOTOMULTIPLIER VOLTAGE DIVIDER DESIGN

As explained in Chapter 5, the gain of a photomultiplier equipped with a resistive voltage divider is dependent on the internal current in the tube. This effect, which may deprive the tube of its valuable linearity of current output with incident intensity, only becomes important in the last dynode stages where the internal current may become a significant proportion of the total bleeder current in the divider.

From a consideration of the network of currents in a tube, a simple expression can be derived for the relative gain change, dG/G, as a function of anode current, i_a, initial bleeder current, i_b, the number of stages, N, and the mean gain per stage, δ. From Philips (1970) this is:

$$\frac{dG}{G} = \frac{i_a}{i_b}\left[\frac{N}{N+1} - \frac{1}{(N+1)(\delta-1)}\right] \qquad (F.1)$$

which can be used to calculate the anode and bleeder current limits consistent with the desired gain stability.

The instrument's 1P28 photomultiplier has N = 9 stages and its voltage dependent mean gain per stage, δ, can be calculated from the manufacturer's listed current amplification. For example, the typical current amplification at 1000V is given as 2.5×10^6, so assuming the gains per stage to be similar, then

$$\delta^N = 2.5\times10^6 = 10^{6.4},$$

and since N = 9,

$$\delta = 10^{(6.4)/9} = 5.14.$$

The mean gain per stage for other voltages can be calculated from the knowledge that, for interstage voltages of less than 200V, the gain per stage is proportional to the interstage voltage (RCA 1970, Philips 1970). The resulting gain characteristics are assembled in table F.1 below.

TABLE F.1: Gain Characteristics for 1P28 Photomultiplier with Purely Resistive Voltage Divider.

Voltage	Mean gain/stage	Relative Gain Change dG/G
500V	2.57	0.836 i_a/i_b
750	3.86	0.865 i_a/i_b
1000	5.14	0.876 i_a/i_b
1250	6.43	0.882 i_a/i_b

It can be seen that, for the usual operating voltages, the bracketed factor in equation (F.1) is largely independent of the voltage and that the equation can be approximated by

$$\frac{dG}{G} = 0.86 \frac{i_a}{i_b} \qquad (F.2)$$

In our case, because the instrument's photomultiplier voltage divider uses zener diodes to keep the first two stages at constant voltage, the above theory must be applied only to the remaining eight resistors. Therefore N = 7 and the total resistor voltage V_r is the difference between the overall voltage and the total zener diode voltage of 250V.

At 1250V, each stage has 125V across it, and so the gain per stage of $\delta = 6.43$, listed in the above table, applies to both zener and resistor stages. Again, the fact that the gain per stage is proportional to applied voltage, (across the dynode resistors only) enables the gain per stage for other voltages to be found and table F.2 to be constructed.

TABLE F.2: Gain Characteristics of 1P28 Photomultiplier with Two Zener Diodes in the Voltage Divider.

Overall Voltage	Resistor Voltage	Mean Gain per Stage	Relative Gain Change dG/G
500V	250V	1.61	0.670 i_a/i_b
750	500	3.21	0.818
1000	750	4.83	0.842
1250	1000	6.43	0.852

Equation (F.1) can again be approximated, in this situation by

$$\frac{dG}{G} = 0.8 \frac{i_a}{i_b} \qquad (F.3)$$

which is little different from equation (F.2) for the 1P28 without the two zener diode stabilisers. It is clear from both equations (F.2) and (F.3) that a high gain stability requires a low ratio of anode current to bleeder current.

The instrument's bleeder current is determined by the photomultiplier high voltage source, which provides a maximum bleeder current of 2 mA at an overall voltage of 1250, and lesser amounts, proportional to the total resistor voltage (i.e. excluding the zener diodes), at other voltages. The

maximum anode currents consistent with gain stabilities of 0.1% and 1.0% are calculated from this data and that from table F.2, and are displayed in table F.3.

TABLE F.3: Anode Current Stability for 1P28 with Zener Diodes

Overall Voltage	Resistor Voltage	Bleeder Current	Max. Anode Current for dG/G = 0.1%	1%
500V	250V	0.5 mA	0.75 μA	7.5 μA
750	500	1.0	1.22	12.2
1000	750	1.5	1.78	17.8
1250	1000	2.0	2.34	23.4

Hence, in the range of usual operating voltages, 500V to 750V, gain stabilities of 0.1% and 1.0% are limited to anode currents of less than approximately 1 μA and 10 μA respectively.

The current limits can be raised by increasing the bleeder current, either in the whole resistor chain, or in just the final stages. The first method involves a more powerful high voltage supply which would be difficult to build with sufficient regulation. The second method is the more elegant, as it supplies the higher bleeder current only to the final high internal current stages, and requires only an additional low voltage high current source, e.g. a maximum of 250V applied over the last two stages at a bleeder current of say 10 ma.

APPENDIX G

NUMERICAL MODEL DETAILS

G.1 Introduction

This appendix provides the details of the computer model which is briefly described in Section 8.1. It is principally concerned with the sources and accuracies of the various components of the model which appear in equations (7.1), (7.2) and (7.3).

These components include: the integration bounds and integration interval (this section); the solar irradiance and detector sensitivity (Section G.2); the interference and blocking filter transmittances (Section G.3); the atmospheric attenuation coefficients (Section G.4); the column ratios (Section G.5); and lastly the Dobson instrument variables (Section G.6).

The integration is extended over the wavelength range in which the instrument electrical response is significant. This range is considered to be bounded by 290 nm at the lower end, where the high atmospheric attenuation provides a cut-off to solar radiation, and by 390 nm at the upper end, beyond which the blocking filter is effective. The infrared leakage bands in the filters and the blocking filter are not significant. These response cut-offs are enhanced by the highly attenuating outer skirts of the interference filters.

The choice of integration interval depends on the scale of the detail in the input spectral data, the accuracy required of the calculations, and the effort needed to set up digitised spectra. A choice of 0.2 nm was made. This reflects

the scale of detail in the most important variable, the ozone absorption coefficient, and enables the width of single interference filters (between tenth transmittance points) to be well represented by at least ten points. There are 400 points in total.

The methods for constructing the 400 point spectra of the variables of the model are outlined in the following three sections.

G.2 Solar Irradiance and Detector Sensitivity

The extraterrestrial source intensity, $U(\lambda)$, of the sun is derived from the composite high resolution near-ultraviolet solar spectrum compiled by Furakawa et al. (1967), a copy of the spectrum on magnetic tape being made available by the National Center for Atmospheric Research, Boulder, Colorado, U.S.A. Covering the spectral region from 208 nm to 360 nm, it gives the positions of over 12,000 minima and maxima in wavelength to ±0.01 nm, and in absolute spectral irradiance to ±30%, with a density of points of up to 150 nm^{-1}. The irradiance is highly variable, ranging from 7 to 180 μW/(cm nm) and showing many changes in excess of 100% occurring within a few hundredths of a nanometre. Figure G.1 shows the variability that can be found within a single 0.2 nm wavelength interval.

A trapezoidal integration of the spectrum over successive wavelength intervals was made to produce an equal-interval, medium-resolution spectrum suitable for the calculations. A 5 nm section of it is shown in figure G.2, while the complete (but partly smoothed) spectrum is represented in figure 8.1.

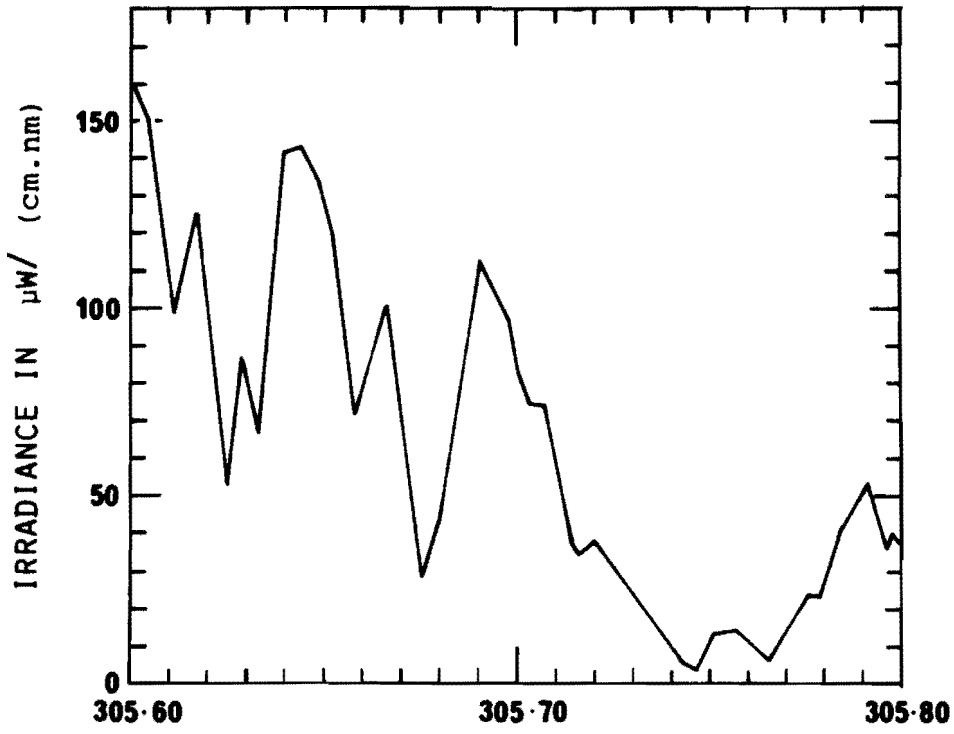

FIG. G.1 HIGH RESOLUTION SOLAR SPECTRUM

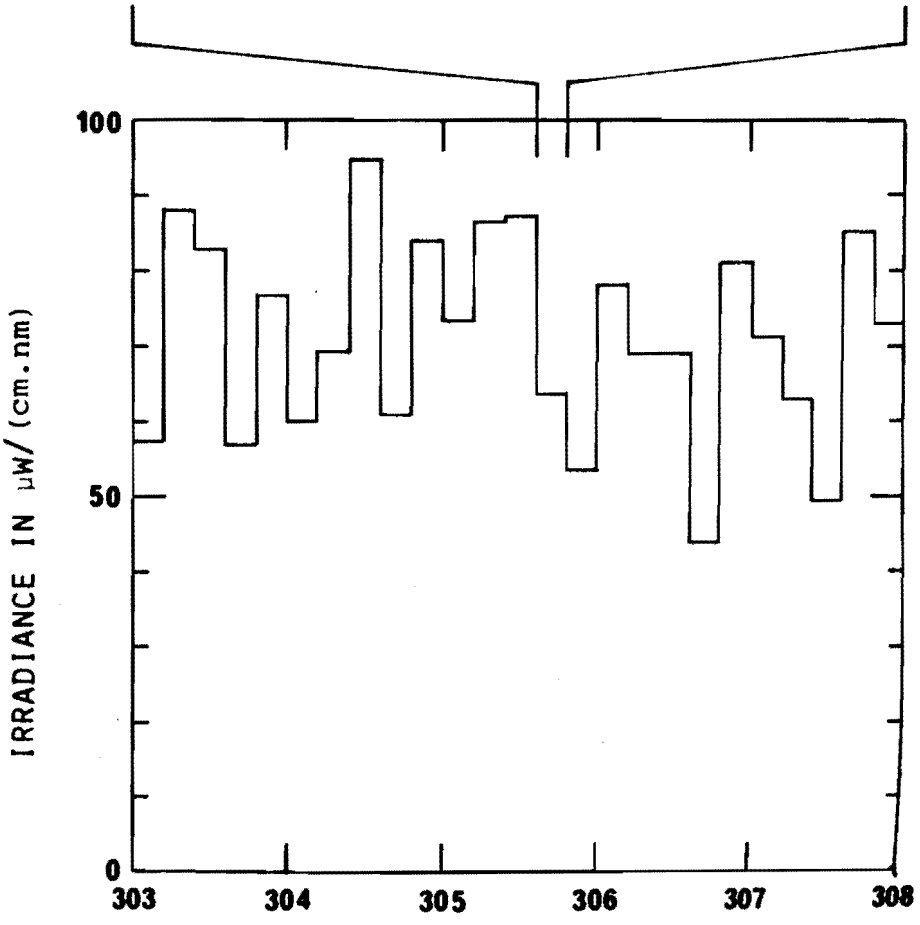

FIG. G.2 MEDIUM RESOLUTION EQUAL INTERVAL SOLAR SPECTRUM

Beyond 360 nm, where the high-resolution data end, the irradiance is approximated by a constant value derived from the solar spectrum of Dunkelman and Scholnik (1959). No great accuracy is needed in this wavelength region as it is very well blocked.

Another equal-interval irradiance spectrum, at 0.1 nm intervals between 300 and 610 nm, has since been published by Thekaekara (1974), and is similar in outline to the author's spectrum. It is less suitable for the purposes of Part III of this thesis owing to its lower resolution, of 0.3 nm, although its absolute accuracy, averaged over 1.0 nm intervals, may be better.

Furakawa et al. indicate that the absolute accuracy of any medium-resolution spectrum based on their high-resolution spectrum cannot be expected to be better than 15 to 20%. However, for our purposes, only the relative spectral irradiance is required, so the corresponding relative accuracy will be greater, probably better than 10%.

According to Tousey (1966), although the total solar radiation output is known to be constant to better than 2%, no similar constancy has yet been shown for either absolute or relative spectral irradiance in the near ultraviolet part of the spectrum. However, there is reason to believe that the near ultraviolet constancy is in fact similar to the total solar constancy, i.e. to better than 2%, which is rather smaller than the experimental uncertainty of 10% mentioned above.

The relative spectral sensitivity $D(\lambda)$ of the detector is taken from the standard S5 spectral response curve which is believed to be characteristic of the RCA 1P28 photomultiplier

tubes used in both the filter and prism instruments. A graph of the S5 response shown in RCA (1970) shows a maximum response, 100% say, at about 345 nm, with smooth decreases to about 85% at 290 nm, and 90% at 370 nm. Within this wavelength region, the relative spectral response, $D(\lambda)$, can be approximated by the parabolic equation

$$D(\lambda \text{ nm}) = 1.0 - 5\text{x}10^{-5} (345-\lambda)^2 \qquad (G.1)$$

or for the i^{th} 0.2 nm wavelength interval from 290 nm, by

$$D_i = 1.0 - 5\text{x}10^{-5} (55.1 - 0.2i)^2 \qquad (G.2)$$

The $D(\lambda)$ spectrum is shown in figure 8.2.

The assumption that the 1P28 photomultipliers belong to a well-defined spectral class is supported by the experiment explained in Appendix A, section 4, which shows two such photomultipliers to be within 2.0% in relative spectral response over any 50 nm range between 300 and 700 nm. This figure is therefore taken as representative of the uncertainty in the expressions for $D(\lambda)$ and D_i, equations (G.1) and (G.2).

It should be noted that temperature changes produce relative spectral response changes (RCA 1970), but the effect is small for our case, being about $1.5\text{x}10^{-3}$ % $^{o}C^{-1}$ nm^{-1} for the 1P28 tube in the 300 to 350 nm region (see Section 5.2).

G.3 Interference and Blocking Filter Transmittance

Complete transmittance spectra in the spectral region 290 to 400 nm were obtained for all the filters on a Cary 14 recording spectrophotometer as is described in Appendix A sections 1 and 2. Each interference filter corresponds to one of the standard total-ozone measurement wavelengths, as can be seen from their spectra, figures 4.1 to 4.6, and consists of a narrow transmittance band of about 25% peak transmittance, and broad wings whose transmittance decreases to about 0.001%.

The blocking filter transmittance, figure 4.10, is about 50% from 290 nm to 315 nm, but decreases very rapidly beyond 340 nm, to become less than 10^{-7} at 310 nm. The broad, low-transmittance infrared band at 850 nm contributes negligible energy when combined with the interference filters and the instrument's detector, and is ignored in the model.

In practice, the great transmittance ranges are accommodated on the linear spectrophotometer chart by periodic scale changes, as can be seen in the typical raw spectrum of figure A.1. Once calibrated, such a spectrum is approximated by a series of straight lines and the coordinates of their intersection points read off for later use in constructing an equal-interval data set. In the less important low-transmittance regions, the points may be up to 10 nm apart, but in the high-transmittance passband region the points are only 0.15 nm apart, thus giving accurate representation of the spectrum where it is needed. A trapezoidal integration over 0.2 nm wavelength intervals yields the final equal-interval spectrum.

Calibration of the Cary 14 can achieve a wavelength accuracy of ±0.05 nm, and a transmittance accuracy on the 10°

and 10^{-1} scales of ±0.2 to 2.0% depending on the actual reading. For the lesser scales, accuracy steadily decreases with decreasing transmittance, partly due to inaccuracy in scale calibration, and partly due to instrumental limitations. Adding to this the intended lessening accuracy of the straight-line spectrum approximation mentioned above, results in a decline in accuracy from ±1% for the 10^{-1} scale to about ±20% for the 10^{-5} scale. Therefore, only in the important high transmittance regions is a good accuracy maintained. Consideration to the uncertainties in the original measured spectra is given in Appendix A, sections 1, 2 and 3.

Since the interference filter spectra depend on temperature, as explained in Section 4.7, it should be noted that all recordings were made in an airconditioned room held at 20±2°C.

G.4 Atmospheric Attenuation Coefficients

The necessary coefficients are the ozone absorption coefficient α, the Rayleigh or molecular scattering coefficient β, and the aerosol scattering coefficient, δ, all of which are wavelength dependent.

The ozone spectral absorption coefficient used was measured at 229°K, corresponding roughly to stratospheric temperatures, by Vigroux (1953) and consists of a set of minima and maxima. It is more clearly tabulated in Valley (1965), from which values were plotted to form the basis for an interpolated continuous absorption spectrum, figure 8.3. The final 0.2 nm spectrum was read from this.

Vigroux's data compares well with the measurements of others and is accurate to about 0.1 nm in wavelength, and to about 1% in absorption, although there is some evidence of larger errors (Hamilton and Walker 1966). The interpolated curve retains this accuracy from 290 nm to about 310 nm, but beyond this the uncertainty of the interpolation increases and may reach 25% in the regions between well-separated data points. However, at the wavelengths where larger uncertainties occur, the absorption coefficient is small, so the actual uncertainty, which is the relevant quantity in most of the subsequent calculations, is also small.

Vigroux's work shows the absorption coefficient to be temperature dependent. Consideration is given to this effect in Appendix D, but at this point it is sufficient to say that the coefficient is accurate to about ±3% for the range of stratospheric temperatures normally encountered. Any pressure dependence is negligibly small.

An expression for the Rayleigh scattering coefficient, as a function of wavelength and ground-level air pressure is derived in Appendix H and is accurate to ±0.5%. A graph of it against wavelength is given in figure 8.2.

The aerosol attenuation coefficient is approximated in the theory by a linearly-dependent function of wavelength, equation (7.15), so that most calculations then require only a knowledge of g, the gradient of this function. The range of $g = \pm 0.0025\ nm^{-1}$, assessed from data given in Rat'kov (1971), is used but it should be remembered that the range encountered at a location will depend on its climate and its proximity to aerosol sources, for example cities, and seashores.

G.5 Column Ratios μ_h, μ_m and μ

The ratio μ_h = Sec $\psi(h)$, where $\psi(h)$ is the solar zenith angle at the ozone layer's nominal centre of mass h = 22 km, is given by

$$\mu_h = (\cos(\arcsin(\ell \sin \psi)))^{-1} \qquad (G.3)$$

where ψ = sea level solar zenith angle,
and $\ell = R/(R+h) = 0.99656$, and R is the earth's radius. Equation (G.3) is a consequence of the simple geometric relationship $\sin \psi(h) = \ell \sin \psi$. At a value of $\mu_h = 4.0$, equation (G.3) is accurate to ±0.5% for a ±10% uncertainty in h.

The ratio μ_m, called the relative optical airmass of air, or just airmass, is a function of solar zenith angle. It has been recalculated recently by Kasten (1966) who approximates it by the following equation

$$\mu_m = (\cos \psi + 0.1500(93.885-\psi)^{-1.253})^{-1} \qquad (G.4)$$

where ψ is in degrees, and which is accurate to 0.1% up to $\psi = 86^\circ$, and to 1% for $86^\circ < \psi < 90^\circ$.

The ratio μ is taken as sec ψ.

G.6 Dobson Instrument Variables

All the relevant differences between the filter and Dobson instruments are contained in the passband transmittance function $F(\lambda)$ and the blocking function $S(\lambda)$.

The Dobson passband transmittance functions used are displayed in figure 8.10, and are very similar to those used by Vanier and Wardle (1969). Although only approximate, the

functions provide an adequate model for the calculations.

The transmittance of the glass blocking filter used in the Dobson changes negligibly across the passbands and may be ignored, i.e. $S(\lambda) = 1.0$.

APPENDIX H

DERIVATION OF MOLECULAR SCATTERING COEFFICIENT

Following Penndorf (1957), a formula is derived here for β, the Rayleigh or molecular scattering coefficient for a vertical path through the atmosphere. In addition to outlining the derivation, this appendix shows how the scattering coefficient can be simply expressed in terms of a site's air pressure.

Penndorf begins with the following expression for $\sigma(\lambda)$, the single molecule scattering cross section,

$$\sigma(\lambda) = \frac{8\pi^3}{3\lambda^4} \frac{(n_s^2-1)^2}{N_s^2} \frac{(6+3\rho_n)}{(6-7\rho_n)} \quad cm^{-2} \tag{H.1}$$

where n_s = refractive index for standard air, (i.e. 15°C, 760 mm Hg, and 0.03% CO_2 by volume)

ρ_n = depolarisation factor

N_s = number density of standard air in cm^{-3}
= 2.5474×10^{19} cm^{-3}

λ = wavelength of light in μm.

The refractive index is wavelength-dependent and the empirical formula of Edlen, given in Penndorf, expresses it as

$$(n_s-1)10^8 = \lambda^2 \left[\frac{6432.8}{\lambda^2} + \frac{2949800}{146\lambda^2-1} + \frac{25540}{41\lambda^2-1}\right] \tag{H.2}$$

where λ is in μm, and which is believed to be accurate to better than 0.1% for 0.2 μm < λ < 20 μm.

Equations (H.1) and (H.2) are easily related by the following expansion.

$$(n_s^2-1)^2 = (n_s+1)^2(n_s-1)^2 \quad \text{which at } \lambda = 0.3\mu$$

$$\simeq (1.003+1)^2(n_s-1)^2$$

$$\simeq 4.0012(n_s-1)^2$$

$$\simeq 4(n_s-1)^2. \qquad \text{(H.3)}$$

The depolarisation factor accounts for the optical anisotropy of the diatomic air molecules, and from a table in Penndorf, is assessed as $\rho_n = 0.034 \pm 0.003$, which gives

$$\frac{6+3\rho_n}{6-7\rho_n} = 1.059 \pm 0.5\% \qquad \text{(H.4)}$$

Combining equations (H.1), (H.2), (H.3) and (H.4) and multiplying out the constants yields

$$\sigma(\lambda) = 5.397 \times 10^{-37}\left[\frac{6432.8}{\lambda^2} + \frac{2949800}{146\lambda^2-1} + \frac{25540}{41\lambda^2-1}\right]^2 \text{ cm}^2 \qquad \text{(H.5)}$$

whose accuracy, from equation (H.4), is 0.5%, and where λ is measured in microns. Since equation (H.5) refers to a single molecule, it is independent of temperature and pressure.

The total molecular scattering coefficient, β, used throughout the thesis (see equation (1.2)), is a dimensionless optical thickness, and should not be confused with the volume scattering coefficient which is similarly labelled by Penndorf.

For a vertical path through the dilute earth atmosphere, above a site of altitude h,

$$\beta = \int_h^\infty \sigma N(z)\,dz \qquad \text{(H.6)}$$

where N(z) is the molecular number density at height z. Since σ is pressure and temperature independent, equation (H.6) may be written as

$$\beta = \sigma \int_h^\infty N(z)dz \qquad (H.7)$$

At this point, Penndorf calculates the integral for an isothermal and a model atmosphere, but a simpler method which relates it to ground level air pressure is proposed here.

The air pressure P_h at the site of altitude h is given by

$$P_h = \int_h^\infty \frac{M(z)}{N_a} N(z)g(z)dz \qquad (H.8)$$

where M(z) = mean molecular weight of air at height z

N_a = Avogadros number

g(z) = gravitational acceleration at height z.

Since the atmosphere is well mixed below about 90 km, in this region the mean molecular weight is constant with a value of $\overline{M(z)} = 28.96$. The gravitational acceleration is more variable but an adequate constant approximation can be made. g(z) is inversely proportional to the distance from the centre of the earth, so that in going from ground level to a height of z = 16 km, which encloses 90% of the atmosphere, the percentage change in g is found to be only 0.5%. Therefore, the use of an average, $\overline{g(z)}$, weighted toward the lower part of this layer, may contribute less than 0.1% error to the integral of equation (H.8), provided that latitudinal and local variations in g(z=0) are taken care of.

Equation (H.8) can therefore be written as

$$P_h = \frac{\overline{M(z)}\ \overline{g(z)}}{N_a} \int_h^\infty N(z)dz, \qquad (H.9)$$

which is accurate to 0.1%, and when compared with equation (H.5) yields

$$\beta = \frac{\sigma N a}{\overline{M(z)}\ \overline{g(z)}} P_h. \qquad (H.10)$$

This equation, along with equation (H.5), enables the easy calculation of the scattering coefficient for any location where pressure or altitude is known. It also clearly defines the relationship of the coefficient to air pressure. This is important, since the periodic variations in air pressure, equivalent to ±3% at mid-latitudes, will be accompanied by corresponding variations in the scattering coefficient. The 0.5% combined uncertainty of other quantities in equation (H.10) is negligible compared to this.

With an average sea level pressure P_{0h} = 1013.3 mb, a mid-latitude weighted $\overline{g(z)}$ = 9.79 ms^{-1}, and an $\overline{M(z)}$ = 28.96 as given above, equations (H.10) and (H.5) give

$$\beta_0 = 2.153 \times 10^{25}\sigma \qquad (H.11)$$

and

$$\beta_0 = 1.162 \times 10^{-11} \left[\frac{6432.8}{\lambda^2} + \frac{2949800}{146\lambda^2-1} + \frac{25540}{41\lambda^2-1}\right]^2 \qquad (H.12)$$

where β_0 is the exponential scattering coefficient for the average air pressure of P_{0h}. At other air pressures, P_h, the scattering coefficient, β, is given by

$$\beta = \beta_0 \frac{P_h}{P_{0h}} . \qquad (H.13)$$

APPENDIX I

LIMITS OF EQUIVALENT ATTENUATION COEFFICIENT AT ZERO AIRMASS

This appendix shows that, in the limit of zero airmass, the equivalent attenuation coefficients, defined by equations (7.6), (7.8) and (7.10), are equal to simple averages weighted by the extraterrestrial response function, $Q_\infty(\lambda)$, i.e. that, for example

$$\lim_{\mu \to 0} \bar{\alpha} = \alpha_0 = \frac{\int_{\lambda_a}^{\lambda_b} Q_\infty(\lambda)\alpha(\lambda)d\lambda}{\int_{\lambda_a}^{\lambda_b} Q_\infty(\lambda)d\lambda} \qquad (I.1)$$

To begin, equation (7.6) is rearranged as

$$e^{-\mu_h X\bar{\alpha}} = \frac{\int_{\lambda_a}^{\lambda_b} Q_\infty(\lambda)\exp-[\mu_h X\alpha(\lambda)+\mu_m\beta(\lambda)+\mu\delta(\lambda)]d\lambda}{\int_{\lambda_a}^{\lambda_b} Q_\infty(\lambda)\exp-[\mu_m\beta(\lambda)+\mu\delta(\lambda)]d\lambda} \qquad (I.2)$$

Now since

$$e^{\gamma} \sim 1 + \gamma \quad \text{for} \quad \gamma << 1 \qquad (I.3)$$

then in the limit as $\mu \to 0$ (and therefore as μ_h and $\mu_m \to 0$) equation (I.2) becomes firstly

$$1-\mu_h X\bar{\alpha} = \frac{\int_{\lambda_a}^{\lambda_b} Q_\infty(\lambda)[1-\mu_h X\alpha(\lambda)-\mu_m\beta(\lambda)-\mu\delta(\lambda)]d\lambda}{\int_{\lambda_a}^{\lambda_b} Q_\infty(\lambda)[1-\mu_m\beta(\lambda)-\mu\delta(\lambda)]d\lambda} \qquad (I.4)$$

and then

$$1-\mu_h X\bar{\alpha} = 1 - \frac{\int_{\lambda_a}^{\lambda_b} Q_\infty(\lambda)\,[\mu_h X \alpha(\lambda)]\,d\lambda}{\int_{\lambda_a}^{\lambda_b} Q_\infty(\lambda)\,d\lambda} \tag{I.5}$$

$$\therefore \quad \lim_{\mu \to 0} \bar{\alpha} = \frac{\int_{\lambda_a}^{\lambda_b} Q_\infty(\lambda)\,\alpha(\lambda)\,d\lambda}{\int_{\lambda_a}^{\lambda_b} Q_\infty(\lambda)\,d\lambda} \tag{I.6}$$

which is just an average of $\alpha(\lambda)$ weighted by $Q_\infty(\lambda)$.

Similar conclusions follow for $\bar{\beta}$ and $\bar{\delta}$.

REFERENCES

Baumeister, P.W. 1965 Interference and Optical Interference Coatings. Applied Optics and Optical Engineering. Academic Press, New York. 1, 8, p285-323.

Blifford, I.H. 1966 Factors Affecting the Performance of Commercial Interference Filters. Appl. Opt. 5, 1, 105.

Bojkov, R.D. 1969 Differences in Dobson Spectrophotometer and Filter Ozonometer Measurements of Total Ozone. J. App. Met. 8, 3, 362.

Born, M. and Wolf, E. 1965 Principles of Optics, 3rd Ed. Pergamon Press, New York.

Brewer, A.W. 1973 A Replacement for the Dobson Spectrophotometer? PAGEOPH, 106-108, p919.

Cary. Instructions for Cary Recording Spectrophotometer Model 14R. Cary Instruments, 2724 South Peck Rd, Monrovia, California 91016.

Craig, R.A. 1965 The Upper Atmosphere, Meteorology and Physics. Academic Press, New York. 509p.

Delano, E. and Pegis, R.J. 1969 Methods of Synthesis for Dielectric Multilayer Filters. Progress in Optics, North Holland, Amsterdam. 7, 2, p69-137.

Dobson, G.M.B. 1957 Observers Handbook for the Ozone Spectrophotometer. In Ann. I.G.Y. 5. Pergamon Press, London. P46-114.

Dobson, G.M.B., and Normand, C.W.B. 1962 Determination of Constants etc. Used in the Calculation of the Amount of Ozone from Spectrophotometric Measurements and an Analysis of the Accuracy of Results. Ann. I.G.Y. 16, part II, 161.

Dunkelman, L. and Scholnik, R. 1959 Solar Spectral Irradiance and Vertical Atmospheric Attenuation in the Visible and Ultraviolet. J. Opt. Soc. Am. 49, 356.

E.M.I. 1970 Photomultiplier Tubes. EMI Electronics Ltd, Electron Tube Division, Hayes, Middlesex, England. 64p.

Furakawa, P.M., Haagenson, P.L. and Sharberg, M.J. 1967 A Composite, High Resolution Solar Spectrum from 2080 to 3600Å. NCAR Technical Note TN-26. National Centre for Atmospheric Research, Boulder, Colorado.

Furman, Sh.A. and Levina, M.D. 1971 Effect of Moisture on the Optical Characteristics of Narrow Band Interference Filters. Opt. Spectrosc. 30, 4, 404.

Goldberg, B. and Klein, W.H. 1974 Radiometer to Monitor Low Levels of Ultraviolet Irradiance. Appl. Opt. 13, 3, 493.

Griggs, M. 1966 Atmospheric Ozone. In Green, A.E.S. The Middle Ultraviolet: Its Science and Technology. John Wiley and Sons, New York. p83-117.

Hamilton, R.A. and Walker, J.M. 1966 A Method of Measuring Atmospheric Ozone Absorption Coefficients. J. Atmos. Terr. Phys. 28, 667.

Hearn, A.G. 1961 The Absorption of Ozone in the Ultraviolet and Visible Regions of the Spectrum. Proc. Phys. Soc. 78, 932.

Hennes, J. and Dunkelman, L. 1966 Ultraviolet Technology. In Green, A.E.S. The Middle Ultraviolet: Its Science and Technology. John Wiley and Sons, New York. p304-377.

Kasten, F. 1966. A New Table and Approximation Formula for the Relative Optical Airmass. Archives f. Met. Geophys. Bioklimat. Series B, Bd 14, Heft.2.

Lissberger, P.H. and Wilcock, W.L. 1959 Filters in Parallel Beams of Light Incident Obliquely and in Convergent Beams. Part II of Properties of All-Dielectric Interference Filters. J. Opt. Soc. Am. 49, 2, 126.

Matthews, W.A. 1971 Atmospheric Ozone. Ph.D. thesis, University of Canterbury, Christchurch, New Zealand.

Matthews, W.A. 1972 Agreement Between Dobson Spectrophotometer and Filter Ozonometer Measurements of Total Ozone. J. App. Met. 11, 1, 239.

Nichols, L.W., Olson, A.L. and Plain, K.E. 1965 Factors Affecting the Performance of Narrow-Band Interference Filters. Appl. Opt. 4, 1, 138.

Osherovich, A.L., Rozinskiy, M.Ya. and Furman, Sh.A. 1969 A comparison between the M83 Standard Ozonometer and an Ozonometer Equipped with Narrow-band Interference Filters. Izv., Atmos. and Oceanic Phys. 5, 10, 1030.

Penndorf, R. 1957 Tables of the Refractive Index for Standard Air and the Rayleigh Scattering Coefficient for the Spectral Region between 0.2 and 20.0 μ and Their Application to Atmospheric Optics. J. Opt. Soc. 47, 2, 176.

Phillips. 1970. Photomultipliers. Phillips Application Book. Electronic Components and Materials Division, Eindhoven. 150p.

Powell, D.B.B. 1971 The Absorption Coefficients of Ozone for the Dobson Spectrophotometer: A Direct Determination of their Ratios and Temperature Dependence. Quart. J. R. Met. Soc. 97, 83.

Raeber, J.A. 1973 An Automated Dobson Spectrophotometer. PAGEOPH, 106-108, 947.

Rat'kov, V.M. 1971 The Effect of Aerosol Attenuation on Spectrophotometric Determination of Ozone. Ivz., Atmos. and Oceanic Phys. 7, 8, 878.

RCA. 1970 Photomultiplier Manual. Item PT-61, Technical Series. RCA Corporation, Electronic Components Division, Harrison, N.J. 07029, U.S.A. 192p.

Thekaekara, M.P. 1974 Extraterrestrial Solar Spectrum, 3000-6100Å at 1Å Intervals. Appl. Opt. 13, 3, 518.

Thomas, R.W., Guard, K., Holland, A.C. and Spurling, J.F. 1974 Ozone Measurement Systems Improvement Studies. NASA Technical Note TN D-7758. National Aeronautics and Space Administration, Washington, D.C. 20546.

Tousey, R. 1966 The Radiation from the Sun. In Green, A.E.S. The Middle Ultraviolet: Its Science and Technology. John Wiley and Sons, New York. P1-39.

Valley, S.L. 1965 Ed. Handbook of Geophysics and Space Environments. Prepared by U.S. Air Force Cambridge Research Laboratories. McGraw Hill Inc., New York.

Vanier, J. and Wardle, D.I. 1969 The Effects of Spectral Resolution on Total Ozone Measurements. Quart. J. R. Met. Soc. 95, 395.

Vigroux, E. 1953 Contribution à l'Étude Expérimentale de l'Absorption de l'Ozone. Ann. Phys. 8, 709-762.

Walshaw, C.D., Dobson, G.M.D. and MacGarry, B.M.F. 1971 Absorption Coefficients of Ozone for Use in the Determination of Atmospheric Ozone. Quart. J. R. Met. Soc. 97, 75.